UNIVERSITY OF SOUTHAMPTON

ABSTRACT

FACULTY OF ENGINEERING

INSTITUTE OF SOUND AND VIBRATION RESEARCH

Doctor of Philosophy

New methods for assessing the control of blood flow in the brain

By Hesam Kouchakpour

Cerebral autoregulation is the process of maintaining blood flow to the brain almost constant despite changes in arterial blood pressure (ABP) with the assumption that changes to other physiological condition are small. Assessment of cerebral autoregulation plays a key role in diagnosis, monitoring and prognosis of cerebrovascular disease clinically. In this work Transcranial Doppler Ultrasound was used to measure middle cerebral artery velocity, arterial blood pressure (ABP) was non-invasively measured using a finger cuff device (Finapres).

Mathematical models that characterize the cerebral autoregulatory system have been used in the quantitative assessment of function/impairment of autoregulation as well as in furthering the understanding cerebral hemodynamics. Using spontaneous fluctuations in arterial blood pressure (ABP) and CO_2 as inputs and cerebral blood flow velocity ($CBFV$) as output, the autoregulatory mechanism has been modeled using linear and nonlinear (Laguerre Volterra Networks), single-input (SI, only ABP) and multi-input (MI, ABP and CO_2) approaches. From these models, a small number of measures have been extracted to provide an overall assessment of autoregulation. It was also investigated whether or not some of the poor performance previously reported can be overcome by improved modeling (characteristics of the nonlinear models) and choice of autoregulation parameter to extract cerebral autoregulation. In this work, lower inter and intra subject variability of the parameters were considered as the criteria for identifying improved measures of autoregulation.

Search for improved analysis is then extended, using the data-driven approach based on subspace distance (SSD). The performance of this method is compared to alternatives previously proposed, using data from healthy volunteers in normo- and hyper-capnia (to induce transient impairment of autoregulation). The subspace distance (SSD) provides a means of determining the distance of an estimated model to others known to have been obtained from normal or impaired autoregulation, considerably. The smallest average distance with respect to each of these sets then determines how far from normal/impaired a given recording lies. For comparison, indexes of autoregulation were obtained from methods used in previous work, including the phase of the frequency response at $0.1\ Hz$ ($P1$), and the 2^{nd} parameter of a 1^{st} order FIR model ($H1$). The main advantage of this method is that it does not require picking parameters but is driven by the data (the model) itself.

The method was found to be promising and provided better distinction between normocapnia and hypercapnia compared to other autoregulatory parameters studied in this section.

Multivariate adaptive filters (multivariate recursive least square ($MI-RLS$)) and multivariate moving window ($MI-MW$) to study the effect of P_{ETCO_2} in the dynamic of time-varying characteristic of cerebral autoregulation were applied to study the multivariate, time-varying characteristics of cerebral autoregulation. Here also $SI-RLS$, $SI-MW$, $MI-MW$ and $MI-RLS$ methods to baseline, hypercapnia and normocapnia measurements from our volunteers individually were applied. Autoregulation was quantified by both time-varying phase-lead and amplitude using pressure pulse input. It was also noticed that multivariate models deal very well with the transient at the beginning of hypercapnia compared to univariate models and autoregulatory parameters extracted from $MI-RLS$ provide the least variation. The results from multivariate time-varying coherence showed that it can provide significantly higher values at low frequencies ($f < 0.05\ Hz$) and the transient between normocapnia and hypercapnia compared to univariate time-varying coherence.

Finally, a new tentative approach of hardware and software system for the measurement of blood flow control was carried out in Southampton General Hospital which allowed the inducement of random, step-wise changes in blood pressure and inspired carbon dioxide (CO_2) level that can be easily and safely repeated and may be applicable as a clinical tool. This experiment benefited from the use of $LBNP$ (Lower-body-negative pressure). It generates a controllable pressure variation, built around the lower limbs of a subject resulting in temporary lowering the blood pressure. The initial assessment of this dataset is presented.

Acknowledgments

It is with immense gratitude that I acknowledge the support and help of my supervisor, Dr David Simpson. Apart from supporting me throughout my PhD with his kindness and knowledge, our meetings were always enlightening the problem domain for me, and proving me with sufficient guidance to investigate the best possible solution.

I would also like to thank Dr. Tony Birch from the medical physics department at Southampton General Hospital for his aid and advice in the experiment arrangement, data collection and medical aspects of this research. I would like to thank Prof Robert Allen for his contribution in this work.

This research would not have been possible without the financial support of EPSRC. Furthermore, in my daily work I have been blessed with a friendly and cheerful group of fellow colleges in SPCG research group.

In the end I cannot find words to express my gratitude to my parents (Alireza and Sedigheh) and my sister (Samaneh) for their continuous support and encouragement.

Abbreviations

$A1.5$	Amplitude at $1.5\ sec$ from PPR
$A8$	Amplitude at $8\ sec$ from PPR
ABP	Arterial blood pressure
AIC	Akaiki
AR	Autoregressive
ARI	Autoregulatory index
$ARMA$	Autoregressive–moving-average
$ARMAX$	Autoregressive moving average model with exogenous input
ARP	Autoregulatory parameter
ARX	Autoregressive with exogenous input
BP	Blood pressure
CA	Cerebral autoregulation
CBF	Cerebral blood flow
$CBFV$	Cerebral blood flow velocity
CCP	Critical closing pressure
CPP	Cerebral perfusion pressure
CS	Cluster separation
CSF	Cerebrospinal fluid
CVR	Cerebrovascular resistance
$CVRi$	Cerebrovascular resistance index
DFT	Discrete Fourier transform
DLF	Discrete Laguerre function
FFT	Fast Fourier transform
FIR	Finite impulse response
FR	Frequency response
FVS	Final value (amplitude) to step input
H	Hidden units in Laguerre network
$H1$	Second coefficient of the FIR filter with 2 lags
HC	Hypercapnia
HCO_2	High CO_2
HF	High Frequency
HR	Heart rate
ICC	Intraclass correlation
ICP	Intracranial pressure
IIR	Infinite impulse response
$LBNP$	Lower body negative pressure
LET	Laguerre expansion technique
LF	Low Frequency
$LOOCV$	Leave-one-out cross-validation approach
LVN	Laguerre Volterra Networks
LVN	Nonlinear Laguerre network
MA	Moving average
$MABP$	Mean arterial blood pressure
MCA	middle cerebral artery
$MCAV$	Mean middle cerebral blood flow velocity
$MCBFV$	Mean cerebral blood flow velocity
MI	Multi-input

$MI-MW$	Multivariate moving window
$MI-RLS$	Multivariate recursive least square
$MISO$	Multi-Input-Single-Output
Mx	Correlation method using Pearson's correlation coefficient
NC	Normocapnia
$NMSE$	Normalized mean square error
$P1$	Phase at $0.1\ Hz$
P_{ETCO_2}	Partial pressure of end-tidal carbon dioxide
P_{ETO_2}	End-tidal O_2
P_{aCO_2}	Partial Arterial O_2
P_{aCO_2}	Partial pressure of CO_2 in the blood
PPI	Pressure pulse input
PPR	Pressure pulse response
R	Resistance
$RHCO_2$	Random high CO_2
RLS	Recursive least squares filter
RoR	Rate of regulation
SDn	Inter-subject variability
SI	Single-input
$SI-MW$	Single-input moving window
$SI-RLS$	Single-input recursive least square
$SISO$	Single-Input-Single-Output
SNR	Signal to noise ratio
SSD	Subspace distance
STD	Standard deviation
T	Circumferential tension
TCD	Transcranial Doppler sonography
TFA	Transfer function analysis
VLF	Very low frequency
$mSDn$	Intra-subject variability
y	Output

Mathematical Notation

a	Scalar a
v	Vector v
M	Matrix M
M^T	Transpose of matrix M
M^*	Complex conjugate of matrix M
$M^H = (M^*)^T$	Hermitian transpose of matrix M
M^{-1}	Inverse of matrix M
$F(x)$	Fourier transform of x
$F^{-1}(x)$	Inverse fourier transform of x
$\log(x)$	Logarithm of x in base of e
$x(i)$	Element i of signal x
$x(t)$	Time domain representation for signal x
$x(f)$	Frequency domain representation of signal x
$a = b$	a is equal to b
$a \sim b$	a is similar to b
$a < b$	$a$is smaller than b
$A \equiv B$	Matrix A is equivalent to matrix B
$\pm$	confidence interval
$\|.\|$	Absolute value
μ_x	Mean of x
σ_x	Standard deviation of x
$E(.)$	Expectation operator
ε	Error
dX	Normalized version of signal x
ΔX	Normalized variation of signal x
$\bar{X}(f)$	Fourier transform of $x(t)$
$\sum_{i=1}^{I} x(i)$	Summation of $x(i)$ for $i = 1$ to $i = I$
$mean(x_i)$	Mean of vector x_i
$\hat{X}$	Estimated of X
$\prod_{i=1}^{I} x(i)$	multiplication of $x(i)$ for $i = 1$ to $i = I$
$G_{xy}(f)$	Cross-spectrum between signal x and y
$Gxx(f)$	Auto-spectrum of signal x
γ	Coherence
$H(f)$	Transfer function
$\phi(f)$	Phase of transfer function $H(f)$
$cov(X)$	Covariance matrix X
$coh(X)$	Coherence
$d(x, y)$	Distance between x and y
C_n	Cepstrum coefficients
$\Gamma_x^2(f)$	Univariate coherence function
$\Gamma_M^2(f)$	Multiple coherence
r	Intraclass correlation
$b_j(m)$	j[th]-order orthonormal discrete Laguerre function
f_h	Polynomial static nonlinearity
Q	Order of nonlinearity
$k_{m,n}(j_1, j_2, \dots)$	Volterra kernels

$c_{m,n}(j_1, j_2, \dots)$	Expansion coefficients of Volterra kernels
$a_{m,n}(j_1, j_2, \dots)$	Coefficients of the r^{th} order kernel expansion
q	Time lag
a_{na}	Autoregressive coefficients of a $SISO$ system
b_{nb}	Moving average coefficients of a $SISO$ system
c_{nc}	Exogenous signal coefficients of a $SISO$ system
θ	Parameter vector
V_N	Loss function
$H(z)$	Rational function of z
w_n	Positive weight in cepstrum
$h(i)$	Coefficients of a causal FIR
H	Matrix of the FIR coefficients
R_{XX}	Auto-correlation matrix
R_{XY}	Cross-correlation matrix
λ	Forgetting factor for RLS method
$k(n)$	Kalman gain vector
$P(n)$	Inverse autocorrelation matrix

Contents

List of tables

List of Figures

Chapter 1 : Introduction

1.1 Overview

Autoregulation is one of the mechanisms in the automatic adjustment of blood flow to supply the required nutrition and remove waste in proportion to the tissue's requirement at any instant in time [2, 3]. For the brain, cerebral autoregulation refers to an active process of the brain by which cerebral blood flow is controlled at steady state despites the changes in the arterial blood pressure to ensure the required supply of the blood for the cerebral tissues. Cerebral autoregulation attracts considerable attention in the literature as it is thought to be an important mechanism in the development of some strokes, and also in the occurrence of the secondary damage, following stroke, head injury and cerebrovascular disease [4]. Having a good assessment of the cerebral autoregulation can potentially be used in clinics and hospitals where the changes in cerebral autoregulation may be observed. These changes can indicate variations in the patient's health and may be used to modify their medical treatment in order to help to manage their therapy and improve their recovery. Autoregulation is impaired by too low or too high cerebral perfusion pressure (CPP) when compared to autoregulation with normal CPP (between 60 to 85 $mmHg$).

The inducement of changes in arterial blood pressure (ABP), middle cerebral blood flow velocity ($MCAV$) and partial pressure of end-tidal carbon dioxide (P_{ETCO_2}) are the most common parameters used to stimulate the regulating mechanisms. Infrared plethysmography (Finapres), transcranial Doppler ultrasound and capnography are used respectively for these measurements as they can be used non-invasively and are commonly available.

The main aims of this project are to propose innovative experimental and signal analysis techniques for the robust assessment of cerebral blood flow control to determine the nature of the autoregulation mechanisms and increase understanding of the dynamic interaction between $CBFV$, ABP and P_{ETCO_2} based on modelling of experimental data using multivariate and data driven methods.

1.2 Layout of the thesis:

In chapter 2 of this thesis a brief summary of the relevant anatomy and physiology of cerebral blood flow and cerebral autoregulation is given.

The technical details for analysis of the response to the pressure and blood flow changes, for both static and dynamic cerebral autoregulation, are presented in chapter 3.

In chapter 4 the system identification methods to assess dynamic cerebral autoregulation by using a previously published model: the Tiecks [5] model, and frequency response, coherence and transfer function gain and phase are discussed which help to identify some challenges that exist in this field. The results from these well-known approaches are used as a ground for new findings and to compare new results to these approaches.

In chapter 5, multi-input (ABP,P_{ETCO_2}) Nonlinear Laguerre network (LVN) is used, to model, and to extract new autoregulatory parameters from the response of the system to pressure pulse (PP) input which has not frequently been extensively investigated. The variability between and within subject is studied. The aim of this chapter is to find the optimal model characteristics for different LVN and to test and compare the performance of these different models in term of assessment of autoregulation.

In chapter 6, subspace distance as a novel and data-driven approach to assess autoregulation is used. The performance of this methodology is studied by comparing it with some well-known autoregulatory parameters.

In chapter 7, time-varying multivariate models using multivariate recursive least square ($MI-RLS$) and multivariate moving window ($MI-MW$) are applied to study the time-varying characteristics of dynamic cerebral autoregulation and the performance is compared with the univariate version of these approaches.

In chapter 8, the new approach in data collection using constant/random lower body negative pressure ($LBNP$) with constant/random high CO_2 (HCO_2) is studied in order to test whether $LBNP$ can produce more variability in $CBFV$ and as the result of that can help to get more robust assessment of autoregulation.

In chapter 9, we conclude the work that has been carried out on this thesis.

1.3 List of original contributions

1. Proposal of optimal method and orders for two-input Laguerre Volterra networks (LVN) with different combinations of inputs and linearity/non-linearity: linear ABP, linearP_{ETCO_2}, nonlinear ABP, nonlinear P_{ETCO_2}, nonlinear interaction between ABP and P_{ETCO_2} with a focus on extracting parameters for assessing autoregulation in the models. Assessment of autoregulation was also done by looking at the variability between and within subjects and the robustness of different autoregulatory parameter estimates were studied.
2. Proposal of a new data-driven approach, and showing the superiority of this method over some other well-known autoregulatory parameters in term of assessing autoregulation and distinguishing between normo- and hypercapnia.
3. Applying uni- and multivariate time-varying methods for the assessment of autoregulation, showing that, having P_{ECTCO_2} as the secondary input can improve the normalized mean square error in the training. The results also showed that the contribution of P_{ECTCO_2} towards the spontaneous changes in $CBFV$ is significantly higher in hypercapnia compared to normocapnia. The result also indicated that the multivariate time-varying model can improve the coherence value at low frequency range and also in the transient between normocapnia and hypercapnia and vice versa. The results also showed that the effect of P_{ECTCO_2} on the variation of $CBFV$ is more significant when the subject is in hypercapnia.
4. Analysis of data collection from random Lower Body Negative Pressure ($LBNP$) in Southampton to induce bigger variations in ABP. Different autoregulatory parameters were used and it was shown that more robust assessment of autoregulation can be achieved with this new data collection approach. The results also showed significant reduction in the variability of autoregulatory parameters from baseline to $LBNP$

1.4 List of publications

1. Kouchakpour.H, Simpson.D.M, Allen.R, *New methods for assessing the control of blood flow in the brain*, in *PGBioMed*. 2009: Magdalen College,Oxford
2. Kouchakpour, H., R. Allen, and D.M. Simpson, *Nonlinear, multiple-input modeling of cerebral autoregulation using Volterra Kernel estimation.* Conference proceedings : Annual International Conference of the IEEE Engineering in Medicine and Biology Society. IEEE Engineering in Medicine and Biology Society. Conference, 2010. **2010**: p. 2375-8.
3. Angarita-Jaimes.N, Kouchakpour.H, Jia Liu, Panerai .R.B, Simpson.D.M, *Optimizing the assessment of cerebral autoregulation from black box models.* Medical Engineering and Physics, 2013.
4. Simpson D.M., Angarita-Jaimes.N, Kouchakpour.H, Allen.R, *Improved estimates of autoregulation from spontaneous variations in blood flow and pressure*, in *XXVth International Symposium on Cerebral Blood Flow, Metabolism and Function & Xth International Conference on Quantification of Brain Function with PET*. 2011: Barcelona, Spain.
5. Kouchakpour.H, Simpson D.M, Allen.R, *Optimizing measures of autoregulation from spontaneously varying blood pressure and flow*, in *IPEM Cerebral haemodynamic meeting*. 2011: Imperial College London.
6. Jia Liu , Kouchakpour.H, Panerai, R.B, Katsogridakis, E. , Zuoen Wang , Simpson, D.M. *Tracking instantaneous pressure-to-flow dynamics of cerebral autoregulation induced by CO2 reactivity*. in *IEEE*. 2013. Osaka: Engineering in Medicine and Biology Society (EMBC), 2013 35th Annual International Conference of the IEEE.
7. Simpson.D.M, Allen.R, Kouchakpour.H , Lea-Banks.H, Panerai.R.B, *Random steps in lower-body-negative pressure to augment blood pressure variability in the measurement of cerebral autoregulation*. in *18th meeting of European Society of Neurosonology and Cerebral Hemodynamics and 3rd meeting of Cerebral Autoregulation Network* 2013. Porto, Portugal

Chapter 2：Literature review

2.1 Cerebral circulation

The brain is the most remarkable and complex biological structure known. The brain weighs only 2% of total body mass, it consumes 20% of the total body oxygen and 25% of total body glucose [6].

In normal condition the amount of glucose supplied to the brain is seven times the necessary requirement, however the supplied oxygen to the brain is about two or three times the required amount. As a result cerebral blood flow may be halved without any distinct change in cerebral function but if it goes considerably below 50%, then failure of normal brain function will very rapidly become apparent due to an insufficient supply of oxygen [7, 8]. It is thus vital for human life, that the brain always received an adequate supply of blood.

2.2 Anatomy

The anatomy of the cerebral circulation was first documented by Willis in 1664 where he described, at the base of the brain, the arterial structures. He described the circle of arteries that distributes most of the blood supply to the cerebral cortex and is now named after him.

Blood is pumped to large elastic arteries from the heart and these themselves branch into smaller arteries. The structure of the arteries changes with their sizes. As the size of the arteries gets smaller their structure changes from having walls with a large amount of elastic tissues and a smaller amount of smooth muscle to structures with walls that have a smaller amount of elastic tissues and a larger amount of smooth muscle. With respect to this structure the arteries can be divided into three categories: elastic arteries, muscular arteries and arterioles. Elastic arteries have the largest diameter and the least amount of smooth muscle. Muscular arteries have relatively thick vessel walls compared to their diameter. The arterioles have small diameters and branch out of the arteries to transport blood from arteries to the capillaries.

There are four main arteries in the neck which supply the blood to the brain as can be seen in Figure 2-1. These arteries are connected at the base of the brain to the circle of Willis, as mentioned above. The four major cerebral arteries are left and right carotid arteries and left and right vertebral arteries (Figure 2-1).

The major cerebral network varies from one individual to another individual significantly. These differences can be in arterial dimension, complete absence of some vessels, point of bifurcation and even inclusion of additional duplicated vessels [9].

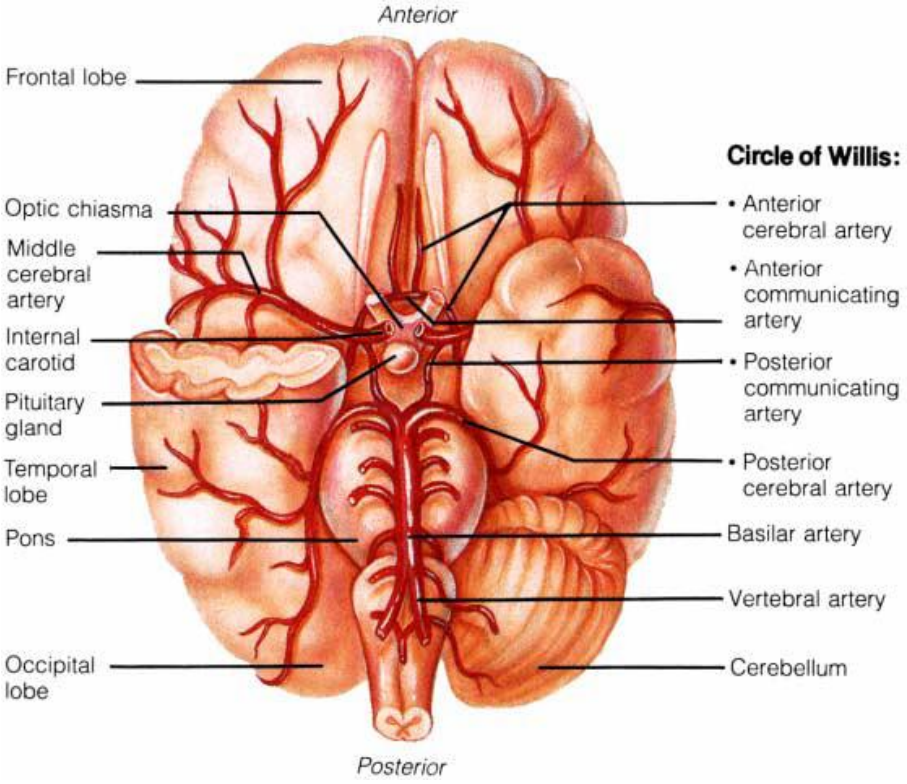

Figure 2-1 Major cerebral arteries that supply the human brain and the circle of Willis [10]

2.2.1 The carotid arteries

The left and right carotid arteries follow the same path through the soft tissues of the neck but with different origins. Both of the common carotid arteries divide to form an internal and external carotid artery; the internal carotid artery is responsible for supplying the blood to the brain while the external carotid artery supplies blood to the face, scalp and the neck. The internal carotid artery travels up into the skull from the behind of the eyes' orbit through the carotid foramen and joins the anterior part of the Circle of Willis. The internal carotid arteries contain barorepectors which are sensors that detect the blood pressure flowing through them. These sensors are located in a thickening of the arterial wall called the carotid sinus. The communication between baroreceptors themselves is done via the sinus nerves which are also responsible for regulating heart rate and strength of contraction. Under normal conditions, the blood flow through both of the left and right carotid arteries are the same and together they are responsible for 80% of the blood flow to the brain while the two vertebral arteries are responsible for the remaining 20%.

2.2.2 The Vertebral and Basilar arteries

The left and right vertebral arteries originate from the subclavian arteries and they enter the vertebral column at the level of the sixth vertebrae. They both then enter the skull through the foramen magnum at the top of the spine and then join together to form the basilar artery which itself terminates in the two posterior cerebral arteries of the circle of Willis. Several small arteries from the vertebral arteries and basilar arteries supply essential blood to the cerebellum, spinal chord and brain stem. Under normal conditions, just a little mixing between bloods in the communicating vessels occurs.

2.2.3 The cerebral arteries

The two hemispheres which form the human brain receive their blood supply entirely from the Circle of Willis. There are three major arteries that originate from the Circle of Willis to supply the blood to each hemisphere, conveniently named; anterior, middle and posterior cerebral arteries. Under normal circumstances, the left and right carotid artery supply the required blood to the left and right anterior and middle cerebral arteries respectively. The basilar arteries as mentioned above, supply the blood to the two posterior cerebral arteries. In other words under normal conditions the right and left carotid arteries supply the right and left lateral and anterior cortex respectively while the Basilar artery supply the required blood to the posterior cortex. Even though no communication between these three arteries is required, they are linked close to their origin, by the anterior communicating artery and each carotid artery is also linked to the corresponding posterior cerebral artery by a posterior communicating artery. As the result of the mentioned arteries and communicators the blood supply to the cerebral hemispheres is not exclusively dependent on just one vessel.

2.2.4 The middle cerebral artery

As mentioned above, the middle cerebral artery (MCA) is one the three major arteries that are responsible for the blood supply to the cerebrum[1]. The MCA is largest artery out of the three and is responsible for supplying a significant proportion of the lateral surface of the cerebral hemispheres such as: cortical regions controlling, auditory, and motor and speech activities. The cerebral blood flow is commonly measured by transcranial Doppler ultrasound (TCD) in the MCA which will be discussed in more details in 2.6 . The MCA is chosen not just because it is the largest vessel, but because it shows the least anatomical variation and also the initial segment of MCA, travels almost horizontally outwards, from the circle of Willis (Figure 2-1), for about $16\ mm$, with little tapering, feeding the main arteries that supply the centre of the brain. It is the fairly straight initial segment of the MCA is used to obtain the majority of TCD measurements [11].

2.3 Cerebral circulation

So far primarily the anatomy of cerebral circulation was discussed. In order to understand cerebral autoregulation it is necessary to look at the blood flow and its dynamics. The dynamics of the blood circulation involves the inter-relationships between blood pressure, blood flow, resistance and the control mechanism that regulate blood flow and blood pressure in the vessels, and which play a critical role in the functionality of the cerebral circulatory system.

2.3.1 Cerebrospinal fluid (CSF)

Cerebrospinal fluid (CSF) circulation exists intracranially in addition to cerebral blood circulation. The CSF is a clear, colourless liquid that fills the ventricles of the brain and the subarachnoid spaces [9]. The CSF supports the central nervous system against trauma. The brain weighs around $1500\ g$ in the air whilst this is only $50\ g$ when immersed in CSF. One of the other responsibilities of CSF is to remove waste products of neuronal metabolism, drugs and other substances which diffuse into the brain from the blood [12].

The brain inside the skull is incompressible and as the result of that the overall combined volume of the brain, CSF and intracranial blood must be maintained at a constant level. This means that if one of these three parameters increases, it is at the expense of other two components to be reduced according to Munro-Kellie hypothesis [13].

[1] The cerebrum with diencephalon, constitute the forebrain. It is the most superior (in human) region of the vertebrate central nervous system.

It has been reported that the rate of formation of the CSF is independent of short-term variation of intracranial pressure [14]. The CSF formation only slightly decreases from $0.35\,ml/min$ to $0.30\ ml/min$ when intracranial pressure (ICP) increases from less that $15\ mmHg$ to more than $25\ mmHg$ [14].

2.3.2 Blood pressure and blood flow

Blood pressure is the measurement of the pressure (force per unit area) that blood exerts on the walls of blood vessel walls. Blood flow can be described as the volume of blood that passes a specific point in a blood vessel at a certain point of time. The flow can be modelled using the pressure difference also known as perfusion pressure between two sections of the vessels. We expect the blood to flow from the point with high pressure (P_1) flows towards the points with low (with respect to P_1) pressure (P_2). The blood vessels have resistance (R) which is oppose the blood flow. The flow can now be mathematically expressed as (Darcy's law):

$$Flow = \frac{P_1 - P_2}{R} \tag{2.1}$$

For the case of the brain, the blood flow in the brain is driven by the difference between the arterial blood pressure (P_1) and the pressure in the skull (intra-cranial pressure[2] $- P_2$). The vascular resistance in the above equation is known as the cerebral vascular resistance (CVR) for the brain mechanisms. The blood flow resistance can be modelled using the Hagen-Poiseuille's law as below:

$$R = (\frac{vl}{r^4})(\frac{8}{\pi}) \tag{2.2}$$

where in the above equation v is the blood viscosity, l is the length of the vessel and r is the blood vessel radius. From the above equation it can be seen that the blood flow resistance is greatly related to the radius of the vessel (r^4) and proportional to the length of the blood vessel and the viscosity of the blood.

Each blood vessel has a critical closing pressure (CCP); the pressure below which the vessel collapse and blood flow through the vessel stops. This can happen under the conditions of shock.

2.3.3 Vascular mechanics

It is known that the blood vessels are distensible. It results in the fact that the width of a vessel depends on two factors: 1. Blood pressure 2. Tension in the wall. The radius of the vessel controls

[2] Elevation of the pressure in the cranium

the amount of tension in the wall in response to a given pressure drop. This principle is commonly known as Laplace's law.

$$T = P.r \qquad 2.3$$

where in above equation, T is the circumferential tension, P is the pressure difference between the inside and outside of the vessel and r is the vessel radius. There is an assumption in writing above equation that the vessel wall thickness is negligible with respect to the inner radius. However this is not the case when arteries or arterioles are studied as they have significantly thick walls with respect to internal radius. In this case the tension can be expressed by:

$$T = P_i r - P_o r_0 = P_i r - P_o(r + h) = \sigma h \qquad 2.4$$

where P_i, P_o, r and r_0 in above equation denote intravascular pressure, extravascular pressure, intravascular radius and extravascular radius respectively and σ is wall stress and $h = r_0 - r$ is wall thickness [15].

2.3.4 Intra-cranial pressure (ICP)

As mentioned in section 2.1 cerebral blood flow to the brain must be maintained in order for the brain to receive required oxygen and glucose and removal of 'waste 'products. This maintenance depends of a balance between the intra-cranial pressure (ICP) and arterial blood pressure, usually quantified by the mean arterial pressure ($MABP$) with the mean value calculated over each heart rate. The overall task of physiological regulation of ICP and CVR is to maintain a constant blood flow. Thus for example when blood pressure falls, physiological mechanisms attempt reduce CVF to maintain flow and prevent ischemia and conversely with an increase in MAP increase cerebrovascular resistance (CVR) to prevent excessive flow.

As mentioned before ICP is the pressure within the rigid skull. High ICP can cause internal or external herniation[3] of the brain, "distortion and pressure on cranial nerves and vital neurological centres [16]".

Inside the skull is the brain (80%), blood (12%) and cerebrospinal fluid (CSF) (8%) [10]. As mentioned before if there is an increase in the volume of either the brain or blood the normal initial response is a reduction in CSF volume within the skull. CSF is forced out into the spinal sac. Thus the pressure within the skull, ICP, is initially maintained. If the pathological process progresses with further increase in volume, venous blood and more CSF is forced out of the skull. So if the brain

[3] Deadly side effect of very high intracranial pressure that occurs when the brain shifts across structures within the skull.

enlarges (megalencephaly which may occur as the result of neurological problems such as: seizures or mental retardation), some of the blood or CSF inside the skull must escape to avoid a rise in pressure. If this process fails, a rapid increase in ICP from the normal range (5-13 $mmHg$) will occur [17, 18].

Non-invasive measurement of ICP, is very desirable but is only currently applicable to a newborn. Pressure changes within the cranium are transmitted through the open fontanelle of the neonate and can adequately reflect changes in ICP .

There have been researches to develop mathematical models to predict ICP non-invasively [19-21], however there has not been any clinical applicability as the ICP prediction is still poor as the result of changes in physiological conditions which lead to ICP changes.

2.3.5 Cerebral perfusion pressure (CPP)

Cerebral perfusion pressure (CPP) is defined as the difference between mean arterial and intra-cranial pressure.

$$CPP = MAP - ICP \tag{2.5}$$

The normal value for CPP is around $80\ mmHg$. If CPP falls below $50\ mmHg$, there is a good evidence of ischemia and reduced brain electrical activity ceases. It has been observed that inadequate CPP ($< 70\ mmHg$) is a major factor in the poor outcome of patients with raised ICP [22].

For the purpose of this project it is assumed that ICP is constant and ABP can be measured instead of CPP. The issues in measuring ICP are discussed in the section 2.3.4.

2.4 Autoregulation processes

The autoregulation system is one of the mechanisms that maintain the blood flow that is required for all the regions in the brain. The target flow is derived from a complex balance of metabolic requirements of the brain. The balance is not yet fully understood [16]. Without having any accurate information about the required blood flow [23] it is impossible to conclude if the autoregulation is functioning correctly or is impaired. A broad range of resting cerebral blood flow (38 to $75\ \frac{ml}{100g\ min}$) is found in the normal population [24]. Theoretically it may be possible to assess autoregulation by

its failure or success in keeping cerebral blood flow in this normal range. However in practice this is not appropriate because in extreme cases cerebral blood flow may go outside the normal region and it could be wrongly assumed that autoregulation has failed, where it is actually responding well to an abnormal blood or brain chemistry abnormality or perhaps the demand. It can be concluded that only measuring cerebral blood flow cannot tell us if cerebral autoregulation is working properly or not [25].

In order to understand the challenges behind autoregulation it is necessary that the mechanism of cerebral autoregulation is tested. The basic system is considered to have blood pressure as the input and cerebral blood flow as the output. It is assumed that an intact autoregulation would maintain the cerebral blood flow approximately constant during a change in the central arterial blood pressure, but it will not be able to maintain flow, if it is impaired. It can be concluded that if cerebral blood flow is changed when blood pressure changes then cerebral autoregulation is unreliable, unless this change in cerebral blood flow was provoked by another known reason, which is normally not the case. In such complex scenarios, it may not be possible to obtain a reliable estimate of cerebral autoregulation.

Before the mid of 1990's, most studies looked at what is now called static autoregulation. In static autoregulation, the steady state relationship between arterial blood pressure and cerebral blood flow is measured. Such studies were the only option, due to the lack of availability of continuous recordings of cerebral blood flow with high temporal resolution [26]. For these static measurements, a measurement of cerebral blood flow is obtained first at a constant baseline ABP and CBF, followed by another steady state measurement that is taken after the autoregulatory response to a manipulation of ABP has been completed [5].

Figure 2-1 shows the three stages associated with the measurement of the cerebral blood flow with respect to changes to arterial blood pressure in classic autoregulation, where the range of blood pressure and blood flow for a healthy volunteer during normal daily activities is shown. At very low and very high pressures where autoregulation is not active, cerebral blood flow will change with arterial blood pressure. At intermediate pressures there is however a plateau region where autoregulation is said to be active and changes in blood pressure will not greatly alter cerebral blood flow. This plateau region, in which the autoregulation is functioning correctly, is from about 50 to $150\ mmHg$. This range can change from patient to patient and is considerably higher in hypertensive patients.

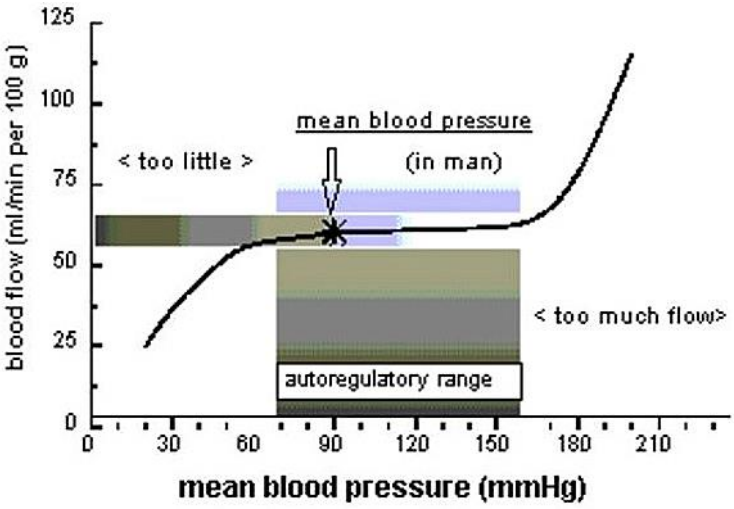

Figure 2-2 Relationship between Arterial Blood pressure and Cerebral blood Flow assuming classical autoregulation [27]

2.5 The importance and pathophysiology of cerebral autoregulation

Assessment of autoregulation plays a key role in diagnosis prognosis and monitoring cerebrovascular diseases clinically. Cerebral autoregulation is vital for assuring that the metabolic needs of the brain are maintained and protect the brain from ischemia due to decreased cerebral perfusion pressure. However this key mechanism can be disturbed, impaired or modified in several brain diseases or injuries. Good and early assessment of cerebral autoregulation can help clinical staff and doctors to monitor the development of brain conditions better and undertake any necessary treatment promptly.

It has been shown by Czosnyka *et al.* [28] that, patients whose cerebral autoregulation was severely impaired or disturbed during the first two days after a severe injury, are more likely to die. It has also been reported [11] that, cerebral autoregulation is asymmetric in the two hemispheres of the brain in patients with head-injuries with lateral brain contusions. The difference in side-to-side hemodynamic reserve of the injured brain can be taken as a fatal outcome following head injury and correlates with the side of contusion or brain expansion [11].

Cerebral autoregulation is a vulnerable mechanism which can deteriorate diffusely in addition to areas of acute or subactute cerebral lesions [29]. Paulson *et al.* [29] listed eight pathophysiological reasons which can lead to the impairment of cerebral autoregulation.

1. Hypertension
2. Diabetes Mellitus
3. Ischemic cerebrovascular diseases

4. Infections
5. Spreading migraine
6. Acute hypertensive encephalopathy
7. Intracranial tumours and other space-occupying lesions

As the result of the discussion here, the monitoring of cerebral autoregulation can be used to guide autoregulation therapy.

2.5.1 The mechanism of cerebral autoregulation

There are different numbers of mechanism that have been suggested to explain the nature of cerebral autoregulation. Three main hypotheses were raised: myogenic, metabolic and neurogenic mechanisms. It has been shown that cerebral autoregulation can be explained by either one of these mechanisms or a by their combinations [30].

The myogenic mechanism theory suggests that smooth muscle of blood vessels reacts to the stretching of the muscle by opening ion channels and leading to muscle contraction, is responsible to changes in transmural pressure [30, 31]. It has been shown that the response of autoregulation is initially within few seconds after changes in transmural pressure and fully completed within $15 - 30$ sec, and is consistent with a myogenic response [29].

A tight coupling between O_2 metabolic supply and brain's demand can explained cerebral autoregulation, or at least part of it [32, 33]. There are many chemical factors that can cause vasodilation

1. Decrease in O_2 or nutrient levels
2. Increase in CO_2 level locally
3. Decrease in pH
4. Increase in adenosine, lactic acid

However the role of these substances in the coupling between flow and metabolism is still unclear [29]. It is known that hypercapnia causes an increase in cerebral blood flow globally. It has been also reported [34]. Although the speed of the autoregulatory response has been linked with the myogenic hypothesis, Paulson *et al.* [29] reported that flow changes may occur essentially in response to metabolic changes.

The studies done on the effect of a neurogenic mechanism on cerebral autoregulation is very diverse and controversial [35, 36]. There are many factors that make it very difficult to reach a comprehensive understanding of cerebral blood flow neurogenic control system. Ursino *et al.* [15] summarized these factors as follow

1. The neurogenic mechanism can be easily be damaged during in vivo experiments
2. We don't have a complete knowledge of nerve supply to cerebral vessels
3. It is difficult to reach nerves that supply cerebral vessels

However the results of wide research on neurogenic control system support the neurogenic hypothesis that autonomic neural control is likely to have a significant effect in cerebral autoregulation [35].

2.6 Technical and experimental techniques for assessing static & dynamic autoregulation

In this section the methods for assessing autoregulation are discussed. As mentioned before, in general, most cerebral autoregulation experiments attempt to measure the regulation of blood flow in the brain by changing the blood pressure in different ways. The reason behind changing blood pressure instead of manipulating the metabolic requirement is that changes in blood pressure are easier to process, control and monitor [37] and also manipulating the metabolic rate is not clinically applicable. Throughout this thesis these changes in blood pressure to assess blood flow regulation are studied.

Experiments to assess cerebral autoregulation can be categorized in to two forms, *static* and *dynamic.* In section 3.1, experiments to assess static autoregulation are discussed. In section 3.2 the methods to measure blood flow and blood pressure in order to assess dynamic autoregulation are presented.

System identification methods to assess dynamic cerebral autoregulation are studied in the following section.

2.7 Static autoregulation experiments

Up to mid1990's, most of the studies that were carried out on cerebral autoregulation were performed under 'steady-state' condition. This was due to the fact that, there was no method of continuous recordings of cerebral blood flow with high temporal resolution.

Cerebral autoregulation (CA), as mentioned previously refers, to the ability of the brain to maintain constant blood flow regardless of the changes in cerebral perfusion pressure (CPP) [3, 29, 38, 39]. Before the development of transcranial Doppler ultrasound (section 3.2.1), evaluation of CA was carried out under steady-state condition. In order to measure autoregulation discussed in section 2.4, cerebral blood flow (CBF) is first measured at a constant baseline value of arterial blood pressure (ABP) and constant CBF. After that another (steady-state) measurement is carried out with a change in ABP provoked in some ways and maintained at a new level for a while (around $10-15$ minutes [40, 41]), and then blood flow is recorded [5].

Most of the experiments carried out using static autoregulation require very time-consuming and/or invasive procedures. This is due to the time needed to maintain the imposed changes on the blood pressure in order for the blood flow to be measured. Most of the procedures carried out in static autoregulation used Xenon [40, 42] or krypton radio-isotope [40, 42] and manipulation of the blood pressure using vasoactive medications [43]. For example the time needed for measuring blood flow after manipulation of blood pressure for Xenon is around 15 minutes. Other methods have been proposed in order to change the mean ABP are: head tilting [44] and lower body negative pressure [18, 45] which did not attract much attention as they could not be carried out for period of long time which is the requirement for static autoregulation.

From the definition of cerebral autoregulation, CPP is required to be measured, but normally the measurement of ABP is used. This is based on the assumption that any change in ABP would be proportional to the change in CPP. This is a valid assumption when the intracranial pressure (ICP) can be considered to be constant. This assumption is more questionable if the patient that is treated has raised ICP, for instance head injury or hydrocephalus [46].

The main disadvantage of static autoregulation is the constrained number of experiments that can be performed on each individual. Most of the works reported in this area are based on two measurements, one before and one after the inducement of changes ABP. This makes it difficult to predict the shape of the autoregulatory response curve for an individual. Some researchers [32, 40], in order to overcome this problem, have accumulated the results for different individuals with the

assumption that the autoregulation for “normal disease-free” subjects have identical autoregulation curves [32], however in different and repeated studies it has been clearly shown that this is not the case and it is vital that each individual should be considered based on their own data [20, 47].

Static autoregulation has some difficulties and problems which may be summarized as follows:

- It is difficult to assess steady state ABP alterations in humans over a large range while keeping other parameters stable [5]. It is common to take two measurements per subject, one just before and one after the induced change in ABP which makes it impossible to measure the shape of autoregulation for individuals.
- In order to capture large spontaneous changes in mean ABP without externally inducing a change in ABP (depending on spontaneous variations) very large intervals e.g. 12 hours measurements are required. However over such large time intervals, it is hard to keep other variables such as P_{ETCO_2} and P_{O_2} constant.
- In order to cancel out the effects of the individual physiological characteristics of volunteer, for the pooled data method, many subjects need to be involved in the measurements [32].
- Static autoregulation is unable to show changes in real time, due to the measuring techniques [16].

As the results of the limitation of static autoregulation, further work in this thesis is concentrated on dynamic autoregulation methods.

2.8 Data collection and measurement Techniques for dynamic autoregulation

In this section some of the most used methods for collecting cerebral blood flow velocity and blood pressure are discussed.

2.8.1 Measurement of cerebral blood flow using Transcranial Doppler sonography

The use of Doppler ultrasound as a non-invasive technique to estimate blood flow velocity was first described in by Satomura and Kaneko [48] in 1960 who measured blood flow velocity by recording the shifted frequency of ultrasound reflected off red blood cells. However it was in the early 1980's when ultrasound devices were developed sufficiently to allow penetration through the skull to carry out relatively quick non-invasive measurements of the blood flow velocity within the intracranial circulation [16]. In order to achieve bone penetration low frequency ultrasound is usually used ($2\ MHz$ is conventional). At low frequencies 1 to $2\ MHz$, the attenuation in bone and soft tissues is considerably less than at higher frequencies. The thickness of the skull varies between regions, and the bone of the temporal region is relatively thin, which makes it an ideal region for the penetration of the ultrasound [16].

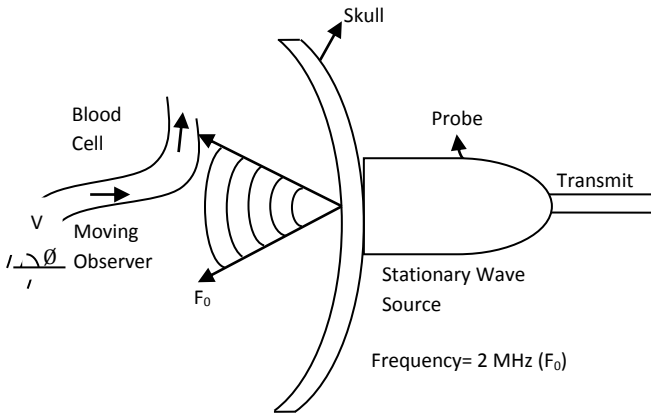

Figure 2-3 Schematic diagram of transcranial Doppler ultrasonography [1]

In the work done by Satomura and Kaneko *et al.* [48] the frequencies used, were in the range of $1\ MHz$ and $20\ MHz$. One transducer transmits and receives the ultrasound beam, and in Transcranial Doppler sonography (TCD) this transducer is nearly always stationary. The moving blood cells back-scatter the transmitted beam and the reflected waves indicate the flow velocity of the blood [16]. These echoes return with a wide range of Doppler-shifted frequencies.

In order to understand the process of the Doppler ultrasound, consider a single blood cell travelling with velocity v as shown in Figure 2-3. The relative speed of the transmitted waveform after hitting the cell is: $c - |v| \cos \phi$, where c is the speed of sound in the medium, ϕ is the angle between the blood cell velocity and the ultrasound wave as shown in Figure 2-3. By using the mentioned equation $c - |v| \cos \phi$, the frequency of the ultrasound hitting the blood cell, f_b say, is [16]:

$$f_b = \frac{c}{c - |v| \cos \phi} f_t \qquad 2.6$$

where f_t is the transmitted frequency. By assuming that there is some reflection by the blood cell, the frequency of the ultrasound reflected back off the blood cell towards the transducer is f_b. In order to calculate the speed of the reflected wave, it has to be considered that the cell has moved a distance of $|v| \cos \phi / f_b$ whilst transmitting one whole wavelength, and as the result of that the relative speed of the reflected waves is $c + |v| \cos \phi$ and the resulting wave frequency received by the transducer (f_r) will be shifted further. By further assuming that there is not full absorption by the tissue or bone, we get some reflected waveform, the received frequency,f_r can be written as:

$$f_r = \frac{c + |v| \cos \phi}{c} f_b \qquad 2.7$$

By replacing eq.2.6 in eq.2.7 we get:

$$f_r = \frac{c + |v| \cos \phi}{c - |v| \cos \phi} f_t \qquad 2.8$$

Since the speed of sound through tissue is $c = 1500\, ms^{-1}$ and the flow velocity in the middle cerebral artery (MCA) is around $0.5\, ms^{-1}$, and $f_d = f_r - f_t$, the equation below gives a good approximation.

$$f_d = \frac{2|v| \cos \phi}{c} f_t \qquad 2.9$$

The above equation gives us a very easy formula to calculate the velocity of the single blood cell just from ϕ ,c, f_b and f_t [1].

In TCD, more than just a single velocity is measured, as the velocity varies across an artery. Usually the whole cross-section of an arterial segment is captured in a single measurement, and some of its branches may be included. This kind of measurement results in having many reflected waves from many cells which contain a mixture of Doppler shifts [16]. Power Spectral distribution of velocities within the target volume is determined by analysing of phase difference between 100 or more

consecutive pulses [16]. The normal pulse repetition frequency[4] is in the order of $10\ kHz$. This signal power is directly proportional to the number of cells travelling at that velocity.

The blood flow which is the required parameter in term of the cerebral autoregulation is proportional to the mean velocity across the artery, if the radius of the vessel is not being monitored and the form of the velocity profile does not change. TCD can enable the measurement of a distribution of blood velocities which means it has the capability to provide the mean velocity.

In practise the mean velocity cannot be accurately and reliably measured. In order to obtain a good accuracy in calculating the blood velocity in clinical measurements, set of conditions needs to be satisfied, such as; the angle between the transducer and the vessel being interrogated is less that 15^o [16], patients should not move and other conditions also stay unchanged. As the result of this issue in most applications maximum velocity (v_{max}) which corresponds to the largest Doppler shift is considered as a more reliable measurement as it is not affected by the assumption made for the mean blood velocity. This maximum velocity corresponds to the blood velocity at the centreline of the major vessel in the sample volume [16].

The TCD measurement explained briefly above has led to the "dynamic" assessment of autoregulation, which consists of real-time measurement of both arterial blood pressure and cerebral blood flow velocity, usually in the MCA as well as arterial blood pressure. Information about the time delay of the control mechanism and the rate of regulation can be extracted from real-time measurement, which can help researchers gain more insight into dynamic autoregulation and the parameters involved with it.

2.8.2 Measurement of blood pressure

It is vital to be able to measure blood pressure accurately in order to assess cerebral autoregulation. The 'gold standard' technique is an invasive approach, which is able to direct hydraulic coupling of the vessel to a pressure transducer, or even better, has a small tip pressure transducer at the end of the catheter inside the blood vessel [49]. The standard procedure to measure the blood pressure is to use a strain gauge pressure transducer, connected to the vessel via a saline-filled rigid-walled catheter. This method can be used to collect the blood pressure in many different vessels including the chambers of the heart, the pulmonary artery as well as the more easily accessible venous and arterial systems. The short rigid-walled catheters provide an excellent frequency response which

[4] Number of pulses transmitted per second

enables the capture of blood pressure fluctuations throughout the cardiac cycle[5]. The main disadvantage of this method is obviously its invasive nature.

Invasive blood pressure measurements such as brachial artery cannulation [50, 51] provide excellent recordings but they are uncomfortable and involve a risks for the subjects. As a result of these disadvantages, non-invasive methods are preferred for measurements on volunteers. The most standard non-invasive method to measure blood pressure is using an arm-cuff. The arm-cuff is first inflated to a pressure above the expected systolic value to occlude flow in the artery. After that the cuff pressure is gradually reduced while an assessment of the blood pressure is made. This is usually done by listening to the Korotkoff[6] sounds. The Arm-cuff provides us with reasonable measurement of the blood pressure that are sufficiently accurate for clinical purposes but measurement can only be made once every about $30\ secs$ [5] which is not fast enough to capture rapid fluctuations of the blood pressure when dynamic assessment of cerebral autoregulation is needed.

The non-invasive measurement of the blood pressure are not fast enough to be used to assess dynamic cerebral autoregulation but can be used in static assessment of cerebral autoregulation with pharmaceutical manipulation of blood pressure. As a result of that most of the studies done in this field [5, 16, 32, 50, 52-54] have used Infrared plethysmogpragy (Finapres) to measure the blood pressure because they ensure accurate results.

2.8.2.1 Infrared plethysmography

This method of continuous assessment of the arterial blood pressure was first introduced in 1976 by Penaz *et al.* [55]. This method uses a small cuff on the finger of the subject which can be inflated through the normal range of blood pressures. The cuff contains an infrared transmitter which is placed on one side of the finger and a receiver on the other side. The infrared light transmitted through the finger is measured. This transmission is found to oscillate with the cardiac cycle. It has been found that the cuff pressure with the largest amplitude oscillations corresponds to the mean finger arterial pressure. The mean value of the transmitted light is measured which corresponds to the mean blood pressure. This is done as a set point for calibration. Once the calibration process is finished, a rapid and continuous inflation and deflation of the cuff is applied through servo control feedback, in order to maintain the transmitted light at a constant level. With the help of the above

[5] Refers to any of the events related to the flow or pressure of blood that occurs from the beginning of one heartbeat to the beginning of the next

[6] Sounds that medical personnel listen for when they are taking blood pressure using a non-invasive procedure

process the arterial pressure waveform can be measured as it is the same as the cuff pressure applied.

The method described is known as the volume clamp technique and is the basis of a commonly used device called the Finapres. Many studies have looked at the accuracy of the blood pressure measured by the Finapres, and the results from all these studies agree that under normal circumstances, there is a good agreement with invasive arterial pressure measurements [23, 54, 56]. However the calibration process is not always accurate, so in order to overcome this shortage the calibration process is usually done every 70 heart beats [57] which is approximately every one minute. The recalibration process gives an unwanted artefact during the assessment of autoregulation but can be turned off. One further concern with using the Finapres for measurement of blood pressure is the unknown influence of peripheral vasoaction in the finger being measured, as it can increase the arterial volume and reduce the transmission of the infrared light through the finger. This can be misinterpreted by the Finapres as an increase in blood pressure, which would result in false trends in the blood pressure recorded by the Finapres.

A completely different method for continuous non-invasive measurement of the arterial pressure is the use of tonometry [58, 59], which uses a pressure transducer applied to the skin and continuously presses and deflates an artery on to a bone surface. A comparison of autoregulation estimated by these two methods has been carried out by Birch *et al.* [60] and shown that the difference between the models is insensitive to peripheral vasoactivity mediated by local endothelial or myogenic mechanisms.

2.9 Assessment of dynamic autoregulation using system identification methods

The dynamic measures of autoregulation focus on the transient response of CBF to the changes of of ICP on CPP (or alternatively ABP when ICP is not available) as cerebral autoregulation acts through vasomotor effectors that control cerebrovascular resistance (CVR) [38]. Active autoregulation generates a rapid response of CVR and regulates CBF towards a baseline level, whereas impaired autoregulation results in a passive response of CBF following the changes of blood pressure. The very first time that the transient response was investigated was in animal studies [61]. After that the first transient response in humans was reported in humans was during the Valsalva manoeuvre which causes rapid changes of ABP [62]. The most common method for inducing a sudden drop of ABP to study dynamic autoregulation was first introduced by Aaslid *et al.* in 1989 [63], and is known as the thigh cuff experiment.

2.9.1 Thigh cuff and Lower Body Negative Pressure ($LBNP$) experiments

As mentioned above Aaslid *et al.* [63] developed a method to induce step changes in arterial blood pressure (ABP) through the deflation of thigh cuffs. In this method the thigh cuffs around both legs are inflated which causes the blood flow in the legs to decrease and after 2 minutes the cuffs are released. As the result of the deflation, the ABP is reduced by about $20\ mmHg$ [3], which is equivalent to a decrease in ABP of around 20% from its baseline. Aaslid *et al.* [63] showed that the step decrease in pressure last for up to 7 seconds before it starts to recover, and takes about 15 to 20 seconds before returning back to its base level. Aaslid *et al.* [63] also showed that in the case of intact cerebral autoregulation, the blood flow velocity recovers to its original level, in about 8 seconds, which is much faster compared to the restoration of ABP. He also observed that in some cases an overshoot in the maximum velocity, of up to 10% above the baseline value, 8 to 12 seconds after the drop in blood pressure.

Another indication of the subject's autoregulatory capacity introduced by Aaslid was the half maximal response time $t_{1/2}$. The half maximal response time was defined as the time taken for the percentage drop in maximum blood flow velocity to be reduced by half. Aaslid *et al.* [26] found that the average value of $t_{1/2}$ for healthy subjects was 3.4 seconds.

Aaslid *et al.* [63] compared the assessment of dynamic autoregulation using the thigh cuff technique with static assessment analysed from a $20\,mmHg$ drug induced rise in ABP, in 10 normal volunteers during normocapnia, hypocapnia and hypercapnia. He suggested that dynamic assessment of cerebral autoregulation has more value since more aspects of autoregulation capacity such as delay and rate of regulation can be extracted from it, whilst static autoregulation can just show the effectiveness of the autoregulation process.

Since the introduction of the thigh cuff test, dynamic autoregulation has attracted much of attention amongst researchers, and extensive studies have been carried out in this area. The reasons for the increasing studies of dynamic autoregulation can be summarized as:

- Transcranial Doppler ultrasonography (TCD) and servo-controlled finger photoplethysmography (Finapres) have enabled the investigation of the relationship between ABP and $CBFV$ of the cerebral circulation as they can be applied noninvasively and can offer very high temporal resolution (< 0.1 seconds for TCD to monitor changes in CBF [16])
- Dynamic AR has the ability to reduce the effect of other parameters such as P_{ETCO_2} and mental activities over short periods of time required for the test.
- Dynamic AR can be carried out safely and repeatedly and avoids major change in ABP remaining within the normal AR control range [16].

As mentioned above, the thigh cuff experiment introduced by Aaslid *et al.* [3] induces a step decrease in BP by rapid deflation of cuffs around both thighs, following an inflation for about 2 minutes.

Another method to reduce BP is lower body negative pressure ($LBNP$) introduced by Schmidt *et al.* [34]. The mechanism behind this method is that if the atmospheric pressure around the lower body (enclosed in a sealed box) is decreased. During the initial stage the effective peripheral vascular resistance of the lower body is lowered and flow to the lower limbs increases causing a drop in central arterial pressure. After this initial stage, it would result in a reduction of extravascular pressure, which itself results in dilation of veins and lowered vascular resistance, resulting in increased in-flow to the lower limbs [64]. Sinusoidal $LBNP$ has been used to produce a periodic variation in blood pressure and has shown to provide a repeatable and controllable stimulus for assessment of cerebral autoregulation [65].

Both the thigh cuff and the lower body negative pressure techniques have been developed to be used in patients in the supine position. A major difficulty in using the thigh cuff method is that it can

be painful [66] and it is not the ideal method for elderly subjects. The discomfort is an issue for lower body negative pressure also, and it cannot be applied in obese subjects. As a results of that these two methods cannot readily be used to assess dynamic cerebral autoregulation (dCA) in elderly patients, and alternative methods to induce oscillations in ABP are needed.

Other proposed methods for a step decrease in blood pressure are placing a hand in iced water or sustained hand-grip, which stimulates sympathetic efferent pathways [17, 67]. But the $CBFV$ response to these changes is diverse.

One of the easiest ways to induce changes in BP to assess dCA is the sit-to-stand procedure. The reduction in BP and decreased in total peripheral resistance upon standing is presumably caused by cardiopulmonary baroreflex mechanisms [7][68]. The advantage of this method is that, it is a useful and feasible method to test dCA in elderly subjects and benefits from being realistic, as it reflects a physiologic challenge that occurs in daily life.

All the methods mentioned above (apart from sinusoidal ($LBNP$)) provide a single-step decrease in the blood pressure and create a single-step challenge in cerebral hemodynamics. An alternative method is creating periodic oscillation of ABP and study the response of CBFV. This approach was first introduced by Birch *et al.* and Diehl *et al.* [65, 69]. Diehl *et al.* [69] used periodic breathing with controlled the frequency of ABP oscillation at $0.1\ Hz$ (6 breaths per minute), on the other hand periodic squatting with oscillation rate of ABP at $0.05\ Hz$ was used by Birch *et al.* [65]. The results from both above studies provided the same information regarding the oscillation of $CBFV$ giving significant phase lead over the changes of ABP, with normal AR. Birch *et al.* [65] reported a phase-lead of 46 ± 14^o at $0.05\ Hz$ and Diehl *et al.* [69] reported a phase-lead of 70.5 ± 29.5^o at $0.1\ Hz$. Both of the mentioned studies agree on phase-lead reduction when autoregulation is impaired. This phase-lead has since been become one of the most important measures of cerebral autoregulation as will be discussed in section 2.11.2.

Other methods that employed technique of periodic oscillation in BP to produce almost sinusoidal oscillation are pressure and oscillatory thigh cuff inflation and deflation [70].

Apart from the methods mentioned above, humans have spontaneous ongoing BP oscillation during their normal daily and nightly activities that vary from 0.02 to $0.4\ Hz$ without the need of external induced BP changes. It has been shown that if spectral analysis of BP over a day is carried out three different frequency bands are distinguishable: the first band at around the respiratory frequency with 12 peaks per minute ($0.2\ Hz$ to $0.4\ Hz$, the high frequency region); the second band due to

[7] One of the body's homeostatic mechanism for maintaining blood pressure

variations in vasomotor tone with 6 cycles per minute (the mid-frequency region, Mayer waves at $0.1\ Hz$); the third band whose cause is still not very well understood with 1 cycle per minute (the low-frequency region, 0.02 to $0.07\ Hz$) [71, 72]. It can be concluded that spontaneous fluctuation of BP and $CBFV$ respectively can be very useful for assessing dCA and form the basis for the easiest method for assessing of dCA, as it does not require externally imposed alteration in the BP, and can thus be used in a clinical setting.

2.10 Modeling of dynamic cerebral autoregulation

In the above section possible methods to create change in BP were discussed. After inducing this change, the relationship between the BP and CBF has to be modelled. In this section the most common and well known methods in this area are presented. In this section all the methods assume that linearity exists between ABP and CBF. The linear modelling of dynamic CA (dCA) can be divided into three different categories: grading autoregulation, time domain analysis, and frequency domain analysis. The common point of all these three categories is that they are all black-box models. In this section some of the most well-known methods in these areas are briefly explained.

In the study of dCA, the system can be assumed as a control system, and the response of $CBFV$ is analysed when a step change or spontaneous fluctuations or induced ongoing in ABP occur. This system can be considered as a system with ABP as the input variable and CBFV as the output variable [73]. By having such a model, the system transfer function and time- and frequency-domain characteristics of CA can be studied (section 2.11.2). Giller *et al.* [73] was the first person to employ the spontaneous fluctuations of ABP and $CBFV$ as the system input and output in order to develop the transfer function of the cerebral autoregulation. In his attempt, the spontaneous data of ABP and $CBFV$ were used to estimate the amplitude, gain of frequency response and coherence, but not the phase of the frequency response. Giller *et al.* [73] showed that the coherence obtains higher values when the autoregulation is impaired compared with healthy subjects (intact autoregulation), indicating that $CBFV$ follows the fluctuations of ABP linearly (passively) with the lack of blood flow control.

In 1995 Tiecks *et al.* [5] devised a methodology using the alteration in cerebrovascular resistance index ($CVRi = MCA/CBFV$) in relation to the change in BP during the thigh cuff manoeuvres. This method used a second order parametric model in order to describe the response of $CBFV$ using 10 pre-defined levels of autoregulation thus defining the autoregulatory index (ARI). In this model ARI of 0 indicates that $CBFV$ passively follows BP (absence of AR) and ARI of 9 indicates that $CBFV$ recovers much faster than BP following a step change in BP. This method has been used as a

starting point for other research that treats cerebral autoregulation as a “black box”, tries to model the system mathematically and identify the coefficients of this mathematical model in order to extract useful information from the time, frequency, impulse and step responses of the identified system [32, 74, 75].

Czosnyka *et al.* [28] used spontaneous variations of ABP and $CBFV$, in order to assess cerebral AR continuously. In this method Pearson’s correlation coefficient (called the index of autoregulation, Mx) between ABP and $CBFV$ in patients with head injury was used. In this study negative and zero correlation coefficients indicate active blood flow control in the brain [76].

In the next section, some of the most common methods for modelling cerebral autoregulation mentioned above are looked at.

2.11 Univariate Ceberal autoregulation models

In this section assessment of autoregulation based on filtering the data and not concentrating on its physiological aspect are studied. Tiecks model nonparametric approaches (coherence, spectra analysis and transfer function) are shown in the following sections.

2.11.1 Tiecks model

Tiecks *et al.* [5] introduced the first model in order to describe the response of $CBFV$ with respect to a pure step change in ABP, to assess the dynamics of cerebral autoregulation In this method a simple, second-order linear differential equation which can be expressed in the form of a state-space model was used to describe the relationship between cerebral blood pressure as the input and cerebral blood flow velocity as the output of this black box model.

Figure 2-4 illustrates the Tiecks model where a sudden drop in blood pressure is generated and the response of the blood flow has been shown for 10 different autoregulation levels with step wise drop of ABP of 10% at $t = 0$ for each step. From top to bottom; $ARI = 9$ denotes "perfect" autoregulation and 0 denotes "absence" of autoregulation or in other words the autoregulation mechanism is completely abolished.

In this state space model state variables $x1$ and $x2$ which were assumed to be equal to 0 initially and after the step change in ABP, the equations are solved in steps of $100\,ms$ (sampling rate, $f = 10\,Hz$). The model can be expressed as below:

$$dP = (MABP - iABP)/(cABP - CCP) \quad 2.10$$

$$x2 = x2 + (x1 - 2D.x2)/(f.T) \quad 2.11$$

$$x1 = x1 + (dP - x2)/(f.T) \quad 2.12$$

$$MCAV = iMCAV.(1 + dP - k.x2) \quad 2.13$$

where dP is the normalized change in mean ABP ($MABP$), $iABP$ is the initial $MABP$, CCP is the critical closing pressure, f is the sampling frequency and $iMCAV$ is the initial $MCAV$ (before the sudden drop). T, D and K indicate time constant, damping factor and autoregulation dynamic gain. These parameters are related to the dynamic autoregulatory index (ARI) [5]. In order to work with this model, for each patient or volunteer the step response of the $CBFV$ is estimated by finding the best-fit step-response using a correlation criterion for that patient. By running the ABP with different combinations of parameters (T, D and K as can be seen in Table 2.1) through the Tiecks model, and simulating $CBFV$ and comparing this with the measured $CBFV$, the autoregulatory index

(ARI) can be estimated. These parameters were related to the dynamic autoregulatory index and to the dynamic rate of regulation ($dRoR$) as shown by Aaslid *et al.* [16] as:

$$RoR = \frac{dCVR}{dt}.\frac{1}{CVR_{baseline}}.\frac{ABP_{baseline}}{\Delta ABP} \qquad 2.14$$

where in above equation CVR is the cerebrovascular resistance which can be calculated using eq.2.1. 'Baseline' in above equation refers to the values before the thigh cuff deflation. The RoR lacks robustness as it only depends on two measured values of ABP and mean cerebral artery velocity ($MCAV$).

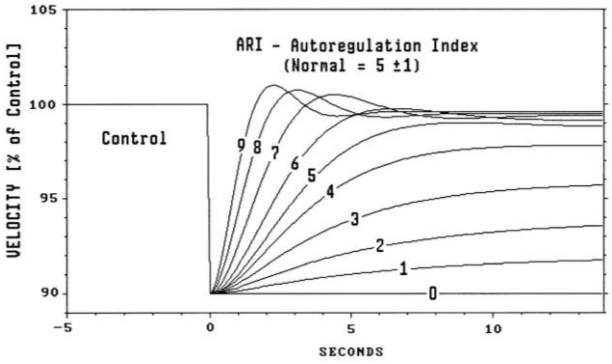

Figure 2-4 Responses of ceberal Autoregulation model to a step change in blood pressure according to the model adopted from [5]

ARI	***ROR***	***K***	***T***	***D***
0	0 ($No\ autoregulation$)	0	2.00	0.00
1	2.5	0.20	2.00	1.60
2	5.0	0.40	2.00	1.50
3	10.0	0.60	2.00	1.15
4	15.0	0.80	2.00	0.90
5	20.0 ("$Normal$" $Autoregulation$)	0.90	1.90	0.75
6	30.0	0.94	1.60	0.65
7	40.0	0.96	1.20	0.55
8	60.0	0.97	0.87	0.52
9	80.0($Fastest\ Autoregulation$)	0.98	0.65	0.50

Table 2.1 Comparison of Autoregulation Index to rate of regulation, $dROR$ is the dynamic rate of regulation

2.11.2 Nonparametric methods using correlation, spectral and transfer function analysis

Over the years, the main tool for analysing the recorded data from spontaneous ABP and $CBFV$ fluctuation and $CBFV$ is frequency domain analysis. Frequency domain analysis of cerebral autoregulation was first devised by Giller *et al.* [73]. In his test, he measured the data over the intervals of more than 30 seconds. His experiment should be considered as an assessment of static autoregulation as he investigated the effects of blood pressure oscillations with periods of around one minutes. Giller *et al.* [73] used the coherence γ between pressure and velocity as :

$$\gamma = \frac{G_{pv}(f)}{\sqrt{G_{pp}(f)G_{vv}(f)}} \quad 2.15$$

where $G_{pv}(f)$ is the cross-spectrum between pressure and velocity, and $G_{pp}(f)$ and $G_{vv}(f)$ are the squared auto-spectra of pressure and velocity respectively. Giller *et al.* [73] suggested that for healthy subjects the coherence is less than 0.25 and this value increased to 77% in the patients with subarachnoid hemorrhage. The author also illustrated that low coherence does not always imply effective autoregulation as it depends on the form of the ABP present at the time. This means that for example if the ABP of one patient does not vary at a given frequency and as the result of that the coherence is low, it would not be possible to predict how efficient blood flow mechanism would be for another experiment on the same subject.

Many works have been carried out on the frequency domain analysis of cerebral autoregulation based on the study of Giller (Kuo *et al.* [77], Diehl *et al.* [78], Panerai *et al.* [32]). In these works, the authors investigated AR via the transfer function $H(f)$ between ABP and $CBFV$ as:

$$\bar{F}(f) = H(f)\bar{P}(f) \quad 2.16$$

Where $\bar{F}(f)$ and $\bar{P}(f)$ are the Fourier transform of the flow $f(t)$ and $p(t)$ respectively. In the above equation the transfer function can be obtained from the cross-spectrum and auto (power) spectrum between pressure and velocity introduced above using the recorded data, as:

$$H(f) = \frac{G_{pv}(f)}{G_{pp}(f)} \quad 2.17$$

By using the equations above the transfer function can be rewritten as:

$$\gamma = H(f)\sqrt{\frac{G_{pp}(f)}{G_{vv}(f)}} \quad 2.18$$

The above equation relates coherence and transfer function. The modulus/phase parts of the complex transfer function are as below:

$$|H(f)| = [H_R(f)^2 + H_I(f)^2]^{1/2} \quad 2.19$$

$$\phi(f) = tan^{-1}\left[\frac{H_I(f)}{H_R(f)}\right] \quad 2.20$$

Where $|H(f)|$ is the gain (modulus) of the transfer function or frequency response and $\phi(f)$ is the phase of the transfer function. In the above equation subscripts I and R indicates the imaginary and real parts of $H(f)$. These two parameters describe the relative amplitude and time relationship between the alteration in ABP and $CBFV$ over a specified frequency range [79].

By using spectral analysis of cerebral blood flow, Kuo *et al.* [77] identified three different frequency ranges for spontaneous fluctuations, which are similar to the three frequency ranges introduced first by Parati *et al.* [80]. These ranges are: very low frequency (VLF,$0.0016 < f < 0.04\ Hz$); assumed to be due to a synchronisation with B-wave[8] fluctuations in ICP, low frequency (LF, $0.04 < f < 0.15\ Hz$), as the results of the VSM activity due to baroreflex, i.e. nerve stimulation of vessels and heart and high frequency (HF, $0.15 < f < 0.4\ Hz$), due to the respiratory cycle. Kuo *et al.* [77] showed that coherence between MCA and ABP are high for LF and HF regions, but low coherence was reported in VLF oscillations. The low coherence in VLF fluctuations tells us that there is little linear relation between ABP and MCA velocity, and as the result of that the true mechanism behind autoregulation that produces fluctuation in velocity in this range is in question. For the reason mentioned above Kuo *et al.* [77] and Diehl *et al.* [78] used the frequency range of $0.04 < f < 0.4\ Hz$ for their calculations. Kuo *et al.* [77] found $\phi(f) = 50^o$ while the phase found by Diehl *et al.* [78] was 70.5 ± 29.5^o both at LF fluctuation (especially $f = 0.1\ Hz$; $P1$). Both authors observed a significant drop in the phase in the HF fluctuation range; 10^o and 18^o found by Kuo *et al.* [77] and Diehl *et al.* [78] respectively at $0.2\ Hz$. They both also observed that the phase falls to almost zero in the HF range and they suggested that this is because autregulation is not active for high frequencies. They both suggested that the reduction of phase for high frequencies can be used to model the autoregulation as a high pass filter. In terms of gain Kuo *et al.* [77] did not comment on this parameter as he did not find a significant relationship between frequency and $|H(f)|$ where increase in $|H(f)|$ was expected with increase in frequency. For instance, they both found approximately the same results for gain such as $|H(f)| = 1.9$ for $f = 0.1\ Hz$, and $|H(f)| = 1.4$ for $f = 0.2\ Hz$ which contradict the high-pass filter criterion, which is due to the dynamic "input impedance principle which states that vessel resistance decrease as frequency increases even if active autoregulation is present" [78].

[8] Slow and rhythmic oscillations in intracranial pressure (ICP)

One of the important factors in assessment of cerebral autoregulation is "false autoregulation". False autoregulation refers to an "alteration of autoregulation in which the apparent maintenance of a constant cerebral blood flow (CBF) when increasing cerebral perfusion pressure (CPP) is due to an increase in brain tissue pressure" [81]. False autoregulation is frequently found in patients after a severe head injury. These patients do not benefit from an increase in $MABP$ to obtain a better CPP as CBF is not modified or may even be reduced [81].

Panerai *et al.* [52] also looked at the frequency domain analysis of cerebral autoregulation on both pre-mature newborns and adult volunteers respectively. The gain $|H(f)|$ showed that for both of these groups (pre-mature newborns and adult volunteers) the gain increased with respect to the increase in frequency. For instance, in the case of adult volunteers $|H(f)|$ rose from 1 at $f = 0\ Hz$ to 1.7 at $f = 0.2\ Hz$ and stayed almost constant up to the point of $f = 0.35\ Hz$ where it again increased to $|H(f)| = 2$ at around $f = 0.48\ Hz$. The results for the phase for the adults volunteers agrees with the results found by Diehl *et al.* [78] and Kuo *et al.* [77] whereas it decreased giving $\phi = 40^o$ for $f < 0.15\ Hz$ and it dropped to 30^o and 0^o for $f = 0.2\ Hz$ and $f = 0.35\ Hz$ respectively. However the results found by Panerai *et al.* [46] for pre-mature newborns did not agree and the observed increased phase with frequency. Panerai *et al.* [46] proposed that the reason that the phase increases with frequency in newborns is that the dynamic input impedance[9] principle is more prevalent in the younger subjects considered in his research. Panerai *et al.* [52] suggested that the first mechanism responsible for the slow response of $CBFV$ to the fluctuation of ABP in the frequency range of $0.02 \leq f \leq 0.2\ Hz$ could be a metabolic mediator. He also suggests that the second mechanism which is responsible for the response of blood flow control for the frequency range of $0.25 \leq f \leq 0.5\ Hz$ is a fast response compatible with a myogenic mechanism.

Another simple parametric approach taken by Simpson *et al.* [74] was to use a first order finite impulse response (FIR) filter and look at the second coefficient ($H1$) from different recordings during normocapnia and hypercapnia. Simpson *et al.* [74] reported strong evidence that the FIR coefficients reflect autoregulatory activity by observing high-pass filter responses and showed significant difference between normocapnia and hypercapnia recordings using $H1$ was also apparent.

[9] The dynamic impedance refers to a circuit with an inductance and a capacitance in parallel at the frequency at which this impedance has a maximum value.

2.12 Assumption of linearity and time invariance

All the models discussed in section 2.11 for the assessment of autoregulation, there is an assumption that our system is linear and time invariant. These assumptions have been made in a large proportion of the literature in the area of assessing cerebral autoregulation, and linear techniques have been used to describe and model the behaviour of dynamic autoregulation (dCA). These assumptions are made in the frequency domain analysis (gain, phase, frequency response function, coherence) and in the Tiecks model described in section 2.11.1).The question of validity of this assumption has been raised by some authors (Panerai *et al.* [82], Mitsis *et al.* [83], Giller *et al.* [84]). This is a crucial question to be addressed because if a system is nonlinear then its behaviour cannot be fully described using linear techniques and a single frequency response function with a single phase and gain. It has been argued [35, 46, 84] that cerebral autoregulation is a nonlinear response when it is studied over a large pressure range see Figure 2-2. One can consider two extreme cases: one with a small step change in blood pressure and one with a massive drop to almost zero blood pressure. In the first case, blood flow drops and is quickly restored to baseline by autoregulation. In the second case, blood flow drops to zero and remains at zero (autoregulation cannot bring it back) [85]. From the above argument, it is obvious that the output (blood flow) and the response of the system depend on the scale of the input (blood pressure), which, by definition, makes the system nonlinear. However the main question is whether it would be a safe assumption to treat the autoregulation response linearly within a limited range of blood pressure.

Panerai *et al.* [46] collected ABP and middle cerebral artery velocity from a large number of healthy subjects. They then used one set of data collected from each subject and by using different mathematical models (4 linear models and one non-linear: Volterra-Wiener kernels[10]) to develop the relationship between ABP and $CBFV$. Then the models for each individual were applied to the second set of data collected and the results were compared for different models. The authors found that the nonlinear model gave much more promising results compared to the linear models when they were applied to the same set of data, on which the model was developed. However when the models were applied to other sets of data, the result from the nonlinear model was relatively poor. The authors argue that the nonlinear models are more flexible and provide a better fit to the data in the training set. However nonlinear models may fail even when tries to fit new recording from the same subject. That means when the coefficients of the model are calculated using the training set of data, they would try to fit the noise as well. Noise can be assumed as non-linearity which includes in

[10] For details see appendix I

our measurements, and when they are applied to different sets of recordings, as they are very sensitive to the training signals, they would not provide promising results in term of signal to noise ratio (SNR). The authors state that it cannot be a solid explanation but acknowledge that the "nonlinear model becomes too sensitive to the particular blood pressure temporal pattern of the training set (over-training)" [46].

Mitsis *et al.* [83] argues that the nonlinear behaviour of cerebral autoregulation has multiple components that operate in different frequency bands. They argue that the assumption of linearity would give satisfactory results when the system is studied over high frequencies ($0.15 < f < 0.4\ Hz$), but nonlinearity would model the data better (data-fitting and grading autoregulation) when low frequencies ($0.04 < f < 0.15\ Hz$) are studied. Mitsis *et al.* [83] used a Volterra-Wiener approach, that utilizes the Laguerre-Volterra[11] network with two filter banks to model the system nonlinearly with two dynamics: fast and slow. Their results prove that nonlinear model provides better results compared to linear models in term of data fitting. They argue that this improvement is due to the representation of the system over the low frequency range.

Another method that has been applied by Chacon *et al.* [82] was the use of a time lagged recurrent neural network to model the relationship between ABP and $CBFV$ as input and output respectively. They showed that this new approach is superior in the prediction of $CBFV$ compared to transfer function analysis, but not to time-domain linear methods. The existence of nonlinear behaviour was also observed in the $ABP - CBFV$ relationship, involving not only an amplitude factor, but possibly a directional effect as well. However they did not comment on the difference between this novel approach and more common methods in term of the assessment of autoregulation.

Autoregulation is known to be nonlinear [35, 85], which raises the question of the validity of linear approaches in assessing autoregulation. However it is been shown that over high frequencies ($f > 0.07\ Hz$), [84] and normal range of blood pressure, the linearity assumption is a safe assumption and gives adequate results [35, 46, 52]. At lower frequencies no models appear to be available to represent the response of the system and neither linear nor nonlinear models proposed so far can accurately predict the relationship between arterial blood pressure and middle cerebral artery velocity. The evidence so far suggests that some nonlinear models can be useful in terms of modelling the behaviour of the system at low frequencies but perhaps due to our lack of knowledge of other extraneous signals, especially cerebral metabolism changes and P_{ETCO_2} variation, a good and accurate model remains to be found.

[11] For details see appendix II

Another assumption that has been made by most of the researchers and authors in the area of quantifying cerebral autoregulation is the time-invariance of the system. It can be said that the mechanism itself is time-varying as mentioned before. So introducing a time-varying model would be sensible choice. However it is possible that the complex mechanisms of the systems that are responsible for autoregulation have time-varying responses depending on the local brain activity and on the history of the blood pressure changes, arterial CO_2 changes and so on. As a result of that the measurements of autoregulation may vary even from minute to minute as the measurements continue.

It has been shown that the autoregulation response varies for healthy subjects [47]. Panerai *et al.* [47] used a period of over 10 minutes of non-invasive recordings of $CBFV$ from both left and right MCA with Doppler ultrasound and simultaneous beat-to-beat ABP [47] and showed that the mechanisms of cerebral autoregulation are time-varying. However the conventional analysis assumes time-invriance and therefore it may be desirable to split the data up into invariant sections. But this is difficult to achieve in practice usually, therefore time-invariance is assumed for short segments of data and estimates are usually taken by averages across those sections. Panerai *et al.* [47] has shown that continuous estimates of dynamics CA can be used to derive continuous cerebral autoregulation index (cAi). He suggested that more work can be done in this area especially on short-term variability of autoregulatory mechanisms. It has been suggested by many authors [53, 86, 87] that time-varying parameters should be given the second priority (after non-linearity) where a more advanced model is considered.

2.13 Multivariate models

In section 2.12, the non-linear characteristic of cerebral autoregulation was discussed. However it is known that the process of blood flow regulation is probably also multivariate [46, 83]. It is known that the variations in $CBFV$ is not entirely driven by pressure. There are other main physiological parameters that are responsible for controlling blood flow such as: arterial O_2 $\left(P_{aCO_2}\right)$, and O_2 $\left(P_{aO_2}\right)$ levels. The reactivity of P_{aCO_2} and P_{aO_2} can be assessed by P_{ETCO_2} and end-tidal O_2 $\left(P_{ETO_2}\right)$. Different studies have investigated the dynamic charactrestics of the $CO_2 - CBFV$ relationship using the measurments of $CBFV$ response to a step change in P_{ETCO_2} [88, 89] or continuous measurement of breath-by-breath fluctuations of P_{ETCO_2} [90, 91]. There are also work done on dynamic cerebral autoregulation by Mitsis *et al.* [35, 92], which used multivariate nonlinear system using both ABP and P_{ETCO_2} as inputs and employed the Laguerre-Volterra network methodology and showed that CO_2 fluctuations and the interaction between ABP and CO_2 have a considerable effect on $CBFV$

variation at low frequency bands. He argued that the results of these studies show, that ABP on its own is not enough to explain $CBFV$ variability in low frequency bands. Kouchakpour *et al.* [93], showed that nonlinear multivariate models of $CBFV$ can improve assessment of autoregulation and can reduce both inter- and intra-subject variability when compared to univariate linear and nonlinear models

2.14 Summary

In this chapter, a brief anatomy of arteries and cerebral circulation were studied. Cerebral circulation and autoregulation process and their importance were also discussed. It is vital to monitor cerebral autoregulation as it plays a key part in diagnosis and monitoring cerebrovascular diseases. Myogenic, metabolic and neurogenic mechanisms which are known to be responsible for the cerebral autoregulation were also discussed.

Next two types of behaviour of cerebral autoregulation; static and dynamic were discussed. The reasons why assessment of the control system in clinical application and research now lean more towards dynamic autoregulation were considered.

Next different models of cerebral autoregulation were studied. Tiecks model which allows to grade cerebral autoregulation into 10 different autoregulatory levels was discussed. By assuming this to be a linear single-input-single-output ($SISO$) system, frequency-, gain-, phase-, step-, impulse-response, coherence and transfer function can be calculated, using linear, time-invariant estimates. More details about how cerebral autoregulation can be assessed using time- and frequency-domain analysis will be given in the next chapter.

Different approaches have been taken by different authors in order to assess dCA. For example, Carey *et al.* [66, 94] used the autoregulation index values using step response analysis and showed that dCA is unaffected by aging. Lipsitz *et al.* [95] and Narayanan *et al.* [96] both used transfer function analysis and showed that elderly normotensive and hypertensive elderly subjects retain dCA, and dCA in healthy elderly subjects is intact in the low frequency ranges.

Although many different models using different approaches have been proposed to assess cerebral autoregulation, none of the methods have been accepted for clinical applications and usage, which gives us the motivation to address this issue and try new methods and investigate them further.

Chapter 3 : Assessment of Autoregulation; Two-input ($\boldsymbol{ABP}$, $\boldsymbol{P_{ETCO_2}}$) models using Laguerre-Volterra Network

Autoregulation refers to the automatic adjustment of blood flow to supply the required oxygen and glucose to each tissue in the body in proportion to the tissue's requirement at any instant in time. In other words for the brain, cerebral autoregulation is an active process of the brain by which cerebral blood flow is controlled at a steady state despite the changes in the arterial blood pressure. Having a good assessment of the cerebral autoregulation by a model that characterizes this system can potentially be used in various number of important clinical and hospital conditions, such as prematurity, birth asphyxia, stroke, head injury, carotid artery disease, hypertension and vasovagal syncope. Spontaneous beat-to-beat variation arterial blood pressure (ABP), breath-to-breath end-tidal carbon dioxide (P_{ETCO_2}) as inputs and cerebral blood flow velocity ($CBFV$) as output are used as signals to model the autoregulatory mechanism (Multi-Input-Single-Output; $MISO$ model). In this study a non-linear multivariate approach, based on Volterra-type kernels estimation models are employed. The results are compared with linear, nonlinear Single-Input-Single-Output ($SISO$) and linear $MISO$ models. The mean squared error is used as the criteria of the performance of each model in assessing cerebral autoregulation. Our simulation results corroborate that for relatively short signals (around 300 seconds), nonlinear multiple-input model based on Volterra-model perform better that other models and can considerably improve the system model error. Results from 13 different healthy volunteers reveal that nonlinear models with additional input (P_{ETCO_2}) have the least inter- and intra-subject variability compared to single-input linear and nonlinear and linear and two-input models. Moreover it is found that simple linear using just ABP as an input perform relatively well when short a data sample is available.

3.1 Introduction

As explained in section 2.9 , it is well documented in the literature that changes in arterial CO_2 tension causes vascular responses in cerebral vessels [29], and this reactivity of cerebral vessels, causes changes in CBF regulation (hypercapnia can cause vasodilation and hypocapnia causes vasoconstriction). The effect of step changes in CO_2 on $CBFV$ has been investigated in number of studies [88, 90]. It has been shown that, this effect is not instantaneous and takes around 20 seconds to develop fully.

In this chapter, the nonlinear dynamic relationship between ABP and CO_2 as inputs, and $CBFV$ as output is studied[12]. In order to simplify the problem of observing changes in arterial CO_2 tension, the breath-to-breath, end-tidal CO_2 (P_{ETCO_2}) variations was used. This measurement as mentioned in section 2.13 can be used as a secondary input in addition to ABP and $CBFV$ as the output in order to test whether routine assessment of cerebral autoregulation and additional CO_2 reactivity have potential clinical usage for patients with cerebrovascular disorders. Panerai *et al.* [90] used the same two-input model to model dynamic cerebral autoregulation (ABP and P_{ETCO_2} as inputs and $CBFV$ variations as output), but employed causal FIR filters to assess the effect of arterial CO_2 on $MCBFV$ in a linear manner. In this study, Panerai *et al.* [90] used spontaneous beat-to-beat fluctuations in $MABP$ and breath-by-breath variability in end-tidal CO_2 in continuous recordings. It was found that having CO_2 alongside with ABP improves the prediction error of the model considerably. He also used impulse response to show the dynamic characteristics of the $MABP$ and P_{ETCO_2} to $MCBFV$. Panerai *et al.* [90] observed no significance interaction between the two inputs.

This chapter starts by employing, a two-input format of Laguerre Volterra Network (LVN) modelling approach (section 3.3.1) to assess the nonlinear dynamic effects of $MABP$ and P_{ETCO_2} on $MCBFV$ and the effect of their interaction [83]. The performances of different models (linear-$SISO$, nonlinear-$SISO$, linear-$MISO$, and nonlinear-$MISO$) are compared and the structure of each model are selected individually for each recording and later a general model structures for all the recordings based on model fit (normalized mean square error; $NMSE$) are presented .

This is then followed by data fitting using multi-input Laguerre-Volterra Network (LVN) and the performance of different models based on their ability to assess autoregulation is studied.

[12] Part of this chapter was presented at IEEE EMBSS [93]

Another issue that is of interest is the robustness of estimated step and impulse response which has been intensively used to assess autoregulation from the models is then investigated [75, 88, 97]. However spontaneous fluctuations of blood pressure and their central frequency is not entrained or synchronized with the changes in ABP (around $0.1\ Hz$) [74] (Figure 3-4).

In this section, a new input (Cosine shape input modulated by a Gaussian, which has more realistic characteristics, i.e. closer to changes observed in spontaneous fluctuations of blood pressure) is used [98] and the response of the system to this input is studied and then compared, with some well-established autoregulatory parameters. Next the issues of inter- and intra-subject variability of the autoregulatory parameters extracted from different models in order to assess the robustness of these methods, was studied. In order to compare the proposed methods (Wiener) to previously used methods, and to determine whether any improvement is due to the methods or just random effects resulting from the specific dataset in question and whether the results are generalizable, a permutation test between the models was used. This is a statistical significance test in which the distribution of the test statistic under the null hypothesis is obtained by calculating all possible values of the test statistic under rearrangements of the labels on the observed data points [99].

3.2 Subjects and measurements

The data used in this study was kindly provided by Prof. D.H. Evans and Prof. R. Panerai, and was collected at the Leicester Royal Infirmary (Leicester, UK). 13 healthy volunteers (age 32 ± 8.8 years) were involved in this study and the study was approved by the Leicestershire Research Ethics Committee. All the measurements were collected with the volunteers in the supine position with their head elevated. Transcranial Doppler Ultrasound (Scimed $\mathrm{QVL}-120$,) was used to measure middle cerebral artery velocity using a $2\ MHz$ transducer, held in position by an elastic headband. Simultaneously arterial blood pressure (ABP) was non-invasively measured using a finger cuff device (Ohmeda 2300 Finapres monitor).

The signals were pre-processed off-line. The maximum velocity envelope from the spectra of the Doppler signal was extracted using a microcomputer-based analyzer that performs a fast Fourier transform (FFT) every $5\ ms$. The ABP signals were digitized at $200\ Hz$. Short periods of evident artefact as well as any spikes on the signals were removed by linear interpolation and the signals (ABP, CBF) were low pass filtered with an eighth-order Butterworth digital filter (applied forward and reverse to give zero phase shift) with a cut-off frequency of $20\ Hz$. The start of each heart cycle was automatically identified (with visual correction) from the ABP signal, after which the average

ABP and $CBFV$s from the right and left MCA were calculated for each heartbeat. This time series was then interpolated with a third-order polynomial, and sampled at a constant rate of $1\ Hz$.

3.2.1 Data analysis

For each measurement, data segments of approximately 300 seconds in duration were available. The recordings of $ABP, CBFV$ and P_{ETCO_2} were converted to a percent change with respect to the mean value of each data segment, in order to remove the dependence on inter-individual variations in mean level.

3.3 Methods

3.3.1 Laguerre-Volterra kernel

The Laguerre-Volterra Network (LVN) methodology was chosen to study the relationship between blood pressure, CO_2 and blood flow in this chapter. The LVN has been shown to be an accurate nonlinear method for short stimulus-response recordings [83] and "is the best implementation of the kernel expansion approach in term of simplicity, to date" [100]. The LVN is a combination of artificial neural networks with the Laguerre expansion technique (LET). The LVN for multivariate models consists of two input layers of two Laguerre filter banks (Figure 3-2) (may be the same set of filters) and a hidden layer with H hidden units using polynomial activation functions. The LVN model consists of individual dual-input static nonlinearities associated with each input-output pair.

The Laguerre functions have been used for the expansion of Wiener kernels due to its orthogonally over a domain from zero to infinity (appendix II) which is in consistent with the kernel domain [100].

The Laguerre expansion technique (LET) for the Volterra kernel estimations is implemented by the use of the orthonormal[13] set of discrete Laguerre functions ($DLFs$) given by [100] as shown in Figure 3-1.

$$b_j(m) = \alpha^{m-j/2}(1-\alpha)^{\frac{1}{2}} \sum_{k=0}^{j} (-1)^k \binom{m}{k} \binom{j}{k} \alpha^{j-k}(1-\alpha)^k \qquad 3.1$$

Where $b_j(m)$ denotes the j^{th}-order orthonormal DLF (the impulse response of the j^{th} filter in the filter-bank), the integer m ranges from 0 to $M-1$ (M is the memory-bandwidth; the length of the

[13] Two vectors in an inner product space are called orthonormal if they are orthogonal and unit vectors.

impulse response), and the real positive number α ranging from 0 to 1, which is the critical DLF parameter that determines the rate of exponential decline of these functions.

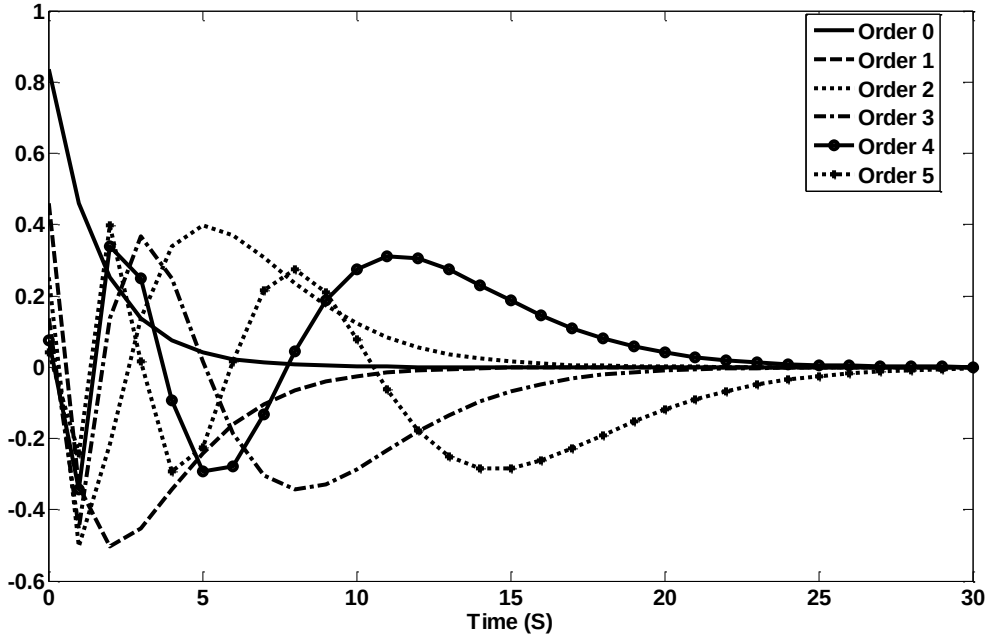

Figure 3-1 Discrete Laguerre functions (DLF) of orders 0-5, for $\alpha = 0.3$ plotted over the first 30 lags ($M = 30$)

The output of the filter-banks ($v_j(n)$) are generated as the convolution of the two inputs ABP and P_{ETCO_2} and the different $DLFs$ and the filter outputs are fully connected to a layer of hidden units with polynomial activation functions [83].

$$v_j^{(i)}(n) = \sum_{m=0}^{M-1} b_j^{(i)}(m) x_i(n-m) \tag{3.2}$$

where, j is the order of orthonormal DLF and i is the input and in this study can be either 1 or 2 representing $MABP$ or P_{ETCO_2} and $b_j^{(i)}$ denotes the basis function that is the impulse response of the j^{th} filter in the i^{th} filter-bank.

The outupt is formed by simple summation of the output of the hidden units and an offset y_0.

$$y(n) = y_0 + \sum_{h=1}^{H} z_h(n) \tag{3.3}$$

$$z_h(n) = f_h[u_h(n)] = \sum_{q=1}^{Q} c_{h,q} u_h^q(n) \tag{3.4}$$

Where Q is the order of nonlinearity and f_h is the polynomial static nonlinearity. $u_h(n)$ is the internal variable of the hth hidden unit and it is composed as a weighted summation of all filter banks outputs:

$$u_h(n) = \sum_{j=1}^{L_1} w_{h,j}^{(1)} v_j^{(1)}(n) \sum_{j=1}^{L_2} w_{h,j}^{(2)} v_j^{(2)}(n) \qquad 3.5$$

As mentioned before the value of α (eq.3.1) determines the convergence of the Laguerre expansion for a given kernel function. So the choice of α is very important in order to achieve an efficient model representation of a system with fast and slow dynamics. In this work, this value was chosen based on the number of filter-banks for each kernel and the length of the impulse response for that input based on the work done by Westwick *et al.* [101]. The equivalent LVN model of our system with two-input, second-order nonlinearity is shown in Figure 3-2.

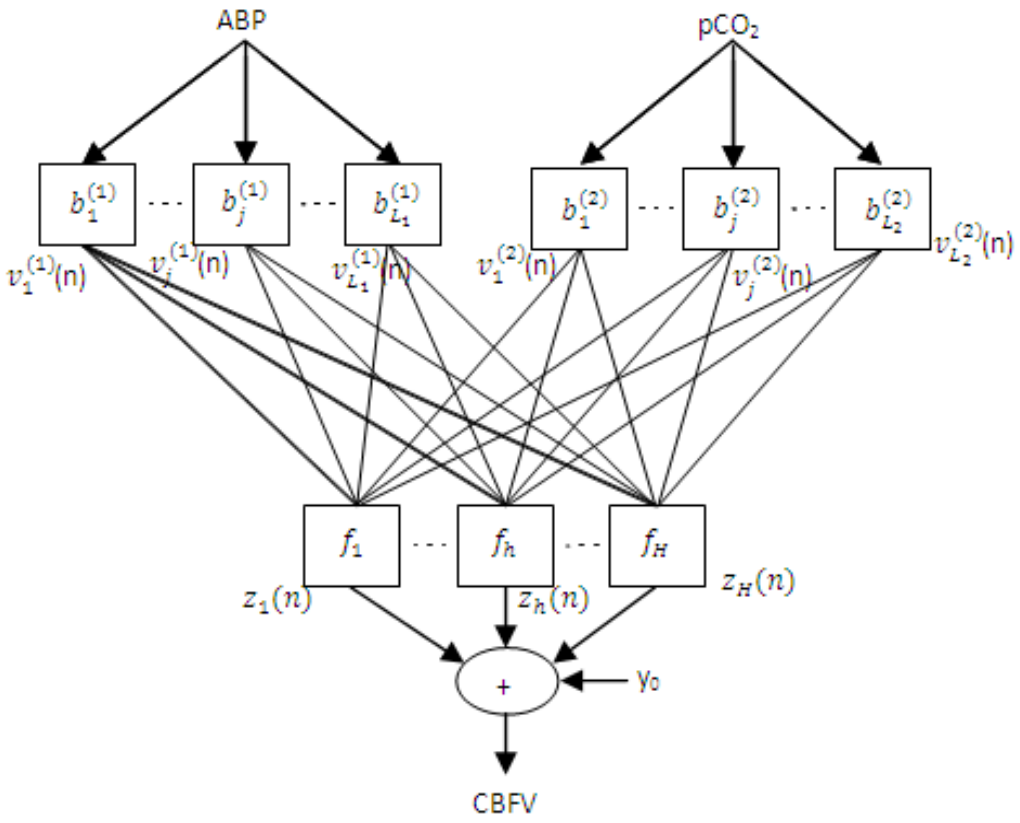

Figure 3-2 The Laguerre-Volterra network (LVN) with two-inputs, with each input pre-processed through a different filter bank ($b_j^{(i)}$) and respectitive filter bank outputs are fed into the hidden units of the hidden layer with polynomial activation functions (f_h), and the output is calculated as the summation of the outputs of the hidden units ($z_h(n)$) and offset y_0 [100].

The system output $y(t)$ according to the Volterra model can be written as:

$$\begin{aligned} y(t) = c_{0,0} + \sum_{j_1=1}^{L_1} c_{1,0}(j_1)\, v_{j_1}{}^{(1)}(t) + \sum_{j_1=1}^{L_2} c_{0,1}(j_1)\, v_{j_1}{}^{(2)}(t) \\ + \sum_{j_1=1}^{L_3}\sum_{j_2=1}^{L_3} c_{2,0}(j_1,j_2)\, v_{j_1}{}^{(1)}(t)\, v_{j_2}{}^{(1)}(t) \\ + \sum_{j_1=1}^{L_4}\sum_{j_2=1}^{L_4} c_{0,2}(j_1,j_2)\, v_{j_1}{}^{(2)}(t)\, v_{j_2}{}^{(2)}(t) \\ + \sum_{j_1=1}^{L_5}\sum_{j_2=1}^{L_5} c_{1,1}(j_1,j_2)\, v_{j_1}{}^{(1)}(t)\, v_{j_2}{}^{(2)}(t) + \ldots + \varepsilon(t) \end{aligned} \quad 3.6$$

where $v_{j_1}{}^{(1)}$ denotes the convolution of b_j with x_i (either $MABP$ or P_{ETCO_2}). It has to be noted that each input may also employ its own set of basis function. The unknown parameters $c_{m,n}(j_1, \ldots, j_{m+n})$ in above equations are the expansion coefficients of $k_{m,n}$ (eq.3.10). The above equation can be simplified by:

$$y = Vc + \varepsilon \quad 3.7$$

Where in the above equation the matrix V is constructed using the output of the filter-banks and ε is the error term and y is the output. It needs to be noted that y, ε and c are all also vectors. For instance, for a second-order system, the *nth* row of the V matrix is in the format of:

$$\begin{bmatrix} 1, v_1^{(1)}(n), \ldots, v_{L_1}^{(1)}(n), v_1^{(2)}(n), \ldots, v_{L_2}^{(1)}(n), \\ v_1^{(1)}(n)v_1^{(1)}(n), v_2^{(1)}(n)v_1^{(1)}(n), \ldots, v_{L_3}^{(1)}(n)v_1^{(1)}(n), v_2^{(1)}(n)v_2^{(1)}(n), v_3^{(1)}(n)v_2^{(1)}(n), \ldots, v_{L_3}^{(1)}(n)v_{L_3}^{(1)}(n), \\ v_1^{(2)}(n)v_1^{(2)}(n), v_2^{(2)}(n)v_1^{(2)}(n), \ldots, v_{L_4}^{(2)}(n)v_1^{(2)}(n), v_2^{(2)}(n)v_2^{(2)}(n), v_3^{(2)}(n)v_2^{(2)}(n), \ldots, v_{L_4}^{(2)}(n)v_{L_4}^{(2)}(n), \\ v_1^{(1)}(n)v_2^{(2)}(n), v_2^{(1)}(n)v_1^{(2)}(n), \ldots, v_{L_5}^{(1)}(n)v_1^{(2)}(n), v_2^{(1)}(n)v_2^{(2)}(n), v_3^{(1)}(n)v_2^{(2)}(n), \ldots, v_{L_5}^{(1)}(n)v_{L_5}^{(2)}(n), \end{bmatrix} \quad 3.8$$

Where the expansion coefficients (c_r) takes into account the symmetries of the Volterra kernels:

$$c_{m,n}(j_1, \ldots j_r) = \lambda_{m,n} a_{m,n}(j_1, \ldots j_r) \quad 3.9$$

Where λ_r depends on the multiplicity of the specific indices $(j_1, \ldots j_r)$ and $(a_{m,n})$ are the coefficients of the r^{th} order kernel expansion. For instance, if all indices are distinct, then $\lambda_{m,n} = 1$; but if the indices form p groups with multiplicities m_i $(i = 1, \ldots, p$ and $m_1 + \cdots + m_p = r)$, then $\lambda_{m,n} = m_1! \ldots m_p!$. The error term ε incorporates possible model truncation error and noise/interference in the data.

The Volterra kernels can be expressed in term of DLFs and the expansion coefficients of $k_{m,n}$ as below:

$$k_{m,n}(j_1, j_2, \dots, j_{m+n}) =$$

$$\sum_{j_1=1}^{L} \dots \sum_{j_{m+n}=1}^{L} \alpha_{m,n}(j_1, \dots j_{m+n}) b_{J_1}(1) \dots b_{j_m}(m) b_{j_{m+1}}(m+1) \dots b_{m+n}(m+n) \quad 3.10$$

It has to be noted that the indices $j_1 \; to \; j_m$ correspond to the first input ($MABP$) and the indices j_{m+1} to j_{m+n} correspond to the second input (P_{ETCO_2}). The value of m and n in the kernels ($k_{m,n}$) denotes the order of that kernel (1 would denote linear model and 2 would denote second-order non-linearity). So $k_{m,0}(j_1, j_2, \dots, j_m)$ or $k_{0,n}(j_1, j_2, \dots, j_n)$ corresponds to the self-kernels, and describes the effect of both linear ($m + n = 1$) or nonlinear ($m + n > 1$) of that input on the output, and if $m, n \neq 0$, then $k_{m,n}(j_1, j_2, \dots, j_{m+n})$ denotes the cross-kernels and describe nonlinear interaction between the inputs and its effect on the output.

The expansion coefficients in the model can be estimated through linear least-squares procedure because they enter linearity into the model [100].

The most important issue when it comes to applying LVN is the determination of the structure parameters L and Q, which determine the size of the matrix V. It is obvious that by going to higher order in Q, we can deal with higher order nonlinearity and the system memory (M) defines the time elapsed for the diminution of the causal effect of an impulsive input stimulus. The key to the efficacy of the kernel expansion is in finding the proper b_j (based on the α value and L), as Q is fixed before choosing other parameters, and the number of columns in the V matrix in eq.3.8 only depends on $L_i, i = 1,2,..,5$ (order of Laguerre Wiener functions; two linear models, two self-kernel nonlinear model and one cross-kernel). In this work the order of nonlinearity was set to 2 ($Q = 2$) due the small data sample and going to the third order would increase the number of kernels and require bigger data sample in order to be able to validate the method. Also going to higher orders would result into over training the validation dataset. Setting the $Q = 2$ the number of columns in matrix V is:

$$(L_1 + L_2) + \left(\frac{L_3 \times (L_3 + 1)}{2}\right) + \frac{L_4 \times (L_4 + 1)}{2} + (L_5)^2 \quad 3.11$$

In above equation, we can set any of $L_i, i = 1,2,..,5$, to zero, and we simply won't have that kernel in our model (for example, setting $L_i, i = 2,..,5$ to zero, would result into a simple linear single-input model).

In the next section normalized mean-square error ($NMSE$) of the output on test data was used as the criterion to select the structure of the multi-input LVN ($L_i, i = 1,2,..,5$) and length of the

impulse response (M_1, M_2). The output prediction $NMSE$ is defined as the sum of squares of the output residuals (difference between true output and the predicted output) of the model prediction normalized by the sum of squared of the true output. In order to avoid over fitting the network, we use training and validation method (training on half of data samples and validation on the other half and vice versa).

3.3.2 Selection of Autoregulatory Parameters

Different approaches have been made to assess autoregulation as described in section 2.9 in both time and frequency domains. A very common method used by [46, 47, 65, 98] to assess autoregulation is to look at the final value of the response of the model to a step or phase-lead at $1/12\ Hz$ [65] and autoregulation index (ARI) [5], developed from time- and frequency-domain analysis have been proposed to assess the status of cerebral autoregulation. The system responses to a step and impulse change are shown in Figure 3-3. As it can be seen in this figure, variability across the subjects is large and they also suffer from considerable inter- or intra-subject variability and may show very large fluctuation over short periods of time [47].

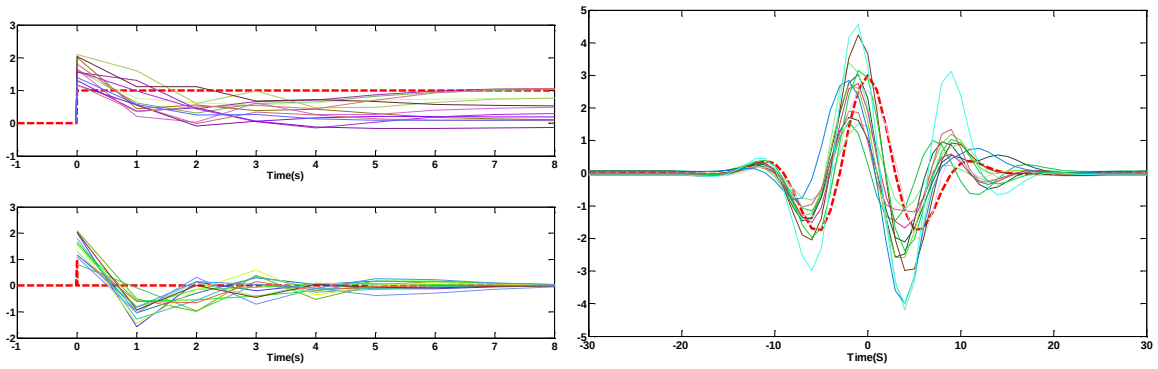

Figure 3-3 Top left: step, Bottom Left: Impulse from a 6 seconds-long FIR model, Right: response to cosine shape input modulated by a Gaussian (pressure-pulse (PP)), for all thirteen subjects. The inputs are indicated as bold-dotted lines and the responses are shown in solid lines. Large dispersion is observed in the step compared to the pressure pulse response.

Simpson *et al.* [102] proposed an alternative test-input to assess model responses shown in Figure 3-3. In this method, instead of feeding a step or an impulse to the system and calculating the response, they used a cosine wave modulated by a Gaussian envelope (pressure pulse, PP) and use the system response to this input. The reason behind choosing this model is that, this input has more realistic characteristics to our real input (spontaneous fluctuations of blood pressure) and its central frequency can be chosen with refer to the autoregulatory system where the variations in the $CBFV$ seem to be entrained or synchronized with the changes in ABP (around $0.1\ Hz$) [103]. The

power spectral density for an arbitrary set of $CBFV$ and ABP and three different inputs (step, impulse and new pulse input) shown in Figure 3-3 are shown in Figure 3-4. As it can be seen, our $MABP$ and $CBFV$ has most of their powers at frequencies between $0.03\,Hz < f < 0.25\,Hz$, however impulse has a flat power spectrum at all frequencies and step input has most of its power at low frequencies which are not feasible with our system in hand. However it can be seen that the PP has more realistic characteristic to our real data in term of power spectra density so more meaningful results are expected from this novel input.

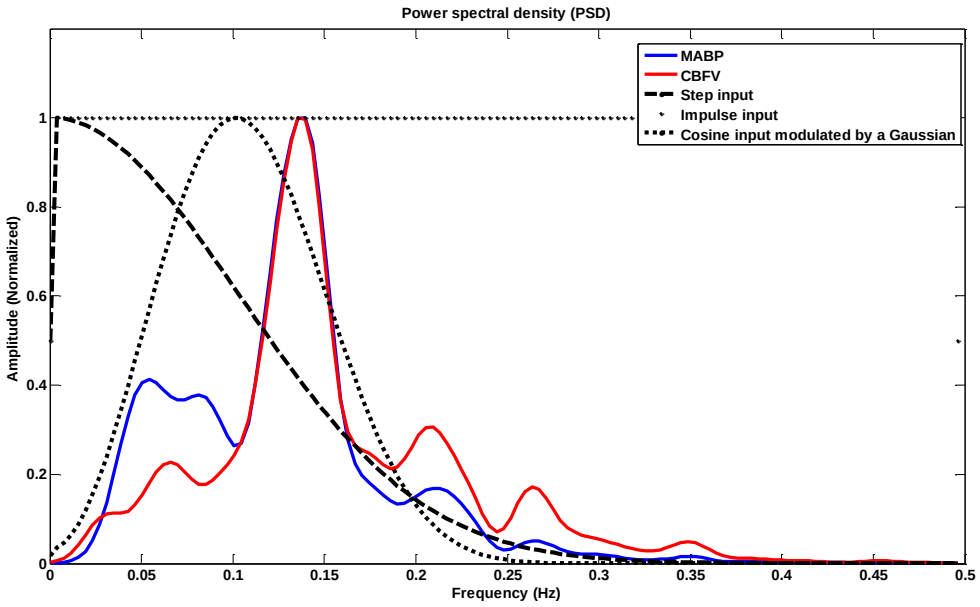

Figure 3-4 Power spectral density for a set of $CBFV$ and ABP, and step, impulse and pressure pulse input.

The high-pass characteristics of the autoregulatory response showed by [18, 77, 103] can be seen in Figure 3-5, from the left-shift (phase lead) in the pressure pulse response (PPR).

In this work, the response of the system to the pulse input for all 13 volunteers during normo- and hypercapnia is studied and the distance between their amplitude at different point are measured, and the ones with the largest difference and highest trend follow across all datasets are chosen.

A typical system response to this pressure pulse and the autoregulatory parameters used from this response are shown in Figure 3-5. demonstrated that, from simulations based on the Tiecks model [5] and preliminary work on the recorded data, pulse response at 1.5 seconds ($A1.5$), and the amplitude at 8 seconds ($A8$) provide good separation of different levels of autoregulation and are used from now on in this chapter for the assessment of autoregulation.

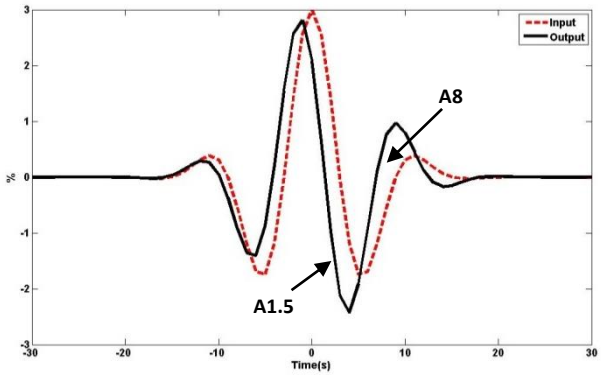

Figure 3-5 The test-input of the shape of pressure pulse response (PPR) in dotted-line and the estimated response in the solid-line. The parameters used to access autoregulation are also shown (amplitude of the response at 1.5 and 8 seconds)

Angarita-Jaimes *et al.* [104] compared some of the most used parameters in the literature. These include the following: The percentage change during the initial segments of the step response (PCS) was calculated from amplitude of the step response after 3 seconds which has shown to provide more robust result than the previously proposed parameter of the final value (non-parametric estimates) [98]. Average phase (Pha) from $0.07\ Hz$ to $0.2\ Hz$, measured from the transfer function analysis proposed by Zhang *et al.* [75]. From the response of the linear and nonlinear models to the step input, the final value (amplitude) is estimated (FVS). Coherence (Coh) over the same frequency range [103, 105], the correlation method (Mx) using the Pearson's correlation coefficient of segments of $\%ABP$ and $\%CBFV$ time series proposed by Piechnik *et al.* [106] have been widely used. The autoregulatory index (ARI) calculated by evaluating the set of models proposed by Tiecks *et al.* [5] using the parameter values given by the authors (for each recording, the model by the authors was applied to $\%ABP$, and the model which provided the highest correlation coefficient between the measured $\%CBFV$ and the generated velocity determined the ARI) is another widely used method. The parametric approach proposed by Simpson *et al.* [74], the coefficients of a first-order (two lags) FIR filter which is the simplest applicable model proposed by and choosing the second coefficient of the filter as an autoregulatory parameter ($H1$) is also approach used in this thesis. Angarita-Jaimes *et al.* [104] found that $H1$ and $P1$ (phase at $0.1\ Hz$) provide the most robust results in term of assessing autoregulation and inter- and intra-subject variability compared to most commonly used autoregulatory parameters mentioned at the beginning of the this section, even though it performs poorly on data fit as shown in Table 3.3.

3.3.3 Statistical Analysis

For each set of data and each model, the predicted output ($CBFV$) was compared to the desired output and the performance was evaluated using the $NMSE$. Accurate model representation was carried out using cross-validation, in which model parameters were estimated on one data segment (training set) and $NMSE$ then calculated on a second segment (validation set). Both segments (training and validation sets) were around 150 seconds long for the same recording. The model parameters were measured with the transient at the beginning (as univariate models have a lag of $6\,sec$ and multivariate models can have a lag of up to 20 seconds) of the training half removed, and then the model performance was measured in the validation half. This procedure was then repeated, swapping training and validation segments [93]. The number of filter-banks ($v_j^i(n)$) for each set of measurements was evaluated using the $NMSE$ between the responses of $CBFV$ to changes in ABP as a linear system (just $k_{0,0}$, $k_{1,0}$ in eq.3.10), and this valued was later used in more complex models (linear and nonlinear multivariate models).

In order for the LVN model to estimate the kernels precisely the number of filter-banks should be large enough, as a smaller number of filter-banks would results in having a LVN model which is just a sub-set of the actual solution.

In this work by scanning through all the models to find the optimum number of filter-banks (1 to 30 for linear kernels and 0 to 3 for nonlinear kernels) are chosen by having $NMSE$ on the validation segment as the criteria repeated on all the recordings. The choice of 30 for linear and 3 for nonlinear kernels come from analyzing dataset. The $NMSE$ for different combinations of filter-banks showed that the lowest $NMSE$ for linear model for different individual measurement was achieved with filter-banks in the range of 4 to 20. However in term of second-order kernels, the largest number of filter-banks that provided the lowest $NMSE$ was with 2 filter-banks and the smallest number of filter-banks that resulted in the lowest $NMSE$ was with no filter-banks which represent no non-linearity (m or $n = 0$ in eq.3.10). The validity of the results based on the criteria of $NMSE$ [93] was proven as higher orders showed to worsen the result on the validation dataset (due to the small sample size).

The filter length was chosen differently for ABP and P_{ETCO_2} as their response is different and based on previous works, filter lengths of 12 seconds for ABP and 20 seconds for P_{ETCO_2} are chosen [23, 39, 74, 97]. For each set of data (ABP, P_{ETCO_2} and $CBFV$), by fixing the filter length, the α (see eq.3.1) was calculated based on the work of Westwick *et al.* [101] (based on the length of the data and the filter length) and the number of filter-banks as shown in Figure 3-2, varied as mentioned

above, and the $NMSE$ for each iteration was calculated. Out of all possible combinations, the number of filter-banks and α that provided the smallest $NMSE$ was chosen as the characteristics of the model for that specific set of data.

It has to be considered that in this work the kernels up to the second order were calculated. In each model the number of filter-banks for each kernels varied from '0' (absence of that kernel) to the maximum of filter-banks for that specific kernel (30 for linear and 3 for nonlinear kernels). It was found that the maximum number of filter-banks for the nonlinear kernels was 2 and for linear kernels this was found to be twenty. In some cases, it was observed that in some set of data, the best model was not the most complex model but a simpler model and adding the nonlinearity did not improve our model prediction.

In this work the "distinction between normo- and hyper-capnia" and "inter-subject" and "intra-subject" variability as the benchmarks for the assessment of cerebral autoregulation were used which will be discussed below.

3.3.3.1 Inter-Subject Variability

We used inter-subject variability (normalized standard deviation; SDn) as an indication of how good an autoregulatory parameter (ARP) separate between NC and HC and thus considered to provide us with the best distinction between intact and impaired autoregulation.

$$X_i = ARP_{NC_i}\ i = 1 \dots 13 \tag{3.12}$$

$$Y_i = ARP_{HC_i}\ \mathrm{i} = 1 \dots 13 \tag{3.13}$$

where in above equations ARP_{NC_i} and ARP_{HC_i} indicate different autoregulatory parameters ($H1, P1, A1.5, A8$) during NC and HC for all 13 recordings. The mean of these parameters are then removed and normalized by the difference between the mean of these two groups (NC and HC) to remove the effect of the scales using:

$$nX_i = \frac{X_i - mX}{|mX - mY|}\ \ \mathrm{i} = 1 \dots 13 \tag{3.14}$$

$$nY_i = \frac{Y_i - mY}{|mX - mY|}\ \ \mathrm{i} = 1 \dots 13 \tag{3.15}$$

where in above equation mX and mY are the mean of the NC and HC across 13 recordings respectively. The inter-subject variability is finally defined as the mean between the variation (standard deviation; STD) of the normalized autoregulatory parameters defined in eq.3.14 and eq.3.15 as:

$$SD_{nX} = STD(nX_i) \quad 3.16$$

$$SD_{nY} = STD(nY_i) \quad 3.17$$

$$SD_n = 100 \times \frac{SD_{nX} + SD_{nY}}{2} \quad 3.18$$

3.3.3.2 Intra-subject Variability

In order to test the robustness of different autoregulatory parameters and the influence of additive noise in the recordings, intra-subject variability ($mSDn$; normalized standard deviation) is evaluated.

$$SD_{X_i} = STD(X_i) \text{ i} = 1 \dots 13 \quad 3.19$$

$$SD_{Y_i} = STD(Y_i) \text{ i} = 1 \dots 13 \quad 3.20$$

where in above equations SD_{X_i} and $SD_{Y_i}$are the standard deviation of the autoregulatory parameters for each recording during NC and HC respectively. As no model can provide a perfect fit to the data, random estimation errors are expected in both model fit and as the result of that in autoregulatory parameters for each recording. By assuming that the underlying autoregulatory response is time-invariant, such random errors would reflect the repeatability of measurements, or the intra-subject variability. In order to assess these, Angarita-Jaimes *et al.* [104], used Monte-Carlo simulations, as they allow not only the errors in model parameters but also the derived autoregulation indexes to be assessed. The idea behind this method is to use computer-generated data to determine the amount of variation in sample statistics. In this work by Angarita-Jaimes *et al.* [104], 100 simulated signals were generated for each of the recordings. Surrogate $\%CBFV$ signals were generated by applying the identified models (SI or MI linear or nonlinear) to the $\%ABP$ signals for that recording, and then adding random noise to simulate residuals. The generated noise was modeled based on the residual error in $\%CBFV$ using an AR (autoregressive) model of order 8 selected based on the Akaike's information criterion [107]. Then for each recording, the standard deviation for the 100 simulated signals for different autoregulatory parameters were calculated, and considered as the intra-subject variability.

By using the standard deviation of autoregulatory parameters for each recordings, intra-subject variability ($mSDn$) can be defined as using below equations

$$mSD_X = \text{mean}(SD_{X_i}) \quad 3.21$$

$$mSD_Y = \text{mean}(SD_{Y_i}) \quad 3.22$$

$$nmSD_X = \frac{mSD_X}{|mX - mY|} \quad 3.23$$

$$nmSD_Y = \frac{mSD_Y}{|mX - mY|} \quad 3.24$$

as:

$$mSDn = 100 \times (\frac{nmSD_X + nmSD_Y}{2}) \quad 3.25$$

Low values of SDn and $mSDn$ thus indicate low dispersion and/or wide separation between groups indicating improved ability to distinguish between normal and impaired autoregulation

In order to calculate the variability (standard deviation) more accurately in this work, a mathematical based approach was used in this work. In the next section, an introduction to this approach is first given and a comparison between this method and Monte-Carlo simulation is presented to validate this technique.

3.3.3.3 Variation; Mathematical Approach

The linear regression is the simplest type of parametric approach which can be written as:

$$y(t) = \Phi^{\mathrm{T}}(t)\theta + e(t) \quad 3.26$$

Where $y(t)$ is a measurable quantity, $\Phi(t)$ is an (n/p) matrix of known quantities and θ is an n-vector of unknown parameters and $e(t)$ is the error.

$$\theta = \left(\Phi^{\mathrm{T}}\Phi\right)^{-1}(\Phi^{\mathrm{T}}y) \quad 3.27$$

The covariance matrix of the unknown parameter estimates θ can be calculated by [108]:

$$cov(\theta) = (\Phi^{\mathrm{T}}\Phi)^{-1}\Phi^{\mathrm{T}}\mathrm{R}\Phi(\Phi^{\mathrm{T}}\Phi)^{-1} \quad 3.28$$

where it is assumed that R is a positive definite matrix:

$$\mathrm{R} = \mathrm{E}(\mathrm{ee}^{\mathrm{T}}) \quad 3.29$$

where in above equation E is the expected value of the entry. The variance of our autoregulatory parameters can be calculated using the covariance matrix of the parameters in the system. The agreement between Monte-Carlo simulation (100 simulations) and covariance matrix for the parameters extracted from the pressure pulse response for all 26 datasets (13 NC, 13 HC) for linear two-input model ($M2$ model in Table 3.4) are shown in Figure 3-6.

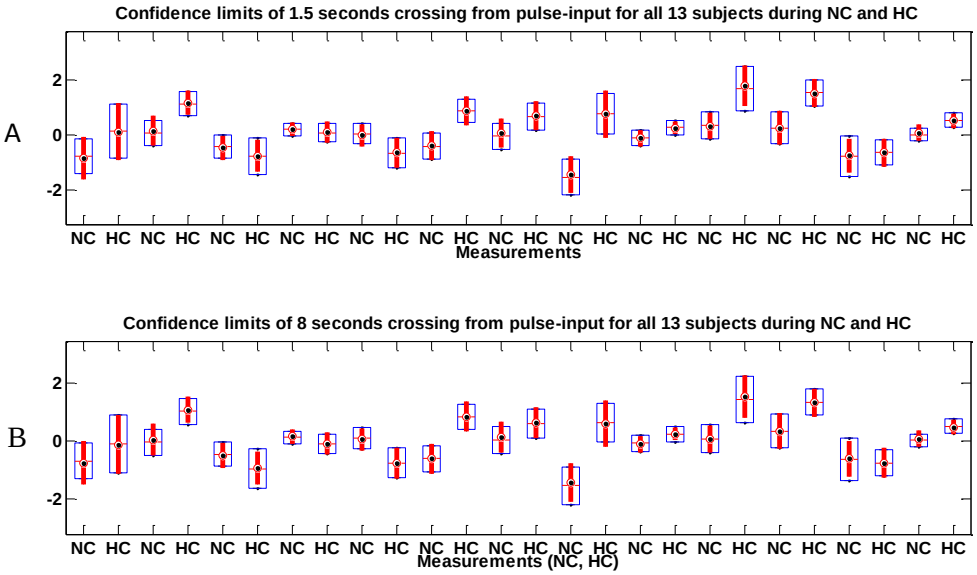

Figure 3-6 Agreement between confident limit (variation and mean) measured by Monte-Carlo simulation (100 runs) in solid-red and covariance matrix in solid-black for all 13 subjects in both normo- and hyper-capnia using linear two-input model ($\%ABP$ and P_{ETCO_2}) for top A) $A1.5$, bottom B) $A8$, the length in the box represents the standard deviation of autoregulatory parameters in that measurement.

The variations measured from covariance matrix is more reliable compared to the Monte-Carlo simulation as the robustness of Monte-carlo simulation depends on the number of repetitions. However as mentioned before covariance matrix is linear approach to measure the variance and consequently the standard deviation, and is not generalizable for different parameters where a linear relationship between the population parameter and the input-output relationship exists.

In the current study, the variation measured from the covariance matrix, of the autoregulatory parameters was used to measure intra-subject variability of different models. Paired t-test were used to test the significance difference between normo- and hypercapnia for all autoregulatory parameters extracted from different models (SI, MI linear and nonlinear). Results are considered statistically significant at $p < 0.05$.

Another approach that has been taken in this work was to look at trend following as the criterion to test how good the autoregulatory parameter is. As an example the $P1$ is expected to decrease from NC to HC as reported by other authors [52, 73, 109]. However this test on its own does not provide any information regarding the significant difference between autoregulatory parameters during NC and HC.

3.3.3.4 NC and HC significant difference

In order to test whether different autoregulatory parameters calculated from different models (SI,MI linear or nonlinear) during NC and HC are significantly different, a null hypothesis that there is no difference in their mean difference was assumed and the difference in their dispersion is measured. The dispersion (intra-subject variablity) is calculated for each subject as:

$$\sigma_i = \left({\sigma_{NC_i}}^2 + {\sigma_{HC_i}}^2\right)^{\frac{1}{2}} \quad i = 1 \dots 13 \qquad 3.30$$

and then a t-test is measured between different SI,MI linear or nonlinear to test the significance between the dispersions from these models.

3.3.3.5 Randomization test

The difference between the models can be tested indirectly by setting up a null hypothesis which says that any difference between the two model means is purely due to chance. If this null hypothesis is consistent with the data then there is no reason to reject this in favor of the alternative hypothesis. This can be interpreted in the same way as for conventional tests of significance: if it is less that 5% this provides some evidence that the null hypothesis is unlikely to be true. Randomization testing is a way of determining whether the null hypothesis is reasonable or not [99].

Significance difference between the inter- and intra-subject variability of different ARP extracted from different model was measured using randomization [99]. Randomization has the downfall that, it is not necessarily possible to generalize the conclusions form a randomization test to a population of interest. “What randomization tell us is that a certain pattern in data is or is not likely to have arisen by chance” [99]. However this disadvantage has very little value for our problem as this lack of generalizability is not in our interest.

This method of statistical analysis can be used when the sample sizes are small. Consider now a randomization test of inter- and intra-subject variability for two different ARP measured from different models. As mentioned before, variability of the ARP can be calculated using its mean and variance. The randomization test on 13 volunteers (26 measurements including both NC and HC), can be based on the idea that if there is no difference then the distribution of these measurements (measurements is 26 in our case) seen in the two inter- and intra-subject variability sample will just be a typical result of allocating the 26 measurements at random into two groups of size 13. The test therefore involves comparing the observed inter- and intra-subject variability (using the ARP mean and variance) difference between the groups with the distribution of differences found with random

allocation. If the inter- and intra-subject variability found from observed result looks like a typical value from the randomization distribution then it can be concluded that the allocation of measurements to the two different ARP in reality does not have any significance difference. On the other hand if the inter- and intra-subject variability from the observed result is unusually different compared to the randomization result, then the data are unlikely to have arisen if the null model is true and it can be concluded that the alternative hypothesis is more plausible. For this matter again 95% as the level of significance was used.

3.4 Results

3.4.1 Model Performance

The mean and standard deviation of $MABP$, P_{ETCO_2} and $MCBFV$ for the 13 subjects are given in Table 3.1.

	$MABP\ (mmHg)$	P_{ETCO_2} (%)	$MCBFV\ (cm/sec)$
Normocapnia	106.82 ± 19.24	5.54 ± 0.38	62.50 ± 11.14
Hypercapnia	112.28 ± 22.65	6.42 ± 0.31	76.58 ± 15.5

Table 3.1 mean ± standard deviation (STD) of $MABP$, P_{ETCO_2} and $MCBFV$, averaged over 13 subjects for normo- and hypercapnia

Typical data segments of ABP, P_{ETCO_2} and $CBFV$ are shown in Figure 3-7. The data are high-pass filtered, zero-meaned to eliminate their effect on intra-subject variability.

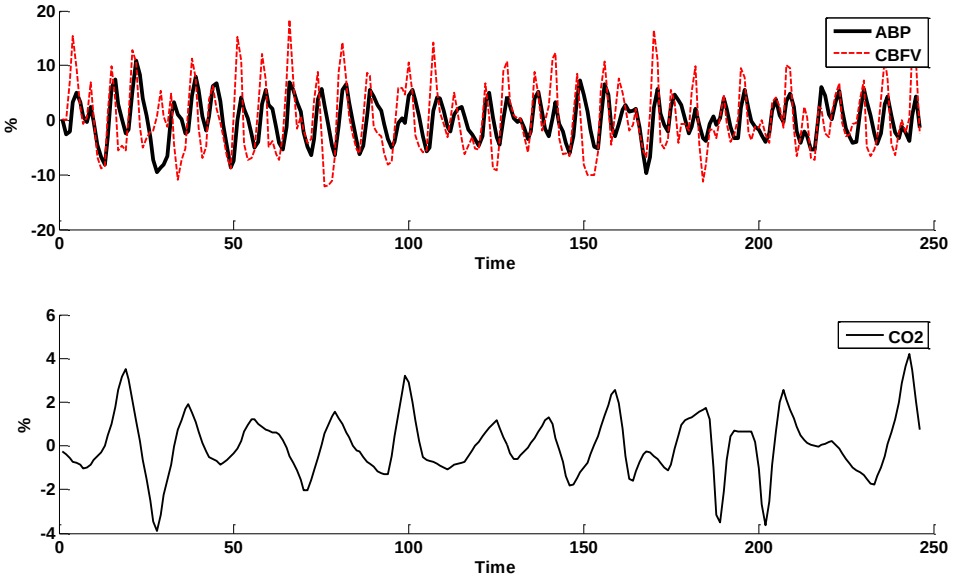

Figure 3-7 Representative segments of ABP, $CBFV$ and CO_2 for one measurement, Top: Cerebral Blood Flow Velocity ($CBFV$) and Arterial Blood Pressure (ABP), Bottom: CO_2. The phase lead characteristics of cerebral autoregulation can be seen in the top figure.

Model	Training NMSE%	Validation NMSE%	Mean number of Parameters used
k_{10} (linear, single-input)	16.21 ± 8.51	16.28 ± 7.08	6
k_{10},k_{01}(linear two-input)	14.49 ± 7.30	15.28 ± 6.44	7
k_{10},k_{20}(nonlinear; self-kernels, single-input (ABP))	15.13 ± 7.44	16.18 ± 7.17	6
k_{10},k_{11}(nonlinear; cross-kernels, two-inputs)	15.17 ± 7.48	16.14 ± 6.97	6
k_{10},k_{01}, k_{20}, k_{02}, k_{11}(nonlinear; self-kernels, cross-kernels, two-inputs)	14.16 ± 7.70	14.59 ± 6.13	9

Table 3.2 mean$\pm$ STD of $NMSE$ across all 13 subjects during training and validation, the last column shows the mean number of parameters that were used for the best combination of filter-banks for each measurement.

The average output prediction achieved in the training and validation for linear, nonlinear single-input (ABP), and linear, nonlinear two-input (ABP,P_{ETCO_2}) LVN models are presented in Table 3.2. The last column of the table show the average number of parameters used. The numbers of

parameters vary from one dataset to another; in some cases the best model based on the $NMSE$ was linear, single-input with only 3 filter-banks whilst in some other cases it was a nonlinear multi-input models with all second-order nonlinear terms, the average number of parameters for each model is given in this table.

For all the measurements, better performance (in terms of $NMSE$) was observed for training data, as expected from theory [101]. The results show that by adding P_{ETCO_2} the $NMSE$ of the LVN model prediction in the validation data reduces compared to single-input linear and nonlinear models. The average reduction in $NMSE$% from the single-input, linear model and single-input, nonlinear model to two-input nonlinear models are 10.38% and 9.0% in validation respectively, indicating the multivariate and nonlinear natures of cerebral regulation. However, the results also showed that for 8 measurements in the first half training, and 3 measurements in the second half training, linear single-input (ABP) gave the best performance in terms of the validation $NMSE$. It has to be considered that no significant test was done on the improvement of $NMSE$ from simpler models to the more sophisticated one. It has to be emphasized that the reason behind this was that as mentioned in section 3.1, the separation and distinction between NC and HC is the criteria in this work and data fit is not the aim in this chapter.

Finding the best number of filter-banks for each dataset is very time consuming as it requires scanning through all possible combinations of filter-banks, for this reason the number of filter-banks that resulted in the lowest mean $NMSE$ across all 13 subjects during NC and HC for linear and nonlinear kernels were chosen.

The results from comparing different models showed that cross-kernel term which is the interaction between two inputs can have great impact on the assessment of autoregulation. As the result of this and in order to show the great effect of the cross-term, the number of filter-banks in the cross-kernel term in model 4 ($M4$ as shown in Table 3.3) was increased. The results show that by fixing the model order the simpler the model the better it can be generalized for different datasets. It is also clear that more complex models (more parameters) perform well on the training data but are not generalizable and perform poorly on the validation set. These results (which are in agreement with the finding of others [110, 111]) suggest that little benefit is achieved from the more sophisticated models when it comes to the validation data and/or the variability between and within subjects (inter- and intra-subject variability) is large in comparison between the differences between models.

Model order							Total number of Parameters used	Training $NMSE\%$	Validation $NMSE\%$
Models	LW Lags	Linear ABP	Linear P_{ETCO_2}	Quadratic ABP	Quadratic P_{ETCO_2}	Cross term			
M1	12	4	0	0	0	0	5	32.4 ± 16.9	42.7 ± 28.5
M2	12	4	4	0	0	0	9	30.7 ± 15.8	81.2 ± 93.13
M3	20	4	4	0	0	4	25	29.8 ± 14.4	88.2 ± 104.2
M4	20	3	3	0	0	7	56	9.6 ± 11.0	230.8 ± 867.2
M5	20	4	4	4	4	4	45	8.6 ± 9.1	115.0 ± 816.6
H1	FIR- 2 coefficients						2	36.4 ±17.5	47.5±25.4

Table 3.3 $NMSE$ comparison for some pre-fixed models

In Figure 3-8 the measured $CBFV$ and the predicted $CBFV$ (whole of the recording) along with the contribution of linear and nonlinear self and cross-terms (with $k_{1,0}, k_{1,0}, k_{0,1}, k_{2,0}, k_{0,2}, k_{1,1}$) for a typical measurement (arbitrarily chosen) data set is shown. In Figure 3-8b the power spectrum for the same dataset is compared with the power spectrum for the entire model prediction and first-order models are compared. It can be seen from this figure that linear models can predict the $CBFV$ at higher frequencies whilst by adding nonlinearity low frequency components, can be explained, consistent with previous work [83].

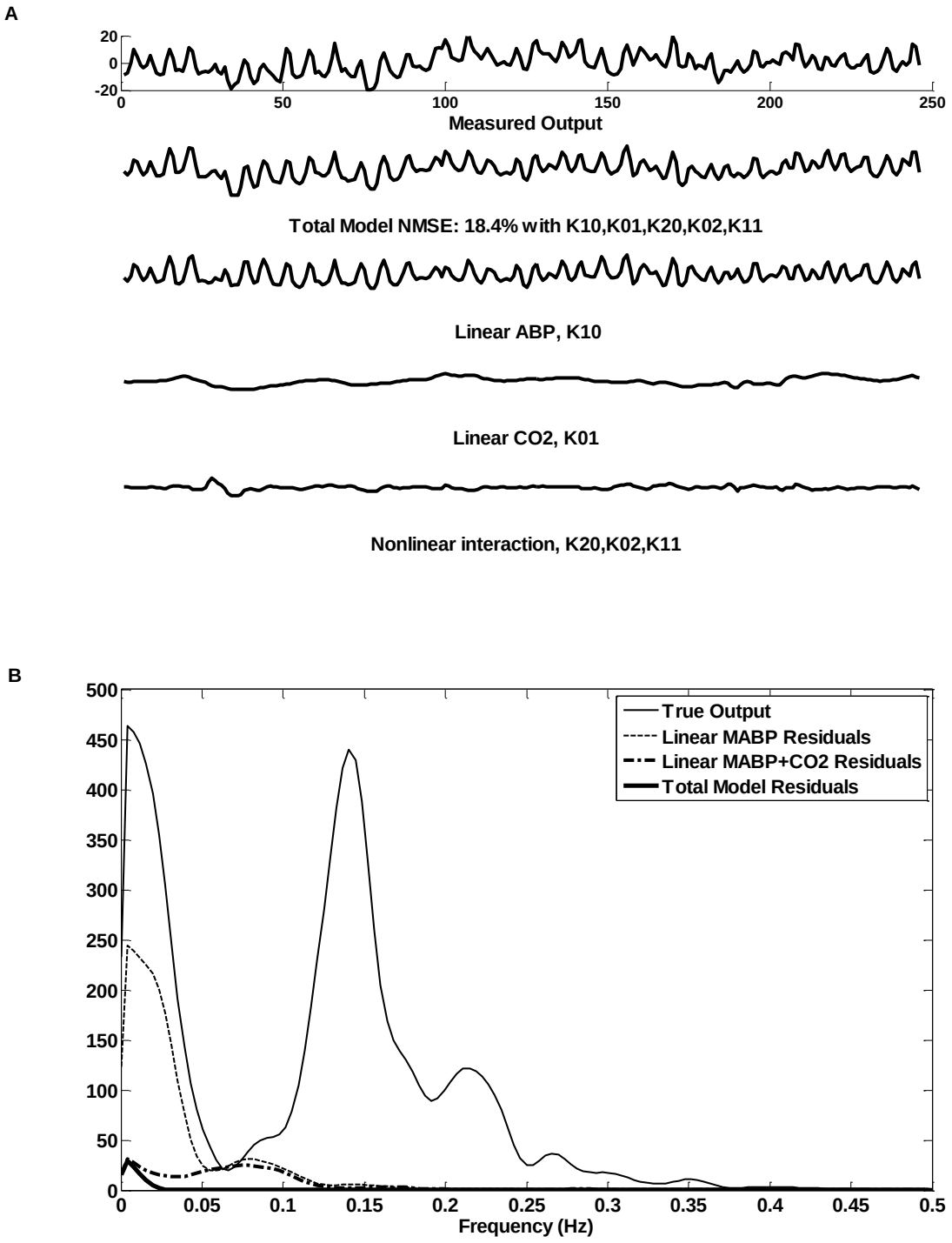

Figure 3-8 Top A) measured $CBFV$ and model prediction (total) for an arbitrary volunteer (randomly chosen), and the contribution of different terms for a typical data segment. B) Spectra of the desired output for the same volunteer and the model prediction (whole model with $k_{1,0}, k_{1,0}, k_{0,1}, k_{2,0}, k_{0,2}, k_{1,1}$) and single-input linear model, two-input linear models.

The contribution of different terms of the LVN are shown in Figure 3-8.A and Figure 3-8.B. In Figure 3-8.A, on the top trace the desired output for the model is shown. The second trace shows the model prediction (two-input, linear and nonlinear terms $k_{1,0}, k_{1,0}, k_{0,1}, k_{2,0}, k_{0,2}, k_{1,1}$), third trace corresponds to the single-input linear model ($ABP - CBFV, k_{1,0}, k_{1,0}$), fourth trace shows the

contribution of the linear P_{ETCO_2} $k_{1,0}$, $k_{0,1}$, and finally the last trace corresponds to the second-order nonlinear terms (self and cross terms as explained in eq.3.10; $k_{2,0}, k_{0,2}, k_{1,1}$). Over the whole thirteen subjects the average contribution of linear ABP toward the total model prediction power was 64% of the overall power of the model prediction, whilst this for linear P_{ETCO_2} and nonlinear terms was, 14% and 22% respectively which is in good agreement with the finding of Mitsis *et al.* [83] where he found 60% for linear ABP, and 17% for P_{ETCO_2} and 23% for nonlinear terms. It was also found that the cross-kernel terms between the ABP and P_{ETCO_2} had a strongest effect on the $NMSE$ than either of the second order self-kernels (15%). The spectra of the desired output ($CBFV$) and the residual of different model prediction for one set of data are shown in Figure 3-8.B, the results are consistent amongst all the subjects. It can be observed that most of the contribution of ABP is at higher frequencies ($> 0.04\ Hz$) which agrees with previous work [105] which states that most of the output signal ($CBFV$) can be explained linearly at these frequencies by $MABP$. It can also be seen that by having P_{ETCO_2} and nonlinearity (specially the cross-kernel terms) as the secondary input, the power spectra of the residual at these low frequencies can be reduced.

The first order $MABP$ Volterra kernel for one subject calculated using the LVN ($M5$) model is shown in Figure 3-9.A. The shape of the response is consistent among all the dataset where it starts with an overshoot, followed by an undershoot and gradually returns to the steady state and in agreement with the finding of previous work on the step response using other methods [32, 46, 52, 75]. The average first-order P_{ETCO_2} Volterra kernel again calculated using the LVN model is shown in Figure 3-9 for one typical subject. The slower response of first-order P_{ETCO_2} compared to $MABP$ is observable (around $10 - 15$ seconds) from these figures. Mitsis *el al.* [83] studied the standard deviation and frequency responses of the above kernels in great detail and observed high-pass and low-pass characteristics on the kernels in the frequency-domain respectively. However no clear method for assessing autoregulation was reported. It is in great clinical interest that a method to distinguish between normocapnia and hypercapnia can be achieved. As only model fitting cannot provide any insight to the question of assessment of autoregulation itself and should be considered as a middle stage when addressing the problem of distinguishing between intact and impaired autoregulation.

Typical second-order $MABP$ and P_{ECO_2} self-kernels and the corresponding cross-kernel are shown in Figure 3-9.B. The second-order kernels show (Figure 3-9.C, d and E) considerable variability amongst the datasets which is in agreement of the finding of Mitsis *el al.* [83]. As previously mentioned Mitsis also studied the frequency responses of the second-order kernels but no meaningful results as a criterion for CBF circulation was reported. In the next section the assessment of autoregulation

using different autoregulatory parameters extracted from the model proposed in this section is studied. The robustness of the models are examined using inter- and intra-subject variability to see the effect of different terms of LVN (linear ABP and P_{ETCO_2} and nonlinear terms).

In this section, the performance of different models entirely based on model fit is studied. The results in this section demonstrated that by having a second order multivariate models data fit can be improved. However it is mentioned that this improvement has little benefit in the validation data when a fix model for all the recordings is used (Table 3.3), however with precise choice of model orders for each recording individually the improvement in the validation set can also be achieved (Table 3.2). The contribution of different linear and nonlinear (each input and their interaction) inputs was also shown. However as mentioned in section 3.4.1, having a good model fit to the data, is not necessarily the best criteria for assessing models in the analysis of autoregulation. It the next section, in the different autoregulatory parameters that can be employed to assess the $CBFV$ control system are investigated.

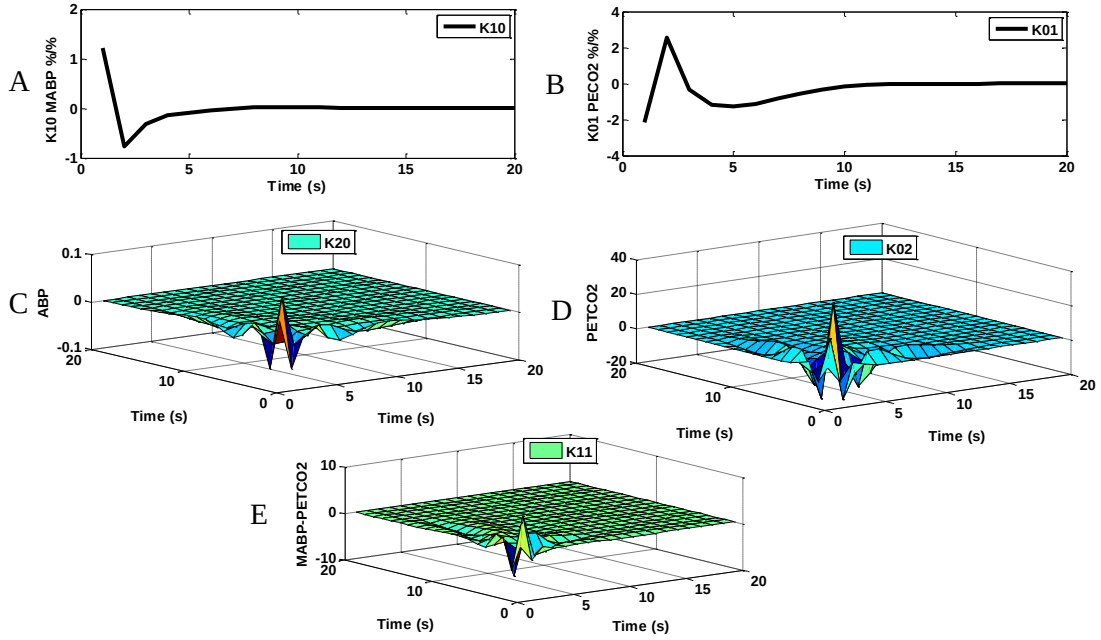

Figure 3-9 Typical Volterra kernels calculated for one dataset from the LVN ($M5$) method A) top left: first-order $MABP$ kernel B) top right: first-order P_{ETCO_2} C) middle left: second-order $MABP$ D) middle-right: second-order P_{ETCO_2} E) second-order cross-kernels $MABP$-P_{ETCO_2}

3.4.2 Assessment of autoregulation

The results from different autoregulatory parameters calculated from single-input (SI) model by Angarita-Jaimes *et al.* [104], showed that for all of the mentioned autoregulatory parameters (ARPs), significant differences were found between NC and HC using paired t-test, with $p < 0.05$, confirming that all respond to the impairement of autoregulation introduced through hypercapnia. In this paper it was found that $A1.5$, $A8$ (section 3.3.23.3.2) calculated from SI, linear and nonlinear models and $H1$ (section 5.3.1.2) provided good separation between NC and HC compared to other parameters studied. They also provided the smallest inter- and intra-subject variability. In order to reduce the number of parameters studied in this section, in this work, these parameters ($A1.5$, $A8$ and $H1$) from SI are used to be compared to the multi-input (MI) linear and nonlinear models,

SDn and $mSDn$ estimates, indicating inter- and intra-subject variability are presented for $A1.5$ and $A8$ calculated from all M models shown in Table 3.3 and $H1$. Variation measured from the mathematical approach discussed in section 3.3.3.3 for different autoregulatory parameters are used to calculate intra-subject variability.

*3.4.2.1 Inter-subject variability (**SDn**)*

A small value of SDn indicats small within group ($NC - HC$) dispersion relative to the difference between the groups, which is evidently the goal of suitable parameter as it provides the clearest distinction between normal and impaired autoregulation. The normalization also aims to allow different parameters with often quite different scales to be compared.

Angarita-Jaimes *et al.* [104] reported that $H1, A1.5$ (linear), $A8$ (nonlinear) and PCS had the lowest SDn. It was observed in this work that magnitude of the PPR at $8\,sec$ for linear and non-linear multivariate models ($M3-5$) has lower SDn (around 50%) compared to H1 (58%) shown in Figure 3-10. Wilcoxon matched pair test also shows significance difference between the magnitude of $A8$ between NC and HC (significance level of 5%) for all models. The results also show that $A1.5$ performed relatively well when a linear model is used but it has very high SDn when two-inputs especially when a nonlinear model is applied. $A8$ proves to be the best parameter when two-input nonlinear models are applied ($M3-5$) and shows to have considerably low model influence.

Previously the advantage of using these novel autoregulatory parameters was reported [104]. However, these results show that nonlinear two-input models, mainly when cross-kernels between

ABP and P_{ETCO_2} is included, have considerably lower inter-subject variability ($M3-5$ in Figure 3-10). This is in agreement with our finding in section 3.4.1.

The effect of cross-kernels is large, compared to self-kernels. The results show that even though some models may not fit the data well; either under-fitting such as FIR filter with only 2 lags or over-fitting. For example $M4$ and $M5$ in Table 3.3, they can provide good autoregulatory parameters ($A8$) as shown in Figure 3-10.

3.4.2.2 Intra-subject variability ($mSDn$)

As discussed in section 3.3.3.2, when the robustness of different autoregulatory parameters with different scales, and the influence of additive noise in the recordings is important, $mSDn$ can be evaluated. The results for intra-subject variability are shown in Figure 3-10 and Table 3.4.

Given that here thirteen standard deviation measurement are available in both NC and HC for each ARP, significance tests can be readily carried out whereas in the case of SDn, this was not possible. The intra-subject variability showed no significant difference between normo- and hypercapnia for any of the autoregulatory parameters studied here, using paired t-test ($p < 0.05$). No significance difference between the $mSDn$ measured from the parameters extracted from the linear model (single-input and two-inputs) was observed ($p \approx 29\%$) which is in agreement with Angarita-Jaimes *et al.* [104]. However pair wise comparison (t-test) between the parameters, showed that the parameters extracted from the models in Table 3.4, circled in Figure 3-10 are significantly different to all other parameters but not different to each other's ($p \approx 19\%$). The results showed that two-input nonlinear models ($M3-5$) provide the best intra-subject variability compared to all other methods and can be used to reduce the observed intra-subject variability.

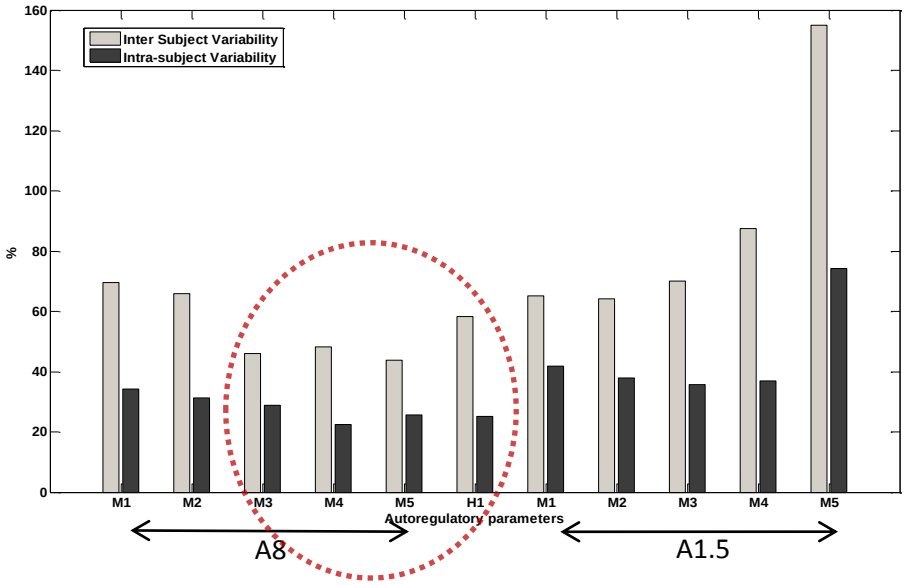

Figure 3-10 Different autoregulatory parameters extracted from different single-input, two-input linear and non-linear models. Dashed circle shows the autoregulatory parameters with the lowest SDn and $mSDn$. The first 5 columns shown with arrows, are for $A8$ autoregulatory parameter and the last 5 columns are for $A1.5$ autoregulatory parameter.

3.4.2.3 NC and HC significance difference

In the previous subsection, the variability of different autoregulatory parameters (ARP) for different models was studied to measure the robustness of different ARP measured from different models. The significance difference for intra-subject variability was also carried out. However it was not possible to test the significance difference for inter-subject variability as it is not possible to do a significant difference test between 2 numbers. Another criterion that can be measured to test the goodness of these ARP, is to test whether these ARP during NC and HC are significantly different or not.

The criterion of how many volunteers (of 13 tested) followed the expected trend of either lower ARP during NC compared to HC ($H1$ and $A1.5$) or vice versa ($A8$). The comparison between $H1$ during NC and HC shows that in 12 cases $H1$ was smaller in NC compared to HC which was in agreement with previous work [32, 52, 74, 75, 112]. The result for autoregulatory parameters extracted from the pressure pulse response ($A1.5$ and $A8$) are shown in Table 3.4. The results show that both of these ARP, perform very well (12 and 13 in most cases) when trend following is the criterion. The results also show that $A8$ extracted from models when cross-terms are used perform notably well with all the volunteers followed the same trend. This result again emphasizes the importance of cross-term when LVN is used. It has to be noted for parameters extracted from

the PPR, in multivariate and nonlinear models, the second-order and cross-kernel terms are set to zero in order to be able to study the response of the system to PP.

Model	Trend Follow		Number of patients passed the significant difference test		Intra-subject Variability ($mSDn$)		Inter-subject variability(SDn)	
FIR , 2 lags, second coefficient ($H1$)	12		10		25.22		58.20	
	$A1.5$	$A8$	$A1.5$	$A8$	$A1.5$	$A8$	$A1.5$	$A8$
$M1$	12	12	4	7	41.73	34.13	65.05	69.54
$M2$	12	12	6	9	37.87	31.39	64.19	65.78
$M3$	12	13	7	9	35.70	28.87	70.16	45.90
$M4$	12	13	6	11	36.91	22.48	87.41	48.20
$M5$	8	13	5	8	74.14	25.73	155.04	43.69

Table 3.4 Summary of analysis between different autoregulatory parameters from different models, lags in above table explain the length of the impulse response. The second column titled with Trend Follow, shows how many subjects out of 13 follow the expected trend; third column illustrates how many subjects passed the significance difference test, and fourth and fifth columns show the inter- and intra-subject variability for different models.

The results from the significant difference test mentioned in section 3.3.3.4 is shown in the third column of Table 3.4 (labeled as 'number of patients passed the significant difference test'). The results show that $A1.5$ extracted from all the models did not perform well as a distinction between normo- and hypercapnia using this significance test (≈ 6 subject passed the significance different test). However $A8$ and $H1$ perform notably well as can be seen in Table 3.4 (10 and 11 respectively).

Up to this point, the performance of various models based on the $NMSE$ and different ARPs, based on their robustness quantified by their variability between and within subjects has been studied. However by looking at Table 3.4, it is very hard to say which ARP from which model is superior to the others. Both $H1$ and $A8$ perform notably well when "Trend Following" or "Significance Test" or even when inter- and intra-subject variability's are the criterions. It can be argued that $M3$ to $M5$ have better performance, compared to $H1$ when variability (especially inter-subject) is considered (46% and 58% respectively). However the significance of this difference is questionable, or even more doubtfully in the case of $M4$ to $M5$ models (48% and 44%).

3.4.2.4 Randomization test

A summary of the results for the randomization test is shown in Table 3.5. Pseudo-random number generator was used to generate 4000 repetitions to determine random assignment of 26 test scores to two groups of 13, and randomization can be made based on that.

Model		Randomization result significance $level$ % (4000 runs)					
		$H1$	$M1$	$M2$	$M3$	$M4$	$M5$
$H1$	SDn	49.62	48.42	36.9	35.37	29.15	47.95
	$mSDn$	49.9	28.8	46	44.07	41.17	38.55
$M1$	SDn	46.72	49.47	26.37	17	11.82	42.9
	$mSDn$	28.75	49.9	44.7	9.8	9.05	4.9
$M2$	SDn	37.55	26.67	49.42	38.87	27.82	26.15
	$mSDn$	42.32	44.67	48	14.17	11.45	6.75
$M3$	SDn	35.3	17.62	40.17	49.12	35.85	21.85
	$mSDn$	45.02	9.55	14.55	49.85	42.45	42.92
$M4$	SDn	27.02	12.02	29.12	35.17	49.37	15.47
	$mSDn$	45.02	9.47	11.85	40.12	49.25	35.32
$M5$	SDn	48.55	44.17	25.5	20.4	16.35	49.62
	$mSDn$	38.92	4.62	6.37	41.37	35.3	49.3

Table 3.5 Results from randomization test on the inter- and intra-subject variability for different models. The results show that no model is significantly different compared with others methods

It can be seen from Table 3.5 that the result of randomizing inter- or intra-subject variability with inter- or intra-subject variability of the same model, is consistent with chance (50%). The results show that no inter- or intra-subject variability calculated from any ARP measured from any model is significantly different to all other methods, in other words some ARP from some methods show significant differences with other ARP from other methods (e.g. intra-subject variability of $M1$ and $M5 = 4.62\%$, or intra-subject variability of $M2$ and $M5 = 6.3\%$) but no method in particular provides strong evidence against the null model, and therefore in favor of the alternative. It has to be noted that it is expected that the above matrix will be symmetric with respect to its diagonal, and the slight differences in the values are the result of using a finite numbers of realisations of the pseudo random generator.

The results also shows that by having a more complete and sophisticated models that provides slightly better results, still a simple model $H1$ performs fairly well (29.15% between $H1$ and $M4$). In other words even though a complex model (nonlinear multivariate model) provides better inter- and

intra-subject variability in these set of measurements, there is no solid evidence that the same model would still provide the same results in other sets of data. In other words, there is no solid evidence that the improvement using nonlinear multivariate models that provided improvement in assessment of autoregulation (less inter- and intra-subject variability) can be repeated in other datasets. It can also be said that no model performed significantly better than the other models.

3.5 Discussion

Spontaneous fluctuations of $MABP$ and $MCBFV$ have been proven to be useful in analyzing the characteristics of autoregulation [2, 35, 69, 73, 74, 98, 113]. However cerebral autoregulation is affected by many other physiological mechanisms [5, 29, 46].

The reactivity of cerebral vessels to CO_2 changes is one of these parameters. Changes in arterial CO_2 tension causes vascular responses in cerebral vessels [29], and this reactivity of cerebral vessels, causes changes in CBF regulation (hypercapnia can cause vasodilation and hypocapnia causes vasoconstriction) [46, 90].

In this chapter, the problem of effective modeling of cerebral autoregulation using spontaneous variation in $MABP$ and P_{ETCO_2} as inputs and $CBFV$ as the output was studied. It has been reported [46] that $MABP - CBFV$ relationship exhibits considerable nonlinearities specially at low frequencies ($< 0.04\ Hz$). The combination of Laguerre expansion with feedforward artificial neural networks in the form of Laguerre-Volterra network, which has been shown to provide a good estimation of nonlinear system with short input-output records, was used to model the cerebral autoregulation system. At first, the characteristics of the LVN were estimated separately for each dataset (all 26 measurements) using $NMSE$ (Table 3.3). Alpha value and consequently number of filterbanks for each input with $NMSE$ as the criterion for each measurement are estimated in the network based on the data and memory bandwidth. It was found that by having two-input nonlinear (second-order) models the performance of the model based on the $NMSE$ improved by 10.38% in validation in relation to the single-input linear model. This result initiated study of the existence of nonlinearity in the autoregulatory system. It was also found that adding nonlinearity or P_{ETCO_2} in all the datasets will always improve our $NMSE$ in the training (as more parameters are involved) but may not necessarily improve our $NMSE$ on the validation segment. It was also shown that the maximum number of filterbanks that reduced the $NMSE$ in the validation data, was twenty whilst this was only 3 for nonlinear ABP and P_{ETCO_2} and the cross-term. This maybe may be due to the small size of the data set. Faster response of P_{ETCO_2} compared to previous works (10 to 15 seconds)

compared to 20 seconds found by some other authors [23, 29, 83, 114]) was observed in this work, however it is unclear how fast autoregulation changes as a result of the transients in partial pressure of CO_2 in the blood. The time required for autoregulation to become impaired following hypercapnia, and the recovery on return to normocapnia is unclear.

By looking at the contribution of each input towards the final model prediction Figure 3-8.A, it was found that $MABP$ explained the biggest fraction of $MCBFV$ variability (64%) which as it can be seen in Figure 3-8.B was at high frequencies. Linear P_{ETCO_2} explained mostly low frequency ranges and had the contribution of 14%, whilst the self- and cross-kernels nonlinear terms had more effect in term of contribution toward power spectra of the predicted $CBFV$ than linear P_{ETCO_2} with the contribution of 22%. It was also observed (Table 3.3) that cross-kernels between $MABP$-P_{ETCO_2} had the most effect amongst the nonlinear terms (2^{nd} order self- and cross-terms for P_{ETCO_2} and ABP) which indicate the importance of this term (in agreement with [83]). The spectral analysis of the $MCBFV$ and the model prediction and the spectra of the residual from different terms of the Laguerre-Volterra network showed that most of the effect of P_{ETCO_2} and nonlinearity lies at low frequencies.

Different indices for the assessment of dynamic cerebral autoregulation base on the changes in P_{ETCO_2} levels which provokes temporary impairment of autoregulation was then studied. The response to a cosine shape input modulated by a Gaussian, (pressure pulse response, PPR) which was introduced by Simpson *et al.* [74] was used, which is more physiologically realistic compared to step or impulse inputs. The results (Figure 3-5) showed the phase-shift characteristics expected of cerebral autoregulation. Next the parameters that provided us with the best separation between good and impaired autoregulation were chosen. Amplitude at 1.5 seconds and 8 seconds ($A1.5$ and $A8$) offered good distinction between intact and impaired autoregulation.

The primary goal of this chapter was to test the performance of different models; however this should only be an intermediate step in answering the question of how to quantify autoregulation when only spontaneous fluctuations in ABP and $CBFV$ are present. High-inter subject variability and poor reproductively have been reported [47, 74]. This work was carried on by looking at a novel approach for assessing autoregulatory parameters using a criterion, the ability to distinguish between NC and HC. This was done by performing a formal analysis to measure the standard deviation using the covariance matrix analysis.

It was found that $A8$ when extracted from two-input nonlinear models, in particular when the cross-kernel terms were included provided the lowest variability (in terms of inter- and intra-subject,

Figure 3-10). The good performance of $H1$ is also very notable as can be seen in Figure 3-10. $A8$ extracted from two-input nonlinear models and $H1$ followed the expected trend (increase in $H1$ and decrease in $A8$ from NC to HC) in 12 and 13 out of 13 subjects respectively.

Intra-subject variability has been reported previously by other authors using repeated recording with only spontaneous variations [47], controlled breathing recordings with a sliding window [110] or repeated thigh cuff tests [90]. Most of the mentioned methods use ARI and showed large intra-subject variability. In this work it was shown that again $A8$ extracted from two-input nonlinear models, especially when cross-kernels were employed alongside $H1$, provided the smallest change of the parameter's magnitude. These results suggest that having model fit ($NMSE$) alone, as shown in Table 3.3, is not a good indicator for assessing autoregulation as $H1$ coming from an under-fitting model (poor training and validation $NMSE$), or $A8$ coming from an over-fitting model (good training and poor validation $NMSE$) $M5$ (Table 3.3), provided the best distinction between intact and impaired autoregulation.

3.5.1 Limitations

It is obvious that a large number of possible parameters can be used to assess autoregulation. In this work only a relatively small number of these were studied, and the current work can thus only indicate the best methods among those analyzed here. In the paper by Angarita-Jaimes *et al.* [104] different autoregulatory parameters, including parameters taken directly from the model ($H1$) were investigated but none were superior to ones presented here. The small dataset (13 volunteers) and small sample size (around 300 seconds) were the main limitations of the study presented in this chapter. It can be argued that the results provided here from different methods are relative to the effect in this particular dataset in question. However the large difference reported from different methods here, can be taken as a hint of which autoregulatory parameters should be considered for further research with a larger dataset. Repeated recordings of spontaneous changes in P_{ETCO_2} and baseline (no P_{ETCO_2}) from the same volunteers should allow testing the repeatability of the methods and more robust estimates of the inter- and intra-subject variability.

There are other factors in addition to noise in the signals, the difference between volunteers and the effect of P_{ETCO_2} which were studied in this chapter, that should be considered when investigating the large scatter reported in the results. Some of these factors are the effect of other physiological

variables such as: P_{O_2}, cerebral metabolic rate, intracranial and venous pressure and brain activity [5, 32, 46].

$H1$ presented in this work measured from a very simple model, provided small variation in term of inter- and intra-subject variability (SDn and $mSDn$). One main advantage of this parameter is its small number of free parameters which does not require big data sample and can be applied to short data recordings.

The effect of large variations in P_{ETCO_2} and ABP should also be considered and to test whether these changes can provide more robust results and smaller inter- and intra-subject variability. This will be address in the next chapter.

3.6 Conclusion

In this chapter, the performance of different models (linear and nonlinear single-input, linear and nonlinear two-inputs) was compared and different autoregulatory parameters were measured. Some of them were extracted directly from the model ($H1$) and some were extracted from the proposed pressure pulse response ($A1.5$ and $A8$). The $A8$ extracted from nonlinear two-input models showed less variability (inter- and intra-subject) when compared to other autoregulatory parameters. This parameter provided the best distinction between intact and impaired autoregulation. However a very simple parameter ($H1$) provided notable good result in term of small coefficient of variation (SDn and $mSDn$) with the added advantage of suitability for use in a very short dataset.

Chapter 4：Evaluation of autoregulation using subspace distance

4.1 Introduction

In the previous chapter, data fit of different Wiener method with the Laguerre expansion technique for all the possible combinations of linear/nonlinear single-input ($ABP \rightarrow CBFV$) and linear/nonlinear two-input (ABP,$P_{ETCO_2} \rightarrow CBFV$) models was studied. Next the inter- and intra-subject variability of different autoregulatory parameters (pressure pulse and $H1$) was compared. It was found that the pressure pulse (PP) as a new autoregulatory parameter extracted from nonlinear two-input model was superior to other autoregulatory parameters and provided very good separation between intact and impaired autoregulation and showed to be a robust parameter to the system noise, amongst other possible autoregulatory parameters studied in section 2.10, which have shown to provide good assessment of autoregulation by previous authors [73-75] on the dataset examined. However as mentioned in section 3.6, there are other parameters that have been proposed in both time- and frequency-domain in the literature which represent the status of cerebral autoregulation which were not examined. These parameters are usually extracted from the estimated step or frequency responses [47, 52, 74, 75] as described in Chapter 3.

In all the above methods, to address the assessment of autoregulation, there is an intermediate step between black box model and setting the autoregulatory parameter which is to test the performance of the model or to get a response of the system (step- or impulse-response) and extract a parameter from it. However we showed in the previous chapter that good data-fit does not necessary lead to good assessment of autoregulation, as both under-fitting; large $NMSE$ in both training and validation (FIR filter with only 2 lags) and over-fitting; small $NMSE$ in training and large in validation (nonlinear two-input model), provided the best distinction between healthy and impaired autoregulation on the dataset examined (Table 3.3).

A major challenge of the methods used for the assessment of autoregulation is the issue of choosing an autoregulatory parameter that could work on different datasets. Furthermore the lack of a “gold standard” for assessment of dynamic cerebral autoregulation does not allow a robust reference, to which alternative methods could be compared. Autoregulatory parameters are sensitive to many physiological variables that can influence CBF (P_{ETCO_2}, brain activity, O_2 content, temperature, etc.)

as has already been observed by other authors [52, 90, 92]. Furthermore, there is a dearth of studies using multiple methods or performing inter-method comparisons [32]. Dynamic cerebral autoregulation can also vary from one patient to another and over time [115]. For example, the choice of phase at $0.1\ Hz$ proposed by Giller *et al.* [73] has been extensively used, but there is no physiological proof that this is the best autoregulatory parameter for every patient. As another example in the previous chapter, it was proposed that careful choice of index (the amplitude at 1.5 seconds or 8 seconds from the PPR) can lead to significant improvement in the ability to distinguish between normal and impaired autoregulation, but large inter- and intra-individual variations in result persist and these parameters were chosen primarily based on visual inspection from the response of the system.

So far all the work that has been done on dynamic assessment of autoregulation has been concentrated on choosing an autoregulatory parameter extracted from different methods from either time-domain analysis such as the correlation coefficient (Mx) between averaged $CBFV$ and ABP over time [73]. Some other works used autoregulatory index (ARI) calculated by evaluating the set of models proposed by Tiecks *et al.* [5] using the parameter values given by the author (for each recording, the model by the authors was applied to $\%ABP$, and the model which provided the highest correlation coefficient between the measured $\%CBFV$ and the generated velocity determined the ARI) [5]. Frequency domain analysis; transfer function analyses (TFA), on gain, coherence and phase [32, 46, 52, 75, 116] or multi-input models (ABP, P_{ETCO_2}) [35, 46, 90, 93, 113, 117]. Most of the autoregulatory parameters are usually extracted from the estimated step or frequency responses [47, 52, 73, 74].

However, this autoregulatory parameter requires long stable TCD signal, typically more than an hour, which is very hard to achieve. Other challenge with Mx is that it does not measure CBF directly and it is only surrogate measure of autoregulation and the observed changes may be as the result of factors that do not have a direct translation to CBF and could be as the result of the calculation method [118].

The objective of this chapter is to propose and test a new data-driven method for assessing autoregulation using subspace distance (SSD) between two autoregressive moving average ($ARMA$) models, without studying primarily the performance of the models in term of data fit and choosing an arbitrarily autoregulatory parameter by visual inspection as used in section 3.3.2.

Martin *et al.* [119] showed that by treating an $ARMA$ model as a complex rational function, one can define a metric on the set of complex rational function, and so measure the distance between two

$ARMA$ models. The subspace distance (SSD) has been used in dynamic models [120], observability of linear hybrid system [121], bioengineering humans [122, 123]. Bissacco *et al.* [123] used SSD to recognize different types of human gait in the space of dynamical systems.

Here, SSD is used to find the distance between new a measurement which is required to be analysed to a group of normocapnia and also to a group of hypercapnia, and decide which group that measurement belongs to by finding which set provides the smallest overall distance. This would also help to construct the distance matrix and perform cluster analysis. In order to test whether this approach is feasible to our system, it is first tested on Tiecks model as it is an acceptable model of autoregulation. Later this method is applied to measure data from volunteers to test the performance of this new approach.

In this chapter, the search for improved analysis is extended, using the data-driven approach based on the subspace distance (SSD) (section 4.3.4.2). The performance of this method is compared to alternatives previously proposed methods including the phase of the frequency response at $0.1\ Hz$ ($P1$) and the 2^{nd} parameter of a 2^{nd} order FIR model ($H1$), which is used in previous studies [46, 52, 73-75] and results from Chapter 3, showed this to be among the best indexes in terms of intra- and inter-subject variability and its ability to distinguish between normo and hypercapnia.

4.2 Subjects and measurements

Signals were recorded from 30 subjects ($25-55$ years old); 27 of them came back for the second recording and with the three subjects that only participated in one session total of 57 recordings were used for this study altogether. Subjects were in the supine position, free from any known cerebrovascular or cardiovascular diseases. The data was collected in the Leicester Royal Infirmary by Dr E. Katsogridakis. ABP was monitored and measured non-invasively using the arterial volume clamping method (Finometer, Ohmeda). Freehand transcranial Doppler (Companion III, Viasys Healthcare) identification of the both middle cerebral arteries (MCA) was performed using $2\ MHz$ probe, which was then held in place by a custom built head frame. A face-mask was connected to the CO_2 delivery system, and by a line to a capnograph (Datex, Normocap 200) to measure end-tidal CO_2 levels. Data were recorded at rest (with only spontaneous changes in ABP) in both normocapnia and hypercapnia (inhalation of $5\%\ CO_2$ for 5 minutes). The mean arterial ABP and $CBFV$ was then calculated by low-pass filtering (cut-off frequency $0.4\ Hz$; zero phase filter) and normalized by its mean value, to give the relative change in these signals. The resultant signals were resampled at $1\ Hz$.

4.3 Methods

In this chapter, the subspace distance (SSD) as a model to measure the distance between two $ARMA$ models is studied. It is shown that the Tiecks can be approximated by a second-order $ARMA$ model. The SSD approach is used to measure the distance between different Tiecks models using their second-order $ARMA$ coefficients to validate the SSD on the dynamic CA system. In order to show the advantage of using SSD by going to the cepstrum domain (section 4.3.4.1), the distance between two $ARMA$ models in the frequency domain is also measured and the results are compared with the findings from the SSD. In the following section, the SSD for measured data is calculated and the distance between different conditions of the volunteers (NC and HC) is measured.

In order to compare the result from SSD to the chosen autoregulatory parameters ($P1$ and $H1$), firstly for all possible pairs of recordings, the distance calculated by SSD for $ARMA$ models and also alternative autoregulatory parameters ($P1$ and $H1$) (all three autoregulatory parameters) are calculated. The distances between all normocapnia, hypercapnia and between normpcapnia and hypercapnia ($NC_{SSD/P1/H1} - NC_{SSD/P1/H1}$,$HC_{SSD/p1/H1} - HC_{SSD/P1/H1}$ and $NC_{SSD/p1/H1} - HC_{SSD/p1/H1}$) measurements are calculated, and the average values are computed as the cluster for that pair and these values are compared with each other (section 4.3.5.1). The $LOOCV$ approach is then used to calculate the average value for each of these groups ($NC_{SSD/p1/H1}$ and $HC_{SSD/p1/H1}$) and then measure the distance between the out dataset and the average value for each of these groups and map that specific measurement to either one of these groups. Finally, cluster separation was used to see which of our used autoregulatory parameters would give us better inter/intra-subject variability.

4.3.1 System Identification

System identification is the field of modeling dynamic system from experimental data [124]. A dynamic system is driven by input variables $x_i(t)$ which are controllable and usually contains of disturbance $v(t)$ which can be controlled, and an output $y(t)$. In the case, our application, the input is arterial blood pressure (ABP) and the output is cerebral blood flow velocity ($CBFV$).

$ARMA$ model, expresses a system function of a discretely sampled process as a rational function in the z −domain. Martin *et al.* [119] showed that by treating an $ARMA$ model as a complex rational function, one can define a metric on the set of complex rational functions, and measure the distance between two $ARMA$ models.

$ARMA$ models with ABP as input and $CBFV$ as output are used to fit data using a least-squares approach for each set of recordings. The estimated filter parameters provide the input to the sub-space distance method. In order to see if SSD can be applied to the assessment of autoregulation, by considering Tiecks model (section 2.11.1), and calculating the $ARMA$ coefficents (re-expressing the Tiecks model in $ARMA$ form) for different ARI's the accuracy of the measured coefficients are measured by comparing the step response of the $ARMA$ models, with the original Tiecks model. The $ARMA$ approach is then used to model real $ABP - CBFV$ relationship and assessing SSD.

4.3.2 Linear parametric models

The general model of a single input and single output system is given by [124]

$$y(n) = G(q)x(n) + H(q)e(n) \tag{4.1}$$

where x,y and e are system input, output and disturbance respectively.

where

$$H(q) = \frac{B(q)}{A(q)} \tag{4.2}$$

$$\mathrm{G(q)} = \frac{\mathrm{C(q)}}{\mathrm{A(q)}} \tag{4.3}$$

and

$$A(q) = 1 + a_1 q^{-1} + \cdots a_{n_a} q^{-na} \tag{4.4}$$

$$B(q) = b_1 q^{-1} + \cdots b_{nb} q^{-nb} \tag{4.5}$$

$$C(q) = 1 + c_1 q^{-1} + \cdots c_{nc} q^{-nc} \tag{4.6}$$

where $a_{1\ldots na}$ and $b_{1\ldots nb}$ and $c_{1\ldots nc}$ are the parameters of the model and 4.1 can be rewritten as

$$A(q)y(n) = B(q)x(n) + C(q)e(n) \quad 4.7$$

The above equation is known as an autoregressive moving average model with an exogenous signal ($ARMAX$ model; Figure 4-1)

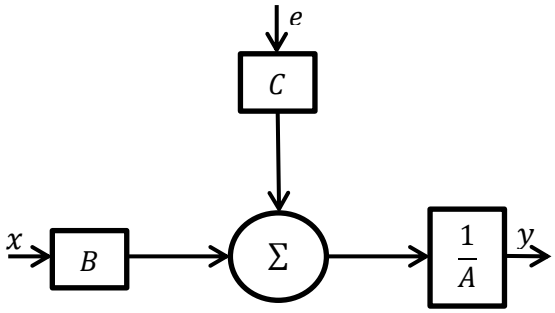

Figure 4-1 $ARMAX$ model

There are several special cases of $ARMAX$ models which are described below:

An autoregressive (AR) model is obtained when $nb = nc = 0$.

$$A(q)y(n) = x(n) \quad 4.8$$

A moving average (MA) model is obtained with $na = nc = 0$.

$$y(n) = B(q)x(n) \quad 4.9$$

An autoregressive moving average ($ARMA$) is the combination of the previous two models and is given when $nc = 0$

$$A(q)y(n) = B(q)x(n) \quad 4.10$$

Another case is when $nb = 0$ is known as autoregressive with an exogenous input (ARX).

$$A(q)y(n) = B(q)x(n) + e(n) \quad 4.11$$

Tiecks autoregulation index (ARI) model (section 4.3.3) is essentially a second order state-space model.

In this work a simple second-order $ARMA$ model ($na = nb = 2$) which is sufficient to re-express the Tiecks model (section 4.3.3) as shown by [47] is used.

Suppose one of above models have been chosen, and parameterized as a model structure which can be rewritten as:

$$y(t) = \varphi^T(t)\theta + e(t) \quad 4.12$$

Where θ is the parameter vector and φ is the regression vector. The e in above equation denotes the prediction error. For the case of $ARMA$ model (eq.4.11), $\varphi(n)$ is given by:

$$\varphi^T(n) = [-y(n-1) \dots - y(n-na)\ x(n) \dots x(n-nb)] \quad 4.13$$

$$\theta = [a_1 \dots a_{na} b_0 \dots b_{nb}]^T \quad 4.14$$

There are different approaches that can be taken to measure the coefficients. Least mean square method is most commonly used.

Least mean square estimate aims to minimize the sum of squared prediction error, which is given by:

$$\hat{\theta} = \arg(min V_N(\theta)) \quad 4.15$$

Where V_N is known as loss function, given by:

$$V_N(\theta) = \frac{1}{N}\sum_{n=1}^{N} e^2(n) \quad 4.16$$

The parameter vector θ that minimises the sum of squared equation errors is given by

$$\hat{\theta} = \left[\frac{1}{N}\sum_{n=1}^{N} \varphi(n)\varphi^T(n)\right]^{-1} [\frac{1}{N}\sum_{n=1}^{N} \varphi(n)y(n)] \quad 4.17$$

$$\hat{y}(t) = \varphi^T(t)\hat{\theta} \quad 4.18$$

Derived from the general form of the $ARMA$ model shown in eq.4.11, the second-order $ARMA$ model can be expressed as:

$$\hat{y}(n) = \frac{b_0 + b_1 q^{-1} + b_2 q^{-2}}{1 + a_1 q^{-1} + a_2 q^{-2}} x(n) \quad 4.19$$

Where a_1, a_2, b_0, b_1, b_2 are the filter coefficients.

The transfer function of a second-order $ARMA$ model can be derived from eq.4.19 as:

$$G(q) = \frac{b_0 + b_1 q^{-1} + b_2 q^{-2}}{1 + a_1 q^{-1} + a_2 q^{-2}} \quad 4.20$$

In the next subsection, the coefficients for a second-order $ARMA$ for 10 pre-defined step responses of the Tiecks model [5] is calculated.

4.3.3 Second-order $ARMA$ model of Tiecks models

The $10\ CBFV$ step responses for the ARI in the Tiecks model [5], were originally defined at $f_0 = 10\ Hz$, however they can be calculated at any desired frequency. The approach for measuring the $ARMA$ coefficient from Tiecks model is shown in appendix III. The a_1, a_2, b_0, b_1, b_2 coefficients of the $ARMA$ model coefficients for 10 different Tiecks models based on the values of T, D, K and f_0 were calculated and are shown in Table 4.1.

Model (ARI)	a_1	a_2	b_0	b_1	b_2
0	0	0	1	0	0
1	-1.8375	0.8400	1	-1.8380	0.8400
2	-1.8475	0.8500	1	-1.8485	0.8500
3	-1.8825	0.8850	1	-1.8840	0.8850
4	-1.9075	0.9100	1	-1.9095	0.9100
5	-1.9183	0.9211	1	-1.9208	0.9211
6	-1.9148	0.9187	1	-1.9185	0.9187
7	-1.9014	0.9083	1	-1.9081	0.9083
8	-1.8672	0.8805	1	-1.8801	0.8805
9	-1.8225	0.8462	1	-1.8457	0.8462

Table 4.1 $ARMA$ coefficients for different Tiecks models $f_0 = 10\ Hz$

The result of the agreement between different using the 10 pre-defined step responses and 10 different coefficients using the $ARMA$ model (Table 4.1) of these models is shown in Figure 4-2.

The Tiecks model originally is defined at $10\ Hz$, however in this work for the assessment of autoregulation, recordings of ABP and $CBFV$ were down-sampled to $1\ Hz$ after being have a low-pass filter applied to them with a Btterworth filter (3^{rd} order) with the cutoff frequency of $0.4\ Hz$. The step responses calculated from their corresponding $ARMA$ models at $10\ Hz$ and $1\ Hz$ are shown in Figure 4-2. The note that has to be considered is that as mentioned before, in the original proposed model by Tiecks *et al.* [5], the sampling frequency of $10\ Hz$ was used. However, different sampling frequency can be used in the original second-order differential equations proposed by

Tiecks *et al.* [5]. The only point that has to be considered is that if lower sampling frequency is used ($f = 1\ Hz$ as used in most of the work in this thesis).

In the next section we introduce the subspace distance proposed by Martin *et al.* [119] as a novel approach to measure the distance between two $ARMA$ models. We use this approach to measure the distances between different $ARMA$ models shown in Table 4.1, measured from the Tiecks models.

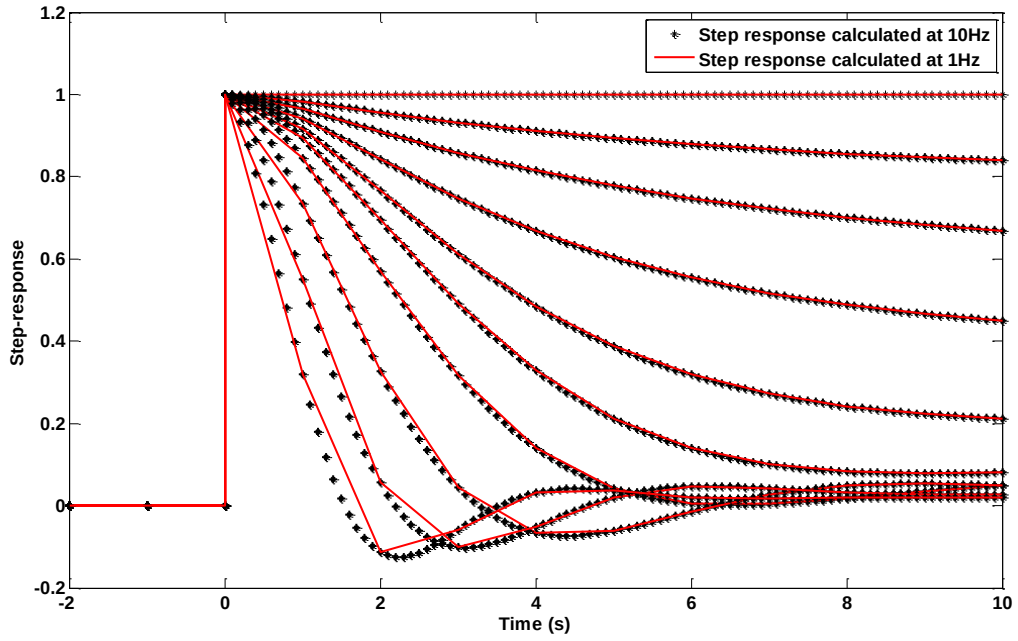

Figure 4-2 Agreement between step responses calculated from $ARMA$ models from Tiecks method at $10Hz$ and $1Hz$

4.3.4 Subspace distance

In the previous section it was shown that the well-established Tiecks model can be realized as an $ARMA$ model with different ARI in the models, corresponding to different $ARMA$ coefficients (Table 4.1).

Eq.4.19 can be written in the z-domain in term of the system function as:

$$H(z) = \frac{\sum_{j=0}^{q} b_j z^{-j}}{\sum_{j=0}^{p} a_j z^{-j}} = \frac{\prod_{i=1}^{q}(1-\beta_i/z)}{\prod_{i=1}^{p}(1-\alpha_i/z)} \quad 4.21$$

Where a_0 and b_0 are defined to be one in this chapter. The α_i and β_i are the positions of the poles and zeros of the model and H is a rational function of z.

Section 4.3.3 described the coefficients a_j and b_j for the Tiecks models for different ARIs. However addressing the question of how two $ARMA$ models can be compared, to find a metric for the space for $ARMA$ models would be very useful.

One approach is to compute $ARMA$ models for subject with intact and impaired autoregulation and then, for a new patient, the $ARMA$ model can be fitted and compared with these two general models and whichever gives the smaller distance would provide an indication of the stage of the new patient.

Martin *et al.* [119] proposed that what is actually required is a method for comparing two spectra. He introduced a purely algebraic approach to model comparison in the cepstrum domain.

4.3.4.1 Cepstrum

Cepstrum has been widely used in literature in processing signals containing echoes in seismology, for measuring properties of reflecting surfaces, in loudspeaker design, for dereverberation, restoration of acoustic recording, estimating parameters of the speech models, or calculating the minimum phase spectrum corresponding to a given log amplitude spectrum [125].

The cepstrum is the inverse Fourier transform of the log magnitude of the Fourier transform (DFT) of a signal.

$$C_n = F^{-1}(log|F(x(n))|) \quad 4.22$$

Where F is the DFT and F^{-1} is the inverse DFT. It has to be noted that C_n in above equation is the cepstrum coefficients and are not the same as eq.4.6 and from this point in this chapter are regarded as the cepstrum coefficients.

As defined in eq.4.22, the cepstrum is the inverse Fourier transform of the logarithm of power spectrum of a signal. If the signal of the system is discrete then its log-spectrum is periodic and the inverse Fourier transform is just a Fourier series

$$\ln(P(z)) = \sum_{n\epsilon\mathbb{Z}} C_n z^{-n} \qquad 4.23$$

The note that has to be considered is that the independent variable n, of the cepstrum has the dimension of time, and is known as "quefrency". "High quefrency" represents rapid fluctuations (small frequency spacing) in the spectrum and "low quefrency" represents slow changes (large frequency spacing) with frequency. Note that quefrency does not say anything about the absolute frequency but only about frequency spacing.

The cepstrum of a discrete-time process is a Hermitian sequence[14] $(C_n)_{n\in\mathbb{Z}}, C_n^* = C_{-n}$ and it is a relatively simple function of the model poles and zeros [126]. Using an $ARMA$ model in the time-domain requires convolution between the time-domain signals, which gives us multiplication in the frequency-domain, and thus addition in the cepstrum-domain. This can simplify the calculation when filters are used for system identification.

*4.3.4.2 Subspace distance (**SSD**)*

Martin *et al.* [119] defines a metric for the set of single input single output ($SISO$) linear time-invariant system $ARMA$ models. This new approach is based on the inner product of the cepstra of $ARMA$ models. If, there are two systems, M and M' be $ARMA$ models with cepstrum coefficients C_n and C_n', $n = 0, \pm1, \pm2, \ldots$

Definition: [119] The distance between M and $M'$with cepstrum coefficeints C_n and C_n' is defined as:

$$d(C, C') = \sum_{n=0}^{\infty} w_n |C_n - C_n'|^2 \qquad 4.24$$

Where w_n in above equation are fixed, positive weights. It has to be noted that the prime symbol $'$ is used in this chapter to distinguish between models.

[14] Hermitian matrix (general form of a sequence) is a matrix whose transpose is equal to the matrix of the complex conjugates of its entries

Definition: Martin *et al.* [119] used the cepstrum domain analysis and proposed that if we have two $ARMA$ models with transfer functions (M, M'), which are stable, (all poles and zeros are inside the unit circle) with cepstrum coefficients for discrete cepstrum, C_n, C'_n, the distance between these models is defined as

$$d(M, M') = \sqrt{\sum_{n=1}^{\infty} n|C_n - C'_n|^2} \qquad 4.25$$

However there are many questions that can arise from this definition. 1. How can a good set of weights be chosen. Does it contain any good system-theoretic properties? e.g. one can argue that the system should be more sensitive to the poles near the unit circle in comparison to the poles near the origin as they indicate strong resonances in the system [119]. 3. One may propose that, the metric does not care whether the models are stable or not. So it is very important not to make a naive comparison between two model coefficients in order to decide how different they are.

It is apparent from 4.25 that it has the Euclidean property:

$$d(c - c'', c' - c'') = d(c, c') \qquad 4.26$$

The above equation can be generalized to $ARMA$ models based on the property of the cepstrum:

$$d(MM'', M'M'') = d(M, M') \qquad 4.27$$

Where M and M' in above equation is the transfer function of the two $ARMA$ models and M'' is an arbitrary stable transfer function. This shows that if two $ARMA$ models are filtered with linear filters (FIR or IIR), their new distance is unaltered compared to the original distance. This is a direct consequence of measuring the metric in the cepstral domain, as convolution of a signal with a filtered impulse response results in the addition of their cepstra. This can be explored further: if there is an $ARMA$ model with $M = \frac{B}{A}$, then by applying a filter with system function $\left(\frac{A}{B}\right)$, the process can be whitened, and if there is another process with system function ($M' = \frac{B'}{A'}$), by applying the same filter to this process, a third process with system function $N = \left(\frac{AB'}{BA'}\right)$ is obtained. If it is assumed that M and M' are two identical processes, then N would be constant (white noise), otherwise it is 'coloured'. So $d(M, M')$ can be regarded as a measure of how coloured (M'/M) is.

Different choices for w_n are discussed by Martin *et al.* [119]. Cepstrum analysis was originally used because if two signals are convolved in the time-domain, their cepstra are combined additively then this characteristic was used by Martin *et al.* [119] as the cepstrum coefficients give information

about the autocorrelation properties of signal. The cepstrum coefficients (c_n) with small values of n are related to time-domain effects that are correlated only on short time scales which corresponds to 'slowly varying' features in the spectrum. Larger values of n in the cepstrum coefficients correspond to strongly coherent elements in the signal and sharper spectral features. This property will later be used when weighting the cepstrum coefficients are applied (cepstrum filtering or homomorphic filtering) [127]. By setting $w_n = n$, Martin *et al.* [119], gave more weight to the cepstrum coefficients at large quefrency and as the result of that bolded the effect of sharper spectral features. Another reason for choosing $w_n = n$, was that, this choice gave a metric in which the infinite summation can be performed explicitly: the metric becomes a finite product in the pole-zero domain [119].

Martin *et al.* [119] started the work first by measuring the distance between two AR models (AR model is a sub-model of $ARMA$ model). It was shown that for two AR models with transfer functions $\frac{1}{a}$ and $\frac{1}{a'}$ with order p and p' and poles $\alpha_i (i = 1, \dots, p)$ and poles $\alpha_i' (i = 1, \dots, p')$ the following equality holds:

$$\mathrm{d}(M, M')^2 = \mathrm{d}\left(\frac{1}{a}, \frac{1}{a'}\right)^2 = \log\left(\frac{\prod_{\mathrm{i}=1}^{p}\prod_{\mathrm{j}=1}^{p'}(1-\alpha_i\alpha_{\mathrm{j}}'^{*})\prod_{\mathrm{i}=1}^{p'}\prod_{\mathrm{j}=1}^{p}(1-\alpha_i'\alpha_j^{*})}{\prod_{\mathrm{i}=1}^{p}\prod_{\mathrm{j}=1}^{p}(1-\alpha_i\alpha_j^{*})\prod_{\mathrm{i}=1}^{p'}\prod_{\mathrm{j}=1}^{p'}(1-\alpha_i'\alpha_{\mathrm{j}}'^{*})}\right) \quad 4.28$$

Now if there are two $ARMA$ models with transfer functions of

$$H(z) = \frac{b(z)}{a(z)}, H'(z) = \frac{b'(z)}{a'(z)} \quad 4.29$$

Where in the above equations the order of the models are p and p'. By taking $H''(z) = \frac{z^{p+p'}}{b(z)b'(z)}$, Martin *et al.* [119] concludes that the distance between two $ARMA$ can be measured from the equation below:

$$d(M, M')^2 = d\left(\frac{b(z)}{a(z)}, \frac{b'(z)}{a'(z)}\right) \quad 4.30$$

Which itself is equal to:

$$d\left(\frac{1}{a(\mathrm{z})\mathrm{b}'(\mathrm{z})}, \frac{1}{a'(\mathrm{z})b(z)}\right) = \mathrm{d}\left(\frac{z^{p+p'}}{a(z)b'(z)}, \frac{z^{p+p'}}{a'(z)b(z)}\right) \quad 4.31$$

As both M and M' are stable, the resulting AR models from the $ARMA$ models are stable as well. In other words, the $ARMA$ models can be treated as two AR models with the transfer functions as shown above.

In the next subsection leave-one-out cross-validation ($LOOCV$) as method to test the performance of different autoregulatory ($H1$ and $P1$) parameters and SSD are be discussed.

The SSD approach is then applied to the different second-order $ARMA$ models corresponding to Tiecks model to illustrate the method and later it will be applied to the recorded data to assess its performance in distinguishing between autoregulation in normocapnia and hypercapnia.

4.3.5 Assessment of autoregulation using SSD

So far in this chapter, having shown that by using subspace distance (SSD) and going to the cepstrum domain the distance between two autoregressive (AR) or autoregressive with moving average ($ARMA$) model can be measured. However the main question that requires answering is whether this new approach can help us with the assessment of autoregulation. In this chapter, different approaches that can be taken for this assessment are studied. As it has been mentioned throughout this thesis, the main task of this work is to be able to distinguish between NC and HC. For this purpose, it is tried in this chapter to allocate a recording to either one of the NC and HC groups using leave-one-out cross-validation approach ($LOOCV$). Another approach that can be taken to study the effectiveness of an approach for assessment of autoregulation is to test the distance between clusters of autoregulatory parameters in NC and HC. These approaches are studied in the next two sections.

4.3.5.1 Leave-one-out cross-validation (LOOCV)

Cross-validation is a method for assessing the quality of the results of a statistical analysis [128]. One of the most common method for cross-validation involves partitioning a sample of data into subsets and performing the analysis on one subset (training set), and validating the analysis on the other subset (validation set). There are four frequently used types of cross-validation: k −fold cross-validation, repeated random sub-sampling validation, 2 −fold cross-validation and leave-one-out cross-validation.

In k-fold cross-validation, the data is randomly partitioned into k subsamples and from the k subsamples, one is retained as the validation data for testing, and the rest as the training data. This process is repeated k times and each of the subsamples are used exactly once as the validation set.

2 −fold cross-validation has exactly the same process as k −fold cross-validation but the data are randomly assigned to two sets, and then training on one subsample and validation on the other one, and vice versa.

In repeated random sub-sampling validation, the dataset is randomly split into training and validation data, and the model is fit to the training data and assessed on the validation data and averaged over the splits. This method has the advantage that the proportion of the training/validation split is not dependent on the number of iterations over the k −fold cross-validation. However as the samples are randomly split, some observations may never be selected in the validation subsample and the result may vary if the procedure was to be repeated (Monte-Carlo variation).

The last method is leave-one-out-cross-validation ($LOOCV$) which uses a single observation from the original samples as the validation data, and treats the rest as the training data. Then this process is repeated as many times as the number of observations that we have (same as k −fold-cross-validation but k is equal to the number of our observations). This process may be very time consuming if the number of observations is large.

In this work $LOOCV$ method is used to test the performance of SSD and other autoregulatory parameters ($H1$ and $P1$) on each volunteer's measurement during normocapnia and hypercapnia, and classify each set of measurements (NC and HC) individually with the rest of the measurements as the reference (training).

4.3.5.2 Cluster separation

In order to be able to compare different autoregulatory parameters in different scales, cluster separation was used as the criterion of measurement for good distinction between normocapnia and hypercapnia. The average distances within each class (NC and HC) and between classes were used to calculate the ratio between their mean difference and the mean (across each group; $NC-NC, HC-NC$ and $HC-HC$) of their standard deviations (variation across each subspace distance; $NC-NC, NC-HC$ and $HC-HC$) in order to remove the effect of mean from the separation between all 27 sets of measurements during normocapnia and hypercapnia.

$$X_{NN_{i,j}} = ARP_{NC_i-NC_j}\ i,j = 1 \dots 27 \quad 4.32$$

$$X_{NH_{i,j}} = ARP_{NC_i-HC_j}\ i,j = 1 \dots 27 \quad 4.33$$

$$X_{HH_{i,j}} = ARP_{HC_i-HC_j}\ i,j = 1 \dots 27 \quad 4.34$$

$$X_{HN_{i,j}} = ARP_{HC_i-NC_j}\ i,j = 1 \dots 27 \quad 4.35$$

The mean and standard deviation (STD) of above matrices are:

$$SDX_{NN} = std\left(X_{NN_{i,j}}\right), mX_{NN} = mean\left(X_{NN_{i,j}}\right) \quad 4.36$$

$$SDX_{NH} = std\left(X_{NH_{i,j}}\right), mX_{NH} = mean\left(X_{NH_{i,j}}\right)$$
$$SDX_{HH} = std\left(X_{HH_{i,j}}\right), mX_{HH} = mean\left(X_{HH_{i,j}}\right)$$
$$SDX_{HN} = std\left(X_{HN_{i,j}}\right), mX_{HN} = mean\left(X_{HN_{i,j}}\right)$$

By using above equations the cluster separation (CS) between the groups can be defined as:

$$CS_{NN-NH} = \left| \frac{mX_{NN} - mX_{NH}}{\frac{1}{2} \times (SDX_{NN} + SDX_{NH})} \right| \quad 4.37$$

$$CS_{HH-HN} = \left| \frac{mX_{HH} - mX_{HN}}{\frac{1}{2} \times (SDX_{HH} + SDX_{HN})} \right| \quad 4.38$$

$$CS = \frac{CS_{NN-NH} + CS_{HH-HN}}{2} \quad 4.39$$

The smaller values of STD would provide higher values of cluster separation so, higher value of cluster separation provides better distinction between NC and HC for the autoregulatory parameter.

4.4 Results

4.4.1 Subspace distance and Tiecks models

Section 4.3.4.2 shows that by having two $ARMA$ models from two systems, SSD can be used to measure the distance between the two models. The Tiecks model has the parameter ARI varying from 0 representing the absence of autoregulation to 9 representing full autoregulation. In this subsection the SSD between different ARI $(0-9)$ is measured. The result is shown in Figure 4-3. In this figure each line represents the ARI of a reference model, and the x-axis in the figure corresponds to the ARI of the Tiecks model to which it is compared. The y-axis corresponds to the subspace distance (SSD), which varies from 0 (when the reference model and test model are the same) to 1.81 (when they are most different). It is evident that the distance between models when both correspond to the same ARi is zero, and as the models differ more, the subspace distance increases. The symmetry of Figure 4-3 can also be observed, so the subspace distance between ARI_i and ARI_j is the same as the subspace distance between ARI_j and ARI_i.

Another notable feature of applying this method to the Tiecks model is that the SSD between any two adjacent ARI is most similar among all the combinations of ARI ($0.1 < SSD_{ARI_i,ARI_{(i+1)}} < 0.4, i = 0, \dots, 8$). This helps to interpret the SSD when applied to measured data with different autoregulatory statues.

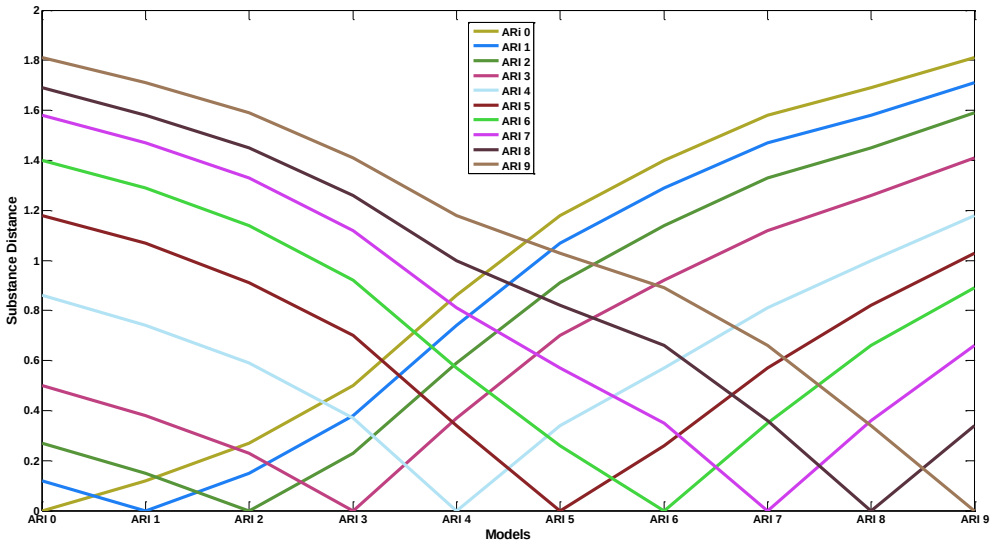

Figure 4-3 Subspace distance between different Autoregulatory indexes (ARI) from Tiecks model varying from $0 - 9$, measured from second-order $ARMA$ models.

The next subsection considers the alternative approach based on distance measures based simply on the frequency responses of different Tiecks models.

4.4.2 Distances in the frequency responses

In the previous section, the Tiecks model was used [5], and the distance between different ARI's in the cepstrum domain using the subspace distance (SSD) were calculated. The previous section demonstrated that the SSD provides a convenient means of distinguishing between different levels of ARIs (Figure 4-3). However, there are evidently many other ways of doing so and therefore in this section this method is compared to one alternative. There are obviously other alternative approaches that could have been taken, however in this work, the original approach taken by Martin *et al.* [119] was used (due to its simplicity and the fact that going to cepstrum domain has the advantage of simplicity as convolution in time domain becomes addition in cepstrum domain) and compared to this alternative. A related question can be raised on why the 2-norm of the logarithm of the cepstrum is used in preference to the 2-nrom of the spectrum itself. In this section, the distance between two models ($ARMA$ models) based on the difference between their gains was measured:

$$D^{i,j} = \sqrt{(\sum_{f=0}^{fs} \left| FR_f^i - FR_f^j \right|^2)} \qquad 4.40$$

Where in the above equation FR_f^i and FR_f^j are the frequency responses of the two models whose distance is to be measured. f_s in above equation is the sampling frequency. The distance is measured over the full frequency range of the models.

The distance between different Tiecks models measured using the above equation is shown in Figure 4-4. The symmetry between the distances is also observable in this figure (distance between $ARI = i$ and $ARI = j$ is the same as the distance between $ARI = j$ and $ARI = i$, i, j vary from 0 to 9). The distance between models varies from 0 (two identical models) to 13.54 ($ARI = 0$ and $ARI = 9$). However the distances between different models are not as separated as Figure 4-3. It can be seen (shown by a dotted circle) that the change in distances between a wide range of ARIs can be quite small, making it difficult to distinguish between them. This can be a problem as if the autoregulation of a subject with $ARI = 6$ deteriorates; it would be very hard to see if it came down to $ARI = 3$ or all the way to $ARI = 0$.

To clarify thus further, it can be seen from Figure 4-4, that the SSD between $ARI = 9$ and $ARI = 8$ is 5.59, and the SSD between $ARI = 9$ and $ARI = 7$ is 9.66, so the difference between two SSD is 5.07. However the SSD between $ARI = 9$ and $ARI = 4$ is 12.29 and the SSD between $ARI = 9$ and

$ARI = 5$ is 12.19, which makes the difference only 0.1, and makes it harder to distinguish between different $ARIs$ levels.

Given that for autoregulation only frequencies between $0.04\ Hz - 0.15\ Hz$ are of main interest [73], the calculations in eq.4.40 were repeated, restricted to this band, with results plotted in Figure 4-5. A similar bunching of lines of result as Figure 4-4 was observed (though now near $ARI = 9$), and same argument as before holds here as it is hard to say whether the condition of a patient which was previously measured at $ARI = 0$ improved to $ARI = 3$ or $ARI = 6$.

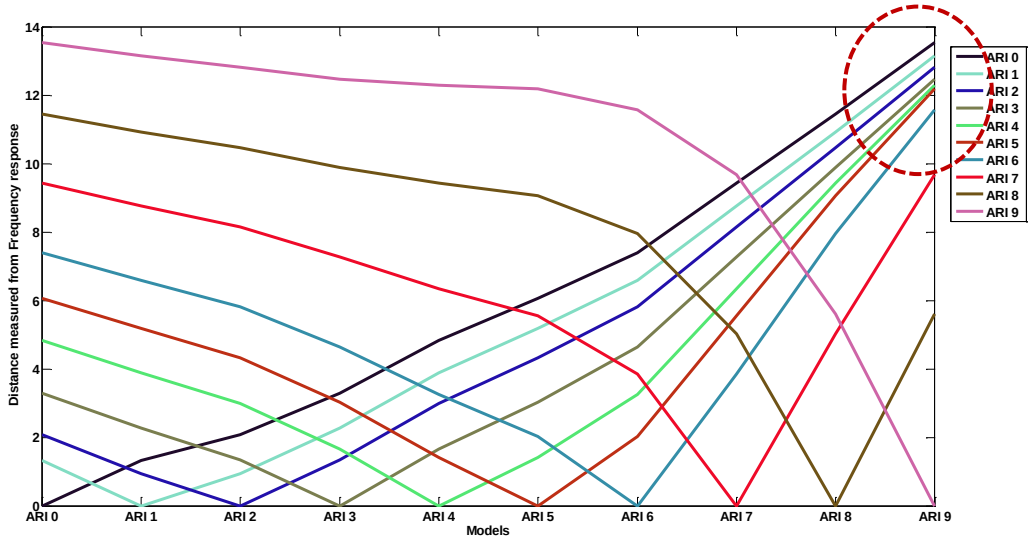

Figure 4-4 Distance between different Autoregulatory indexes (ARI) from Tiecks model varying from $0 - 9$, calculated from the frequency response over the whole range of the frequencies, using the second-order $ARMA$ models. Each line represents a different level of autoregulation in the reference model, and the value on the x-axis that for in the test model. The red dotted circle indicates the area where the SSDs are very close to each other and would make it very difficult to distinguish between them.

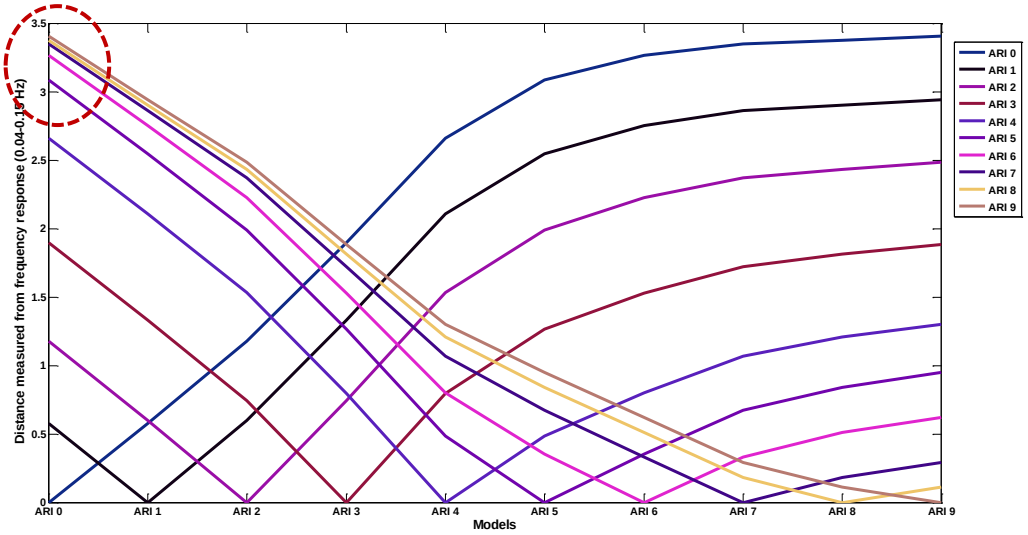

Figure 4-5 Distance between different Autoregulatory indexes (ARI) from Tiecks model varying from 0-9, calculated from the frequency response over the frequency range of $0.04 - 0.15Hz$, and using the second-order $ARMA$ models. Each line represent a different level of autoregulation in the reference model, and the value on the x-axis that for in the test model. The red dotted circle indicates the area where the SSD are very close to each other and making it almost impossible to distinguish between them

In the next section, the SSD method mentioned is applied to measured data in both the NC and HC conditions.

4.4.3 Recorded data

In this section, recorded data are used, and the SSD method was applied to measure the distance between NC and HC in the same subject (pairwise measurements) and then the distance between the estimated $ARMA$ models from different subjects during NC and HC. In order to measure the pairwise distance between the measurements, matrix of format shown in Figure 4-6 was created. As can be seen this matrix is symmetric with respect to its diagonal (with zero in the diagonal), so the matrix has $\frac{113\times114}{2} = 6441$ unique entries. From this number $\frac{56\times57}{2} = 1596$ belong to the SSD between $NC - NC$ and, 1596 to $HC - HC$ and the rest (3249) is the distance between $NC - HC$. The distance between $NC - HC$ itself forms a square matrix, where the diagonal is the distance between the i^{th} measurement during NC and HC. In order to make this matrix compatible with the SSDs measured from the other two groups ($NC - NC$ and $NC - HC$), the upper triangle of this square matrix (57×57) was used.

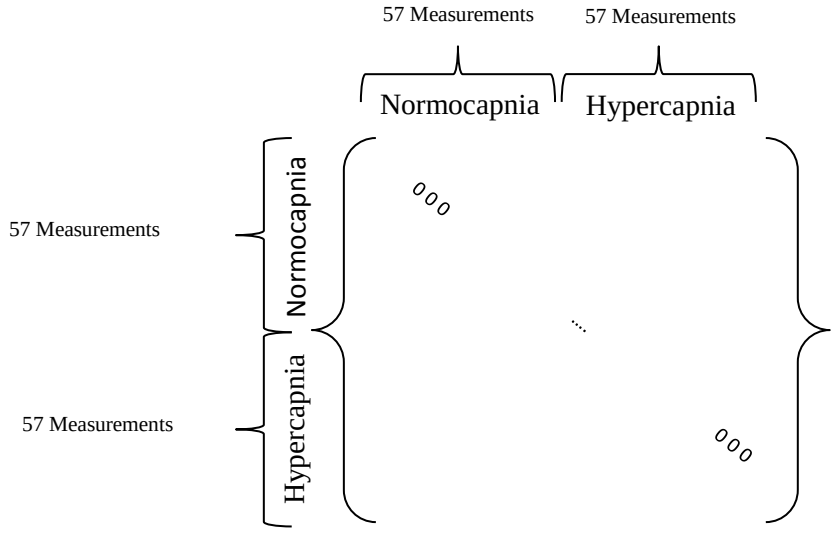

Figure 4-6 Format of the matrix created to measure the subspace distance between $NC-NC$, $NC-HC$ and $HC-HC$

Table 4.2 shows mean of the pairwise SSD between recordings during $NC-NC$, $NC-HC$ and $HC-HC$ for all 57 measurements in NC and HC shown in Figure 4-6 and explained above. It can be seen from this table that the SSD between $NC-HC$ is larger than the other two ($NC-NC$ and $HC-HC$). This finding is in agreement with the initial expectation that the models from different autoregulatory conditions tend to be more different than the models of measurements with the same autoregulatory status (intact or impaired).

Subjects	Normocapnia SSD	Hypercapnia SSD
Normocapnia	1.06 ± 0.23	1.27 ± 0.28
Hypercapnia	1.27 ± 0.28	1.05 ± 0.24

Table 4.2 Mean$\pm STD$ of the subspace distance for 57 recordings between normo-nomo, hyper-normo and hyper-hypercania

Evidence so far suggests that SSD provides a means of comparing models with each other. However in order to compare the results obtained from SSD, to other autoregulatory parameters discussed at the beginning of this chapter ($P1$ and $H1$), the Euclidian distance between measurements of these autoregulatory parameters are assessed. For the autoregulatory indexes ($P1$ and $H1$), the distance between two measurements (all possible pairwise comparison) are calculated, as the difference between their autoregulatory parameter, and matrices in the same format as the matrix shown in figure 6.5 are created using eq.4.41 and eq.4.42.

As explained in SSD, the Euclidian distance between the normocapnia measurements ($NC - NC$) and between hypercapnia measurement ($HC - HC$) and between normocapnia and hypercapnia ($NC - HC$) form a sub-matrix of our matrix in Figure 4-6 with zero on diagonal (Euclidian distance between a measurement and itself is zero). The mathematical formula for calculating the Euclidian distance for $P1$ and $H1$ are shown below

$$\mathrm{D}_{\mathrm{P1}_{i,j}} = \left|\mathrm{P1}_{\mathrm{nc}_i/\mathrm{hc}_i} - \mathrm{P1}_{\mathrm{nc}_j/\mathrm{hc}_j}\right| \; i,j = 1,\dots,57 \qquad 4.41$$

$$\mathrm{D}_{\mathrm{H1}_{i,j}} = \left|\mathrm{H1}_{\mathrm{nc}_i/\mathrm{hc}_i} - \mathrm{H1}_{\mathrm{nc}_j/\mathrm{hc}_j}\right| \; i,j = 1,\dots,57 \qquad 4.42$$

where in above equation, $\mathrm{P1}_{\mathrm{nc}_{i,j}/\mathrm{hc}_{i,j}}$ or $\mathrm{H1}_{\mathrm{nc}_{i,j}/\mathrm{hc}_{i,j}}$ represent $P1$ or $H1$ during either normocapnia or hypercapnia and would lead us to create the matrix of format shown Figure 4-6. As the matrices for $P1$ and $H1$ are symmetrical, only one side of the diagonal was used for our calculations. This would result in having ($\frac{113\times114}{2} = 6441$) paired-wise Euclidian distances for each group ($NC - NC, HC - HC$ and $NC - HC$ and $HC - NC$).

Subjects	Normocapnia $P1$	Hypercapnia $P1$	Normocapnia $H1$	Hypercapnia $H1$
Normocapnia	0.26	0.27	2.18	1.91
Hypercapnia	0.27	0.18	1.91	1.08

Table 4.3 Mean of the Euclidian distance of $P1$ and $H1$ for 57 volunteers between normo-nomo, hyper-normo and hyper-hypercapnia

Table 4.3 shows the Euclidian distance for $P1$ and $H1$ for all the groups ($NC - NC$,$HC - HC$ and $NC - HC$). As it can be seen from this table, the distance between $NC - HC$ for $P1$ is slightly higher (0.27 for $NC - HC$ compared to 0.26 for $NC - NC$ and 0.18 for $HC - HC$), whilst this is not the case for $H1$.

4.4.3.1 Statistical analysis

In order to evaluate the performance of this approach (SSD for assessment of autoregulation), $LOOCV$ is applied. In order to remove the effect of each subject, both of the recordings from the same subject are removed (from the dataset).

The result from 57 different $LOOCV$ on SSD is shown in Table 4.4. In this approach, by removing each subject's NC and HC, 56 subjects during NC and HC (118 total) are left. The average value of SSD of the left-out recording with the 56 recordings during NC and HC is calculated. The distance that has the smallest value with that specific group would be the category for the recording in hand.

Misclassification would refer to a condition when the left out subject's SSD between its NC or HC with the groups of NC or HC respectively is larger than distance to the other family. The misclassifications for SSD are indicated by a star in this Table 4.4.

The results show only 7 misclassification using the SSD whilst these are 14 and 16 for $P1$ and $H1$, respectively. Some of these misclassifications were from the same recordings but there was no overall pattern that suggested these misclassifications was dependent of the recordings or volunteers. The results from two sample z-test of two proportions shows that misclassification of 6 in SSD is significantly different to both misclassification for $P1$ and $H1$ with $p < 5\%$ ($p = 4\%$) and $p < 5\%$ ($p = 2\%$) however, $P1$ and $H1$ are not significantly different ($p = 32\%$).

$LOOCV$	Normo-Normo	Hyper-Hyper	Normo-Hyper	Hyper-Normo
1	1.35	0.42	2.46	1.66
2	0.89	0.52	1.79	0.9
3	0.64	0.71	0.81	2.1
4	1.08	0.76	1.36	1.88
5 ∗	1.12	0.11	0.39	1.39
6	0.68	0.75	1.71	2.05
7	0.49	0.34	1.05	1.43
8	0.84	1.13	1.71	2.42
9 ∗	1.61	0.75	2.57	1.33
10	0.45	0.87	1.65	1.28
11	0.5	0.57	1.43	1.65
12	0.38	0.5	1.4	1.24
13	0.27	0.53	1.66	1.87
14	0.83	0.62	2.14	2.02
15	1.06	1.43	1.22	2.61
16 ∗	1.88	0.64	1.76	0.96
17	0.48	0.61	1.45	1.31
18	0.95	0.76	1.14	1.44
19 ∗	1.31	1.07	1.02	0.82
20 ∗	1.43	0.64	0.5	1.89
21	1.05	0.36	1.68	1.11
22	0.94	1.44	1.81	1.13
23 ∗	1.6	0.67	0.31	0.87
24	0.65	0.23	0.84	1.17
25	1.02	0.7	2.26	1.97
26	0.38	1.07	1.69	1.35
27	0.41	0.67	0.99	1.24
28	0.72	0.96	0.76	0.77
29	1.63	2.2	1.73	2.09
30	0.7	0.22	1.73	1.58
31	0.68	0.13	0.85	1.36
32	0.48	0.26	1.05	1.24
33	0.64	0.81	1.78	1.35
34	0.94	0.95	2.17	1.26
35	0.34	0.24	2.22	1.26
36	0.56	0.22	0.93	2.57
37	1.63	1.74	2.05	2.22
38 ∗	1.03	1.59	2.25	0.98
39	1.07	0.29	1.75	1.5
40	0.91	0.42	1.95	1.14
41	0.22	0.68	1.44	1.12

42	0.33	0.48	1.35	1.58
43	0.79	0.91	1.45	0.61
44	0.49	0.48	1.2	1.05
45	0.15	0.32	1.37	1.16
46	0.46	0.42	0.98	1.74
47	0.26	0.29	1.43	1.64
48	1.18	0.76	2.14	1.43
49	0.46	0.83	1.15	2.23
50	1.44	0.36	2.21	1.48
51	0.84	0.78	1.66	2.11
52	0.33	0.71	1.36	2.0
53	1.51	0.41	2.18	1.76
54	0.61	0.81	1.11	2.11
55	1.08	0.85	1.51	1.47
56	0.67	1.31	1.04	1.3
57	0.58	0.49	0.68	0.7

Table 4.4 Result from 57 $LOOCV$ on volunteers data with arterial blood pressure (ABP) as input and cerebral blood flow velocity ($CBFV$) as output. The second column in this table is the SSD between the left out measurement during NC and the average $ARMA$ model calculated over all other 56 NC measurements, the second column is the SSD between the left out measurement during HC and the average $ARMA$ model calculated over all other 56 HC measuremnets, the third and fourth columns represent the SSD between the left out NC,HC measurement with the average $ARMA$ model calculated over all other 56 NC, HC respectively. It is expected that the distance between for example the left out NC measurement with the reference $ARMA$ model during NC be smaller that when this is compared with the reference $ARMA$ model during HC. The ones that do not follow the expected trend for both NC and HC are indicated with a star.

The result for the cluster separation is shown in Table 4.5. The results from cluster separation shows that SSD gives us better separation compared to $P1$ and $H1$.

Model	Normo/Normo		Hyper/Normo		Hyper/Hyper		Cluster Separation Normalized
	$Mean$	STD	$Mean$	STD	$Mean$	STD	
SSD	1.06	0.23	1.27	0.28	1.05	0.24	0.83
$P1$	0.26	0.2	0.27	0.19	0.183	0.14	0.29
$H1$	2.18	2.26	1.91	2.00	1.08	0.86	0.23

Table 4.5 Mean cluster separation between normo/normo, hyper/normo and hyper/hypercania, using subspace distance (SSD) and phase at 0.1 Hz ($P1$) and second coefficient of FIR filter with 2 lags ($H1$)

4.5 Discussion

The conventional approach to assess autoregulation is to model the relationship between ABP and $CBFV$ ($SISO$ approach) and from this model an autoregulatory parameter is extracted. In term of the assessment of autoregulation, this thesis has concentrated on choosing an autoregulatory parameter from different methods in both time or frequency domain, using linear or nonlinear system identification methods [5, 11, 39, 46, 75, 90, 93, 106, 116, 129, 130]. These parameters are usually extracted from the estimated step or frequency responses [47, 52, 73, 74]. There are other approaches to assessment of autoregulation that does not require choosing a parameter from the step or frequency responses such as correlation coefficient (Mx) between cerebral perfusion pressure (CPP) and blood flow velocity (BFV) [28, 118], however this approach does not measure CBF directly and provides a surrogate measure of autoregulation [118].

In this chapter a new data-driven approach for assessing autoregulation using subspace distance (SSD) between two $ARMA$ models is proposed which avoids the need for prior choice of the autoregulatory parameter. It has to be noted that whilst there are many alternative approaches that could have been chosen, the original approach by Martin *et al.* [119] is used.

In this chapter, it is first shown that by applying SSD to the $CBFV$ responses proposed by Tiecks [5], good and effective separation between all 10 autoregulatory responses ARI can be achieved. To this end an $ARMA$ model is used (with order $2,2$) and adapted for a sampling frequency of $1\ Hz$. It is shown that the step responses obtained from the different sampling frequencies are in good agreement (Figure 4-2).

Next, it is showed that by going to the cepstrum domain, the distance between to $ARMA$ models can be measured as the difference between their cepstrum coefficients [119, 131]. Moving to the cepstrum domain has the advantages of simplicity (convolution in time domain is addition in cepstrum domain) and reduction of the dimension of the spectral vector [132]. Based on the simulation using Tiecks models, it is shown that in dynamic assessment of autoregulation, going to the cepstrum domain, gives clearer separation between different levels of than simple distances between frequency responses (Figure 4-4 and Figure 4-5). Then $ARMA$ models with order $2,2$ are applied to the ABP and $CBFV$ data recorded in volunteers and the SSD between different combinations of normocapnia and hypercapnia ($NC-NC, HC-HC$ and $NC-HC$) are calculated. The results show that the SSD between two different conditions ($NC-HC$) are greater than the distance calculated from two measurements with the same condition ($NC-NC$ or $HC-HC$); 1.27 for $NC-HC$ compared to 1.06 and 1.05 for $NC-NC$ and $HC-HC$ respectively. The Euclidian

distance for $P1$ and $H1$ are calculated for all the conditions ($NC - NC$, $HC - HC$ and $NC - HC$). The results of the mean of the distances for these three groups are shown in Table 4.3.

In order to test the benefit of this novel data driven approach using SSD, similar methods on some more conventional autoregulatory parameters are employed [73-75] and are used in previous chapters. Comparisons are made using $LOOCV$ (section 4.3.5.1). The results from this test shows considerable superiority of SSD over $P1$ and $H1$ with only 7 misclassifications compared to 12 and 14 for $P1$ and $H1$, respectively. Next cluster separation is used as a criteria of how separated the three difference groups ($NC - NC$, $HC - HC$ and $NC - HC$) are from each other.

Inter- and intra-subject variability is a big issue when it comes to the assessment of cerebral autoregulation [47, 74, 97, 102]. There is no 'gold standard' in the assessment of autoregulation [47, 74, 133, 134]. In order to study the variability of this novel approach and compare it to our other autoregulatory parameters, cluster separation is used. The result showed the advantage of using SSD over $P1$ and $H1$ with the cluster separation of 0.83 for SSD, compared to 0.29 and 0.23 using other two autoregulatory parameters respectively (Table 4.5).

One requirement in applying SSD as a method for assessing autoregulation is the need to choose the order of the $ARMA$ models, which might have a major effect on results. In this work $ARMA$ model of order $(2,2)$ is used to facilitate comparison with the initial simulations based on the Tiecks model. This model order has also been used by other authors [97]. In order to probe this choice further, the method is also applied using a simpler model of $2,0$ $ARMA$ model (FIR filter with only 2 lags which was originally used by Simpson *et al.* [102]) and almost similar results were found. The reason behind choosing the original $ARMA$ model with $2,2$ was to be compatible with our original order chosen for the Tiecks model and to be in agreement with the literature [97], however as mentioned, with simpler model, slightly better result are achieved, which suggest further investigation can be carried out in this section (maybe AIC to calculate the best model order).

An important point that has to be considered is that, in order to measure the SSD between two models, it is not required that both models have the same orders (they only need to be stable), and the distance can be measured from two $ARMA$ models with different orders and structures. This might be appropriate when recordings have very different durations (where the principle of parsimony would indicate that for shorter recordings lower model orders are indicated) or recordings may show very different spectral characteristics. However in this work, average $ARMA$ model is used as the reference model and using models with different orders cannot be applied.

The results from $LOOCV$ showed 7 misclassification for SSD and 14 and 16 for $P1$ and $H1$, respectively. The results one-tailed z-test of two proportions showed that classification using SSD was significantly different compared to $P1$ and $H1$, however classification using $P1$ and $H1$ showed no significant difference. The poorer result may be result from the effect of each subject in both training and validation (even though they were measured in two different seasons, but deeper analysis is required in this area).

One issue in using SSD as a method to assess cerebral autoregulation is that the $ARMA$ models are required to be stable [119]. However this will not always be the case (especially with higher order models), but with small order $ARMA$ models this is usually the case. In the case of assessment of autoregulation in the dataset in hand, no measurement found to be unstable with the chosen orders in this chapter.

Another issue of using the SSD is that the models fed to the model are required to be single-input-singe-output ($SISO$) models. However, it may be possible that this model can be extended to measure the distance between multi-input-single-output ($MISO$). This may permit the inclusion of for, example P_{ETCO_2}, which the previous chapter showed to improve the assessment of autoregulation. However, multivariate model of SSD has not be done and could be the next stage in this work.

Another issue using SSD that has arisen, is the big dispersion of autoregulatory parameters within the groups, as can be seen from the large standard deviation in each group shown in Table 4.5 compared to their mean values. This indicates that it is hard to separate the groups from each other and grey area between the groups still exists as reported by others [93, 97, 102]. However the results from cluster separation shows better separation between these groups using SSD compared to $P1$ and $H1$. The results suggest that the grey area between the cluster of SSD of $NC-NC$, $NC-HC$ and $HC-HC$ are separated better compared to $P1$ and $H1$.

4.6 Conclusion

The results from this work show that subspace distance can provide a novel approach for assessing autoregulation, and the results suggest better performance than more conventional alternatives. The method requires that the models are stable. The main advantage of this method is that it does not require the choice of parameters to quantify autoregulation to be picked by the researcher, but is driven by the data (the model) itself. The method is found to be promising, but requires further evaluation with larger datasets. Orders of the $ARMA$ models are chosen based on the model orders

chosen previously used in Tiecks models. However model investigation on the order of $ARMA$ model using probably AIC would be ideal as the choice of the order $ARMA$ plays an important role in applying SSD. Multivariate SSD can also be the next step in applying SSD to cerebral autoregulation as we have already shown in Chapter 3 that including P_{ETCO_2} can improve the assessment of autoregulation.

Chapter 5 : Multivariate time-varying analysis of cerebral autoregulation in response to changes in P_{ETCO_2}

In this work, the contributions of spontaneous beat-to-beat mean arterial blood pressure (ABP) and breath-by-breath carbon dioxide of end-tidal CO_2 (P_{ETCO_2}) on fluctuations of beat-to-beat cerebral blood flow velocity ($CBFV$) variation using linear time-varying models in normal subjects at rest is studied.

Cerebral autoregulation has been widely studied using linear filter system using arterial blood pressure (ABP) and cerebral blood flow velocity ($CBFV$) as input and output respectively. The time-varying characteristic of cerebal autoregulation during step-wise changes in arterial P_{ETCO_2} using adaptive filters has already been studied [114]. The aim of this chapter is to investigate time-varying characteristic of dynamic cerebral autoregulation using multivariate (ABP and P_{ETCO_2}) adaptive filters (multivariate recursive least square ($MI-RLS$) and multivariate moving window ($MI-MW$)). Here single input RLS ($SI-RLS$), single input moving window ($SI-MW$), multi-input moving window ($MI-MW$) and $MI-RLS$ methods are also applied to baseline, hypercapnia and normocapnia (second baseline; after hypercapnia) measurements from volunteers, individually. Autoregulation is quantified by both time-varying phase lead and amplitude using pressure pulse response (PPR) as discussed in section 3.3.2, it is noticed that the multivariate models can remove the transient at the beginning of hypercapnia compared to the univariate models and autoregulatory parameters extracted from $MI-RLS$ provide the least variation over time (1 and $2.69\ rad$ for the mean of variations for the phase at $0.1\ Hz$), as well as the largest separation between normo- and hypercapnia. The analysis of experimental measurements from healthy volunteers shows that by using time-varying multiple coherence of $CBFV$, with ABP and P_{ETCO_2}, significantly higher values in the transient phase between normocapnia to hypercapnia compared to the values obtained from univariate time-varying coherence function at these stages. The results illustrate that at low frequencies and for the transients, the low value of univariate coherence may be due to the effect of P_{ETCO_2} on the variations of $CBFV$.

5.1 Introduction

The coherence function between ABP and $CBFV$, exhibits low values in the low frequency region, which questions the validity of the linear $ABP - CBFV$ relationship of the cerebral autoregulation at these frequencies [135, 136]. More sophisticated system identification can be applied to study the effect of nonlinearity and non-stationarity of cerebral autoregulation [23, 35, 92, 93, 137] although this is not universally accepted. They showed that by including P_{ETCO_2} and nonlinearity and the cross-effect of P_{ETCO_2} on ABP (section 2.9), variation in $CBFV$ can be almost fully explained. Peng *et al.* [91], used a multivariate coherence function with ABP, P_{ETCO_2} and end-tidal oxygen (P_{ETO_2}) as inputs and showed that multiple coherence provide significantly higher values at $f < 0.05\ Hz$ compared to the corresponding univariate coherence with ABP which indicate that alongside nonlinearity and non-stationarity in the system and signals respectively, other physiological signals also have great impact on $CBFV$ [90, 138].

On the other hand, there is large inter- and intra-subject variability in the assessment of autoregulation when short periods of data was analyzed using only spontaneous variations in ABP and $CBFV$ [47, 74, 90, 114, 133, 139, 140]. It is known that increasing arterial CO_2 causes cerebral vasodilation, and impairs cerebral autoregulation temporarily. This can be exploited by switching between ambient air and in air/$5\%\ CO_2$ mixture to assess cerebral autoregulation to investigate impairment statuses [46, 88, 90, 93, 114, 141-143]. Liu *et al.* [114] studied the speed of the changes in autoregulation as a result of transient in partial pressure of CO_2 in the blood (P_{aCO_2}).

In this chapter, the assessment of autoregulation using multivariate time-varying methods is explored. The aim of this chapter is to assess the transient changes in autoregulation as the result of breathing $5\%\ CO_2$ using both ABP and P_{ETCO_2} as inputs to adaptive filters and comparing it to a univariate model with just ABP as input.

In the next section, the data acquisition procedure is introduced. Then the adaptive filter methods are described, followed by a description of the autoregulatory parameters used for the assessment of cerebral autoregulation are outlined. In the following section, the results of tracking time-varying dynamic autoregulation are shown, followed by discussion and suggestions for future work.

5.2 Methods

5.2.1 Data Collection and processing

The same dataset used in the Chapter 4 was used in this work (section 4.2). Participants were asked to assume a supine position. After a brief settling down period, brachial ABP was measured and the thigh cuffs were placed. Once connected to the inflation system, a trial inflation/deflation cycle was performed to familiarize participants with the procedure. ABP was monitored non-invasively using the arterial volume clamping method (Finapres, Ohmeda 2300, Louisville, CO, USA). Freehand transcranial Doppler (SciMed QVL 120, SciMed, Bristol, UK) identification of the right middle cerebral artery (MCA) was performed using a $2\ MHz$ probe, which was then held in place by an elastic head-band during data acquisition. Following a 5 minutes baseline recording, each participant underwent four more 5 minutes recordings, corresponding to all possible combinations between the two sequences and the two high thigh cuff pressure settings. All manoeuvres were performed in a random order. However for the sake of this chapter, only the baseline and high CO_2 (5%) and second baseline (normpcapnia) recordings are used.

The mean arterial ABP and $CBFV$ are then calculated by low-pass filtering (cut-off frequency $0.4\ Hz$; zero phase filter [39, 46]) and the mean was removed from the signals. The resultant signals were resampled at $1\ Hz$.

5.2.2 System identification

As mentioned above the segments of data obtained at baseline, hypercapnia and second baseline (normocapnia) are visually inspected and the mean values were removed. From the time series for ABP $[p(n)]$, P_{ETCO_2} $[c(n)]$ and $CBFV$ $[v(n)]$, the latter is modeled as below [144] where $v(n)$ is modeled with $p(n)$ and $c(n)$ as inputs.

$$v(n) = \sum_{i=0}^{L_{pv}-1} h_{pv}(i)p(n-i) + \sum_{j=0}^{L_{cv}-1} h_{cv}(i)c(n-j) + e(n) \quad 5.1$$

where $e(n)$ is noise and $h_{pv}(i)$ and $h_{cv}(i)$ are the coefficients of the causal FIR filter which are estimated using a multivariate least-squares fit, using

$$H = R_{XX}^{-1}R_{Xy} \quad 5.2$$

Here H is the matrix of the FIR coefficients

$$H = [h_{pv}(0) \dots h_{pv}(L_{pv} - 1), h_{cv}(0) \dots \ h_{cv}(L_{cv} - 1)]^T \quad 5.3$$

In above equation L_{pv} and L_{cv} are the lengths of the FIR filters for h_{pv} and h_{cv}, respectively. $R_{XX} = \begin{bmatrix} R_{pp} & R_{cp} \\ R_{pc} & R_{cc} \end{bmatrix}$ is the auto-correlation matrix of the inputs and $R_{XY} = \begin{bmatrix} R_{pv} \\ R_{cv} \end{bmatrix}$ is the cross-correlation matrix between the inputs and $v(n)$.

The above equations for the multivariate model can be simplified to a univariate model by removing one input. For instance, by removing the effect of P_{ETCO_2} the auto-correlation and cross-correlation matrices employed in eq.5.2 would become, $R_{XX} = [R_{pp}]$ and $R_{XY} = [R_{pv}]$.

In this work, 6 and 20 seconds are chosen for L_{pv} and L_{cv} respectively. These values are chosen based on the previous work done by other authors [29, 90, 91, 141]. It has been shown that these impulse response lengths can cover most of the important effects of ABP and P_{ETCO_2}.

In order to estimate the time-varying characteristics of autoregulation, a sliding-window version of above equation with a window size (WS) of $60\ sec$ [53] are used to be able to capture variations in $CBFV$ and the characteristics of cerebral autoregulation. The H matrix is recalculated for each window and the window is advanced by one sample steps. Different autoregulatory parameters are then calculated from H to quantify cerebral autoregulation as is explained later.

5.2.3 Multivariate *RLS* analysis

The univariate RLS model previously used by Liu *et al.* [114] was extended to a multivariate RLS method as [144]

$$k_p(n) = \frac{\lambda^{-1}P_p(n-1)p(n)}{1+\lambda^{-1}x(n)P_p(n-1)x(n)}, \qquad (0 \le \lambda \le 1) \tag{5.4}$$

$$k_c(n) = \frac{\lambda^{-1}P_c(n-1)c(n)}{1+\lambda^{-1}x(n)P_c(n-1)c(n)}, \qquad (0 \le \lambda \le 1) \tag{5.5}$$

where in the above equations $0 < \lambda < 1$ is the forgetting factor and $P(n) = \mathrm{R}_n^{-1}$ is the inverse autocorrelation matrix of the input signals at sample n and $k(n)$ is the Kalman gain vector. The error at the n^{th} sample was the calculated using

$$e(n) = v(n) - H(n-1)^T x(n) \tag{5.6}$$

Where $x(n)$ in above equation is a vector and $H(n-1)^T$ in above equation is

$$H(n-1) = \begin{bmatrix} H_{pv}(n-1) \\ H_{pc}(n-1) \end{bmatrix} \tag{5.7}$$

$$H_{pv}(n-1) = \left[h_{pv}(n) \ldots h_{pv}(L_{pv}-1)\ 0\ 0 \ldots 0\right] \tag{5.8}$$

$$H_{cv}(n-1) = [h_{cv}(0) \ldots\ h_{cv}(L_{cv}-1)] \tag{5.9}$$

In order to be able to put two rows of different length (as the length of impulse response for ABP and P_{ETCO_2} are chosen differently) into one vector, H_{pv} was zero-padded to have the same length as H_{cv}. This was also done for $x(n)$.

$$x(n) = \begin{bmatrix} x_p(n) \\ x_c(n) \end{bmatrix} \tag{5.10}$$

$$x_p(n) = \left[p(n-L_{pv}) \ldots p(n)\ 0\ 0 \ldots 0\right] \tag{5.11}$$

$$x_c(n) = [\, c(n-L_{cv}) \ldots\ c(n)] \tag{5.12}$$

These are updated sample by sample using

$$H(n) = H(n-1) +\ e(n)k(n) \tag{5.13}$$

where

$$k(n) = \begin{bmatrix} k_p(n) \\ k_c(n) \end{bmatrix} \tag{5.14}$$

Next $P(n)$ for each input was updated and the output $y(n)$ are calculated and the error from the measured $v(n)$ is updated.

$$P_{c/p}(n) = \lambda^{-1}P_{c/p}(n-1) - \lambda^{-1}k_{c/p}(n)x_{c/p}(n)^T P_{c/p}(n-1) \quad 5.15$$

$$y(n) = H^T x(n), e(n) = v(n) - y(n) \quad 5.16$$

where in above equation c/p indicates either c or p.

In order to improve the performance of the models, the system is initialized with $H(n)$ calculated from a multivariate FIR filter (Wiener filter) using the whole set of data. This helps to reduce the large error at the beginning of the process whilst the RLS method converges. In this study, same values used by Liu *et al.* [114] for $\lambda = 0.98$ is used, as these values showed relatively low error estimation at the beginning of the adaptation of the datasets.

5.2.4 Multivariate Coherence function

$P(f), C(f)$ and $V(f)$ as the frequency-domain transforms of $p(t), c(t)$ and $v(t)$ are computed using an FFT algorithm. The power spectrum and the cross spectrum of these signals can be measured using [124]:

$$G_{pp/cc/vv}(f) = E[(P/C/V)^*(f)P/C/V(f)] \quad 5.17$$

$$G_{pv/cv}(f) = E[(P/C)^*(f)V(f)] \quad 5.18$$

where $G_{pp/cc/vv}(f)$ are the power spectrum of $P(f)$ or $C(f)$ or $V(f)$ and $G_{pv/cv}$ is the cross-spectrum between ABP or P_{ETCO_2} and, and the expected value of the complex product is obtained with the Welch method by smoothing the spectra with a 128 −point Hanning window (128 seconds; which gives good resolution to study the effect of cerebral autoregulation at around $0.1\ Hz$) with 50% overlap.

The univariate coherence function $\Gamma_P^2(f)$ between p and v is defined by:

$$\Gamma_P^2(f) = \frac{\left|G_{pv}(f)\right|^2}{G_{vv}(f)G_{pp}(f)} \quad 5.19$$

The coherence function tells how much of the output can be linearly explained by the input over different frequency ranges.

It has also been shown [138] that the complex transfer function $H_{pv}(f)$ and $H_{cv}(f)$ can model the output signal with $p(t)$ and $c(t)$ as inputs using

$$Y(f) = H_{pv}(f)P(f) + H_{cv}(f)C(f) \quad 5.20$$

By using above equations the system auto-spectrum of the model input can be written in matrix form as:

$$G_{YY}(f) = E[Y^*(f)Y(f)] \quad 5.21$$

By using above equations and the definition of coherence as the explained variation of the output over the total variation, the multiple coherence $\Gamma_M^2(f)$ is defined as:

$$\Gamma_M^2(f) = \frac{G_{YY}(f)}{G_{vv}(f)} \quad 5.22$$

In this chapter, both the univariate and multivariate coherence at different samples are calculated to be able to capture the autoregulatory parameter characteristic as the state of autoregulation changes:

$$\Gamma_M^2(f, t_i) = \frac{G_{YY}(f, t_i)}{G_{vv}(f, t_i)} \quad 5.23$$
$$i = N - WS, \dots, N$$

Where t_i in the above equation is the sample time, N is the length of the signals (in samples) and WS is the window size. Thus the coherence is estimated using the last WS samples of the measured $p(t), c(t)$ and $v(t)$.

5.2.5 Autoregulatory parameters

By applying univariate and multivariate time-varying models (RLS and moving window) discussed in the previous section, different autoregulatory parameters can be extracted as the characteristics of the models changes with time using these different techniques. In this work, time-varying autoregulation is estimated using the phase lead between $p(t)$ and $v(t)$ at $\frac{1}{12} Hz$ which has been widely used [65, 73, 98] as an indication of the status of cerebral autoregulation. Birch *et al.* [139] reported a mean phase-lead of 46 ± 14^o at $0.05\ Hz$ and Diehl *et al.* [69] reported a phase-lead of 70.5 ± 29.5^oat $0.1\ Hz$. Both of the mentioned studies agree on phase-lead reduction when autoregulation is impaired. This phase-lead has since been become one of the most important measures of cerebral autoregulation. In this work, the impulse responses for the ABP (H_{pv}), calculated from the different univariate and multivariate time-varying moving-window and RLS filters are transformed into frequency domain by FFT, and the phase angle (phase lead) is estimated at $1/12\ Hz$ for each estimate.

The amplitude at $8\ sec$ ($A8$) of the response of the system to a pressure pulse input (PPI) as introduced in section 3.3.2 is also considered. It was shown that this novel input has more realistic characteristics as our real input in term of power spectrum as shown in Figure 3-4 [102]. This has also been shown to be superior to phase at $1/12\ Hz$ for the assessment of autoregulation in terms of inter- and intra-subject variability and robustness (section 3.3.3.1 and 3.3.3.2). In this method,

instead of feeding a step or an impulse to the system and calculating the response a cosine wave modulated by a Gaussian envelope is used. It is shown Figure 3-4 that this input has more realistic characteristics compared to step and impulse input, with respect to those observed in spontaneously varying ABP and its central frequency can be chosen considering the autoregulatory system where is often selected around $0.1\,Hz$ [73, 139]. This allows us to study autoregulation in frequency bands where autoregulation is known to be working. It can also be seen that PPI has a wider frequency range around $0.1\,Hz$ which enables to capture more information around this frequency which would result in better assessment of autoregulation.

The time-varying models introduced in section 5.2.2 are then applied on recorded ABP, P_{ETCO_2} and $CBFV$ to capture the time-varying characteristics and multivariate structure of cerebral autoregulation during baseline, hypercapnia and normocapnia. The changes of the phase lead and the amplitude at 8 seconds from the pressure pulse response (PPR) are also looked at to firstly observe how fast the autoregulatory parameters change following step-wise changes in P_{ETCO_2}, and secondly to study the effect of multivariate time-varying models compared to univariate time-varying models. In the next section, the results from these models are presented.

5.3 Results

The mean$\pm$ standard deviation of ABP, P_{ETCO_2} and $CBFV$ averaged over the time of recordings for all 57 recordings are given in Table 5.1. The results here are in agreement with literature which indicates the increase of $CBFV$ in the hypercapnia stage. The results from the paired-wise test shows that the increase in $CBFV$ during hypercapnia stage is significantly different to both baseline and normocapnia stage ($p < 0.05$), whilst it was the case for ABP ($p = 0.055$).

	Mean$\pm STD$ of ABP	Mean$\pm$ STD of P_{ETCO_2}	Mean$\pm$ STD of $CBFV$
Baseline	88.34 ± 14.58	39.47 ± 3.21	56.45 ± 11.31
Hypercapnia	94.55 ± 18.41	47.94 ± 2.89	70.73 ± 16.44
Normocapnia	89.55 ± 13.44	37.96 ± 3.21	54.16 ± 11.77

Table 5.1 $Mean \pm STD$ of ABP,$PTCO_2$ and $CBFV$ for all 57 measurements

Table 5.2 presents the normalize mean square error ($NMSE$) for the comparison between the desired $CBFV$ and the model outputs averaged over all the measurements in baseline, normocapnia and hypercapnia. It can be observed that the $NMSE$ for the multivariate RLS improved 16.56% relative to $SI - RLS$. A decrease in variability across subjects is also noticed (11.64%). The same improvement is also observed from multivariate to univariate moving window models (32.51% and

31.96% respectively). A paired t-test is then employed to analyse the statistical significance of the difference between the univariate and multivariate models. The results illustrates that the $NMSE$ from the multivariate models are significantly different with the significant level of ($p < 5\%$). However the results also show that the multivariate RLS and moving-window methods are not significantly different ($p = 11.43\%$). This illustrates that the multivariate RLS and moving window models are not significantly different in terms of model fit.

Model	$NMSE \pm STD$ (%)
Single-Input RLS	47.41 ± 11.55
Multiple-Input RLS	39.56 ± 9.86
Single-Input Moving Window	52.99 ± 13.86
Multiple-Input Moving Window	35.76 ± 9.43

Table 5.2 Normalized mean square error ($NMSE$ %) for different signal processing models

Figure 5-1 shows the results for the autoregulatory parameters; phase lead and $A8$ averaged over 57 measurements calculated during different stages (baseline, hypercapnia, second baseline; normocapnia). It can be noted that in hypercapnia there is a transient from normocapnia to the opening of the valve of CO_2 (Figure 5-3). There is also an adaptation period for the coefficients and the corresponding autoregulatory parameters which can be seen at the beginning of all the stages as is shown in Figure 5-1. The positive phase indicates that $CBFV$ leads ABP which is in agreement with other studies [65, 69]. The results also show that phase lead and $A8$ both decrease with the incensement of P_{ETCO_2} which impairs autoregulation as shown by other authors [65, 69]. It can be seen from Figure 5-1, that the average autoregulatory parameters over all 57 recordings extracted from different models provide almost the same results when they are in the normocapnia stage, however the results differ when the subject are in the hypercapnia stage. This indicates that the effect of variation in P_{ETCO_2} on $CBFV$ is more apparent when the subject experiences hypercapnia.

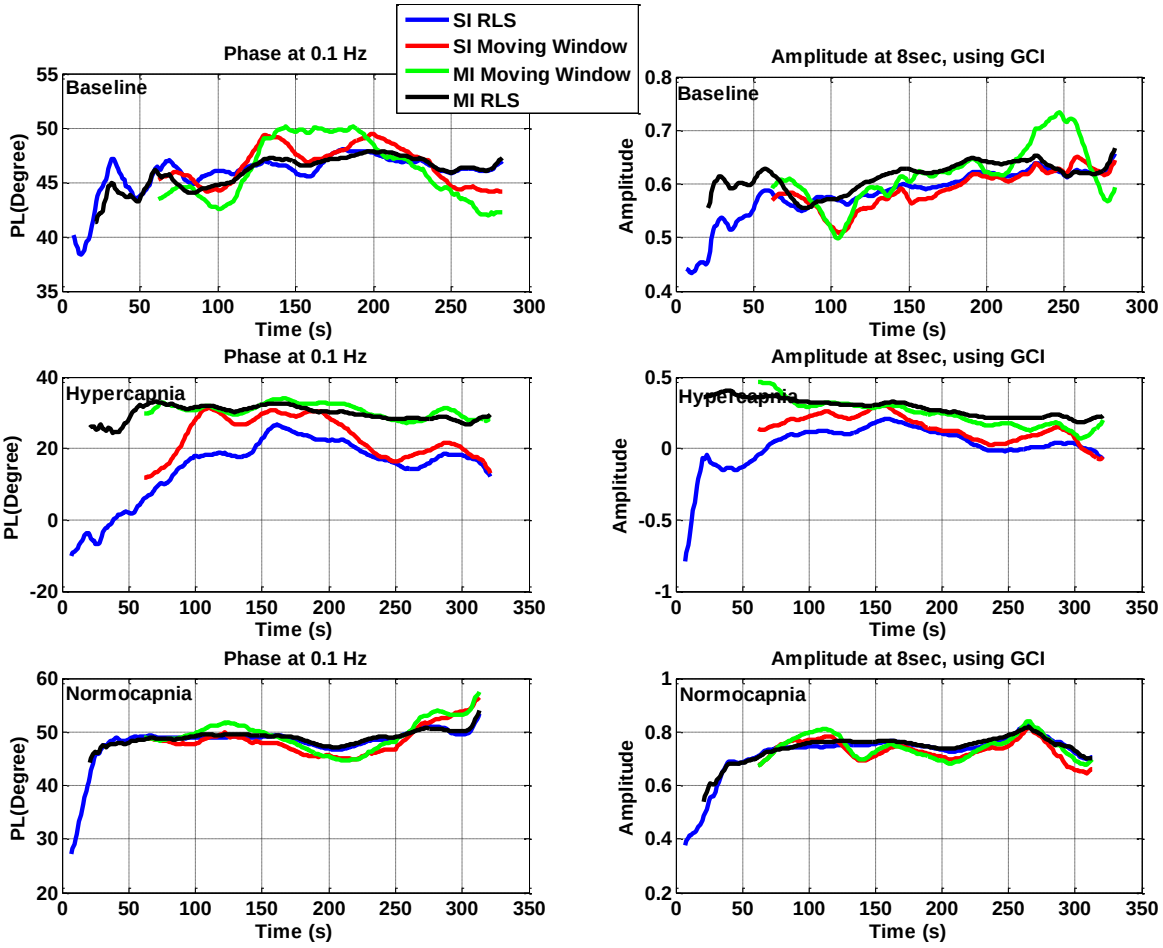

Figure 5-1 Phase at $0.1\ Hz$ and amplitude at $8sec$ averaged over all 57 measurements for different CO_2 levels

It has to be noted that the filters are initialized using a univariate or multivariate FIR filter to reduce the adaptation period at the beginning of the procedures. This adaption period can be seen at the start of all autoregulatory parameters (lower values at the start).

Different autoregulatory parameters are then synchronized at the hypercapnia stages based on the trigger of step-up or down of P_{ETCO_2} as shown in Figure 5-2 the 4.6% of P_{ETCO_2} was used as the trigger point. The top row shows the first 200 seconds of the autoregulatory parameters at the onset and the bottom row shows the last 200 seconds of the autoregulatory parameters in the hypercapnia stage. It can be seen that P_{ETCO_2} takes up to almost 85 seconds from opening the valve to reach hypercapnia (to the dashed line in Figure 5-2). In order to synchronize different autoregulatory parameters, the point of hypercapnia is used as the trigger of hypercapnia. The mean of the synchronized phase lead and $A8$ based on the trigger of P_{ETCO_2} are shown in Figure 5-2. It can be seen from the top row in Figure 5-2, that the delay in the phase leads due to slowness of CO_2 response calculated from the SI models are more evident at P_{ETCO_2} step-up compared to step-down.

The mean value of $CBFV$ during normocapnia (Table 5.1) and its increase at the onset of hypercapnia and its decrease when in baseline are in agreement with previous works [46, 63, 88, 112, 142]. As mentioned before, phase lead and $A8$ both decreased during hypercapnia as autoregulation is impaired and returned at the end of hypercapnia as reported previously [46, 73, 90, 142]. Liu [145] also showed that autoregulation deteriorates rather more slowly during the onset of hypercapnia compared to its recovery on return to normocapnia. However, here it is shown that that by including P_{ETCO_2} in the models the transient of the autoregulatory parameters can be reduced at the onset of P_{ETCO_2} (Figure 5-2). The results show that at the onset of hypercapnia the univariate models require around $150\ sec$ to reach a plateau whilst multivariate models show a much more abrupt change. At the offset of P_{ETCO_2} the results have more consistency between the models with the difference being at the mean values (Figure 5-2, bottom row)

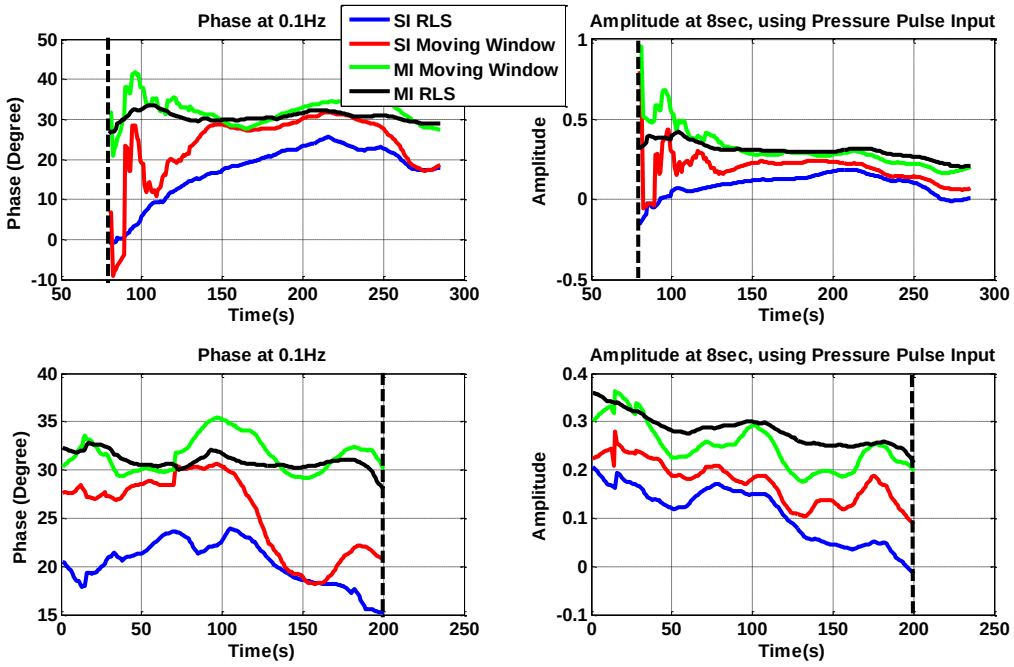

Figure 5-2 the first $200\ sec$ and the last $200\ sec$ of phase at $0.1\ Hz$ and amplitude at $8\ sec$ at the onset (top row) and offset of hypercapnia (bottom row), shown with the dashed line averaged over 57 recordings

Figure 5-4 shows the mean results of the last 200 seconds of the normocapnia followed by the starting 200 seconds after the onset of hypercapnia (opening of the valve; Figure 5-3) of the synchronized autoregulatory parameters.

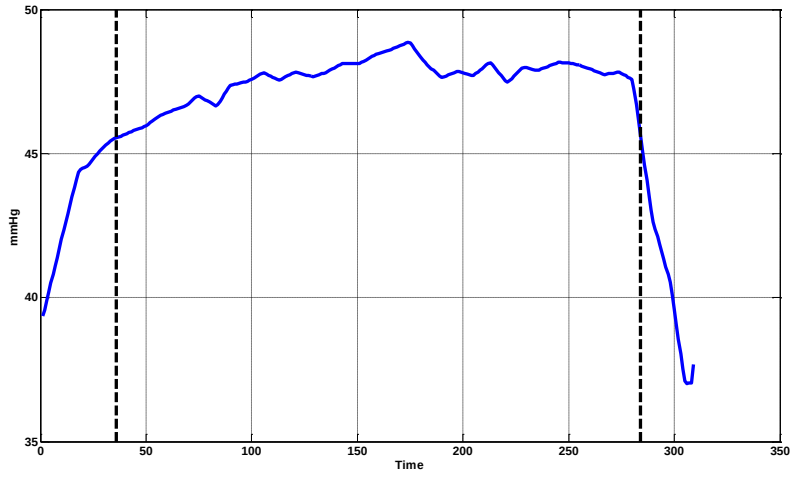

Figure 5-3 P_{ETCO_2} during hypercapnia averaged over all recordings, The dashed lines show the triggers of the onset and offset of high CO_2

Figure 5-4 also shows the last 200 seconds before the offset of hypercapnia followed by the first 200 seconds of the normocapnia of the adjusted autoregulatory parameters with respect with the onset and offset of high CO_2. The standard deviations of these parameters at different stages are also shown in the figure with vertical bars. The results showed wide inter-subject variability which was expected as shown previously [97, 98, 139]. The vertical bars in this figure, corresponds to the STD of the mean values, during the window of 100 to 150 seconds or 350 to 400 seconds. The reason behind choosing these windows are to be able to compare the models after passing the transient stage.

At the onset of hypercapnia, the models are adapting to the change from normocapnia to hypercapnia. As the last 200 seconds of normocapnia is used for the comparison between NC and HC, as this stage the initial transient while the RLS filter adaptation has passed as can be seen Figure 5-1.

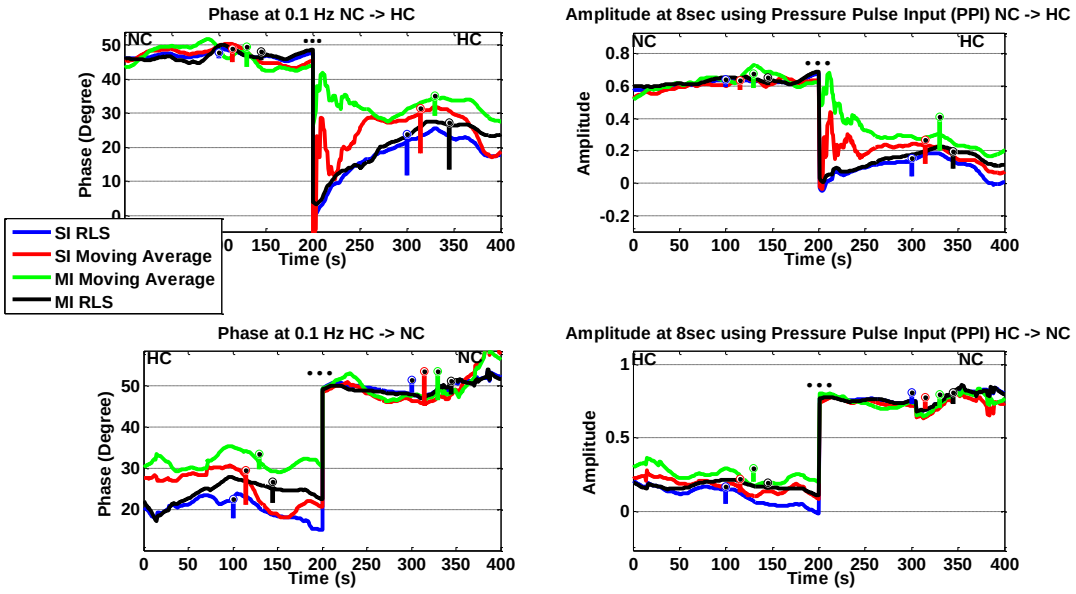

Figure 5-4 The last 200 seconds normocapnia followed by the first 200 seconds of hypercapnia at the onset of hypercapnia (top row) and the last 200 seconds of hypercapnia followed by the first 200 seconds of normocapnia (bottom row), averaged over 57 recordings phase at 0.1 Hz and amplitude at 8 seconds. The vertical lines correspond to the STD of the models averaged over windows of 100 to 150 seconds and 300 to 350 seconds. The discountinouty between different protocols should be considered (shown with three dots)

It has to be noted that, there would appear to be a discontinuity between normocapnia and hypercapnia in above figure at 200 seconds, this is an artifact because two sets of results are shown together in the above figure. Another point that needs to be considered is that, the adaptation is stopped at the end of each recording and each stage (baseline, hypercapnia and second baseline) and is started again for the next recording or stage; consequently, the sets of results are not dependent.

Table 5.3 shows the mean$\pm STD$ of the autoregulatory parameters along time across all the measurements for the different 200 seconds segments mentioned above. The results show the decrease of 16.81 to 9.36 from univariate to multivariate RLS method in the hypercapnia at the start of the onset of high CO_2 using the phase lead. It has to be noted that a smaller mean and the higher STD value for univariate models in the hypercapnia stages were as the result of the transient at the beginning of the process. The reduced STD from the multivariate model compared to univariate model shows the ability of multivariate model to deal with the transient.

This reduction in STD was also considerable when the last 200 seconds of hypercapnia at the offset of P_{ETCO_2} is considered. Standard deviation and mean values are not good indications of a good model in terms of the assessment of autoregulation, as they are related and it is hard to compare results of small STD with small mean with large STD with a large mean value.

Table 5.4 shows the results for the cluster separation which can be used as a criteria of how separated the results from different groups are. Cluster separation (section 3.4.2.3) uses the mean and the standard deviation of each segment and measures the average between their standard

	Phase at $0.1\ Hz$			
Model	NC in $NC-HC$	HC in $NC-HC$	HC in $HC-NC$	NC in $HC-NC$
Single-Input RLS	46.87 ± 8.63	17.81 ± 16.81	20.31 ± 12.28	49.36 ± 5.01
Multiple-Input RLS	46.97 ± 7.83	30.75 ± 9.36	30.92 ± 7.34	49.38 ± 4.42
Single-Input Moving Window	46.92 ± 14.44	26.09 ± 17.41	25.40 ± 18.31	48.46 ± 8.51
Multiple-Input Moving Window	46.60 ± 15.60	31.72 ± 12.68	31.63 ± 13.19	49.23 ± 9.08
	Amplitude at 8 seconds ($A8$) ($\times 10^{-2}$)			
Single-Input RLS	61.60 ± 18.29	9.70 ± 38.74	10.95 ± 25.97	77.09 ± 10.73
Multiple-Input RLS	63.34 ± 17.30	30.38 ± 20.13	28.24 ± 15.36	77.08 ± 10.19
Single-Input Moving Window	60.60 ± 27.38	19.22 ± 31.63	17.52 ± 30.41	73.68 ± 16.24
Multiple-Input Moving Window	62.90 ± 32.57	30.49 ± 27.29	24.92 ± 27.69	74.95 ± 18.46

Table 5.3 Averaged $mean \pm STD$ for phase $0.1\ Hz$ and amplitude at $8\ sec$ during different data sections for different models at the onset and offset of CO_2

deviation normalized by the difference between their mean values (eq.4.37-eq.4.39). Bigger values in cluster separation correspond to better separation between NC and HC. The results show that for the RLS models, in phase lead, the separation can be improved by 190% and 123% for the onset and the offset of hypercapnia respectively whilst these values were -25.51% (i.e worse) and 121% for $A8$. The results also show that the univariate and multivariate moving window methods perform poorly compared to RLS methods. It has to be noted that for these analysis the transient at the beginning of the data are removed.

	Phase at $0.1\ Hz$		Amplitude at $8\ sec$	
Model	$NC->HC$	$HC->NC$	$NC->HC$	$HC->NC$
Single-Input RLS	8.32	15.46	12.62	13.59
Multiple-Input RLS	15.88	19.13	9.40	16.48
Single-Input Moving Window	5.15	5.93	8.06	13.80
Multiple-Input Moving Window	4.90	6.90	4.30	10.79

Table 5.4 Cluster separation value for the onset and offset of CO_2 for different time-varying models

By using the coherence function discussed in section 5.2.4. Figure 5-5 shows the time-varying univariate coherence measured between ABP as input and $CBFV$ as output and time-varying multivariate coherence measured with ABP, P_{ETCO_2} as inputs and $CBFV$ as output, averaged over all 57 recordings. In this work, the data are synchronized by the trigger of onset and offset of P_{ETCO_2} and show the last $200\ sec$ of normocapnia and first $200\ sec$ of hypercapnia after the trigger of the valve. In this figure, the coherence as a function of both time and frequency can be observed.

It is apparent from the results that univariate coherence provides lower values at low frequencies ($f < 0.05\ Hz$) at all the stages of measurement ($\Gamma_p^2(f) < 0.30$). However at these frequencies the multivariate coherence function provides much higher values ($\Gamma_M^2(f) > 0.45$) for different levels of P_{ETCO_2} which is in agreement with the finding of previous authors [91, 138]. It is also observed multivariate coherence provided higher values ($\Gamma_M^2(f) > 0.58$) when the subject is in hypercapnia (impaired autoregulation). It has to be noted that as the recordings were low-pass filtered with cut-off frequency at $0.4\ Hz$.

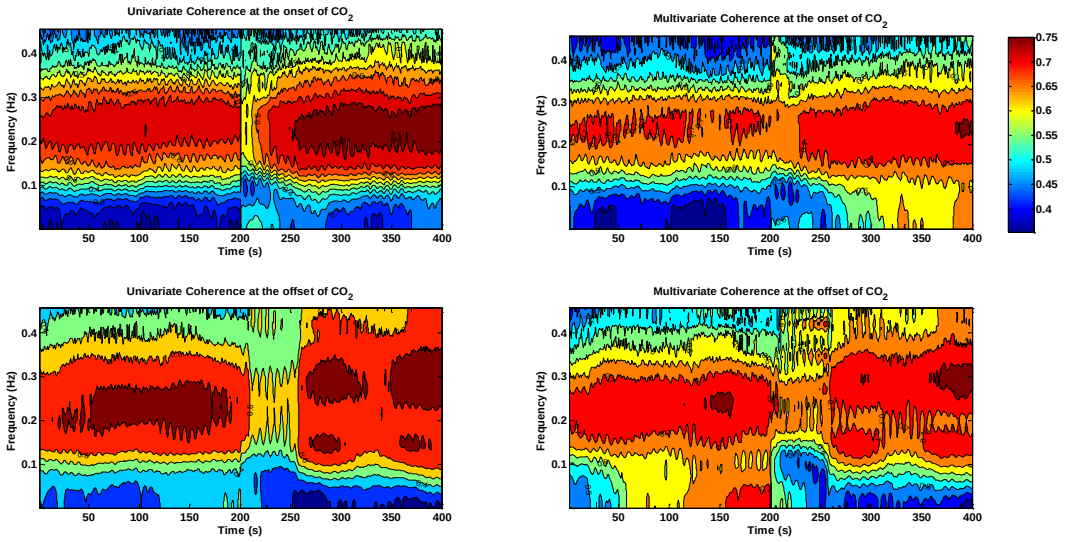

Figure 5-5 Univariate (left column) and multivariate (right column) coherence function at different times at the onset and offset of CO_2 averaged over all 57 recordings

It can also be seen from above figure that at the transient between baseline to hypercapnia at the onset of hypercapnia and also at the transient between hypercapnia to normocapnia at the offset of hypercapnia, coherence measured from the univariate model provides lower values ($\Gamma_p^2(f) < 0.53$) compared to coherence calculated from multivariate mode ($\Gamma_p^2(f) > 0.68$) in the frequency ranges $0.12 < f < 0.32\,Hz$. However the results at other frequency bands or in the steady state of the measurements provide similar results. This illustrates that the contribution of the additional input ($P_{ETCO_2}\ term$) is firstly at low frequencies which is consistent with the finding of [35, 46, 93], and it can also improve the linear model fit and hence ability to explain of $CBFV$ at higher frequencies($0.12 < f < 0.32\,Hz$) when the transient section is studied.

A paired t-test analysis is also carried out in order to check the significance difference between univariate and multivariate coherence function at different frequency range and also at different times.

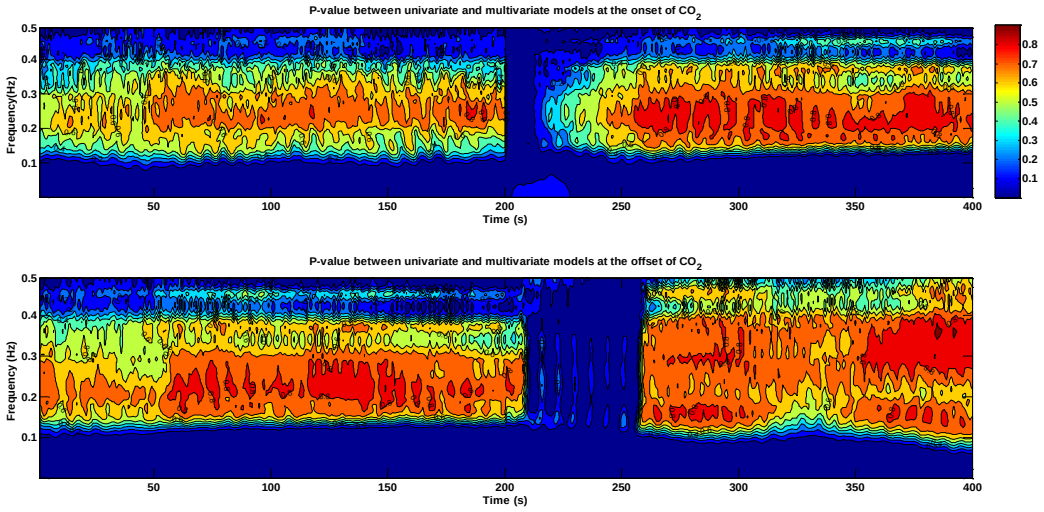

Figure 5-6 paired t-test between univariate and multivariate coherence functionat different times at the onset and offset of CO_2 averaged over 57 recordings

Figure 5-6 illustrates the results of this test. The trigger between normocapnia and hypercapnia and vice versa is at $t = 200$ seconds. It is apparent from Figure 5-6 that time-varying multivariate coherence using ABP and P_{ETCO_2} provides significanltly different results when it is compared to univariate coherence with just ABP at both low frequencies ($f < 0.05\,Hz$) and in the transient between the onset and offset of $PETCO_2$ (top figure). However the results show that time-varying models are not significantly different at frequencies $0.05 < f < 0.4\,Hz$ in steady stage which indicates that univariate time-varying models with only ABP is adequate to explain the characteristics of $CBFV$ at those frequencies.

5.4 Discussion

Univariate and multivariate time-varying analysis of the dynamics of cerebral autoregulation using RLS and moving-window analysis have been carried out in this study. This is achieved by using the relationship between $ABP \rightarrow CBFV$ and $ABP, P_{ETCO_2} \rightarrow CBFV$ during step-wise changes in P_{ETCO_2}. The results showed that by adding $P_{ETCO_2}$to univariate model ($ABP - CBFV$) in addition to the improvement to the model fit, better assessment of autoregulation in term of better separation between normocapnia and hypercapnia using autoregulatory parameters used in this chapter (phase at $0.1\ Hz$ and amplitude at 8 seconds using PPI) can be achieved. The results also show that the effect of P_{ETCO_2} toward the spontaneous changes in $CBFV$ is significantly higher in hypercapnia compared to normocapnia. It is also shown that multivariate coherence provided higher values at the transient phase between normocapnia to hypercapnia and vice versa and it is also shown that it is significantly different to univariate models during this transients and at low frequencies ($f < 0.1\ Hz$) (Figure 5-6).

Many authors have used univariate models using ABP as input to study $CBFV$ variability. However it is known that ABP is not the only factor for the spontaneous changes in $CBFV$ [23, 35, 90, 93]. CO_2 is one of many factor or a specially important one and it has vasodilatory effect on cerebral vessels, increasing $CBFV$ [73]. Different studies have been carried out to characterize the dynamic relationship between $CO_2 - CBFV$ by either measuring the response of $CBFV$ to a step change in end-tidal CO_2 [88, 89], or by continuous recording of breath-by-breath spontaneous fluctuations in CO_2 [39, 74, 98, 114]. The multivariate analysis of the dynamic cerebral autoregulation using linear and nonlinear methods has also been studied [35, 90-93]. Mitsis *et al.* [92] and Kouchakpour *et al.* [93], showed that P_{ETCO_2} as the secondary input can improve the model fit and further showed that the nonlinear interaction between ABP and P_{ETCO_2} has also a major contribution toward $CBFV$ variability. Peng *et al.* [91] also showed that the low values of coherence in low frequency range ($f < 0.04$) is partly due to the effect of CO_2. Mitsis *et al.* [35] and in section 3.3.2 confirmed this result by showing the power spectra of the residual using multivariate nonlinear model can be brought down to almost zero over the whole of the frequency range ($0 - 0.5\ Hz$) which suggest that $CBFV$ variability can almost be explained to a very large extent using nonlinear model with ABP and P_{ETCO_2} as inputs.

It is also known that the dynamic relationship between ABP and $CBFV$ is time varying [85, 87]. Liu *et al.* [114], showed that the dynamic relationship between ABP and $CBFV$ can be studied using time-varying adaptive RLS method. Liu *et al.* [114] used phase lead as the autoregulatory parameter

to assess autoregulation and found that the cerebral autoregulation responses to the P_{ETCO_2} step-up are significantly slower than those to the P_{ETCO_2} step-down. Peng *et al.* [146] used CO_2 reactivity to modify the phase relationship between ABP and $CBFV$ in the low-frequency band. Payne *et al.* [146] suggested that the low value of the synchronization index at low frequency does not mean that ABP and $CBFV$ are not related but they relationship is distorted in that frequency range by CO_2. He showed that by including CO_2 the estimated phase shift of $ABP - CBFV$ system can be increased significantly in the low-frequency band.

In this work the univariate time-varying adaptive RLS algorithm is modified to include the effect of P_{ETCO_2} on the variation of $CBFV$, both univariate and multivariate moving-window methods are also applied to assess cerebral autoregulation. The results show that multivariate models improve the model fit compared to univariate models for RLS and moving-windows by 16.55% and 32.08% ($NMSE$) respectively. Phase lead and amplitude at 8 seconds from the response of the system to a pressure pulse response (PPR) are used as autoregulatory parameters to assess autoregulation. The results show reduction in the autoregulatory parameters when the subjects went from normocapnia to hypercapnia in all the models. However multivariate RLS method shows better cluster separation compared to other univariate time-varying adaptive methods.

The results from the coherence function using both univariate and multivariate models also show that the impact of P_{ETCO_2} on the variation of $CBFV$ is higher when the subject in hypercapnia compared to normocapnia.

The results from the time-frequency coherence function also show that the low values of coherence at low frequencies is partly due to the effect of P_{ETCO_2}, which is in agreement with the finding of Peng *et al.* [91], but also the low values at the transient between normocapnia and hypercapnia can be increased by including P_{ETCO_2} which has not been noted previsouly. The results also show that the improvement in separating NC at the onset and offset of CO_2 from HC for $SI - RLS$ and $MI - RLS$ is small and large scatter between subjects is observed. However the results from cluster separation of phase lead demonstrate that the multivariate time-varying models provide better results compared to the corresponding univariate models. The significance test comparing univariate and multivariate time-frequency coherence (Figure 5-6) show that the improvements in the low frequency range and at the transient between normocapnia to hypercapnia and vice versa are significant which shows the importance of P_{ETCO_2} in the assessment of autoregulation. P_{ETCO_2} and ABP are not the only parameters to affect $CBFV$ variability (even though they can explain most of the variability), so models to study the effect of other parameters such as O_2 may improve the estimation of the dynamics of the cerebral autoregulation system. This can be used as the next step.

It has to be noted that the difference between RLS and MW models is raised based on the choice of the window length and the value of λ. As the result of these differences, it is impossible to simply and objectively compare the performance of these two approaches as their initialization is different [86]. However the results suggest that by adding P_{ETCO_2} as a secondary input to the univariate model, in both cases the analysis can be improved in term of both model fit and the assessment of autoregulation.

5.5 Conclusion

In this chapter the dynamic relationship between arterial blood pressure and cerebral blood flow velocity was viewed as time-varying and nonlinear and time-varying algorithms (RLS and moving window) are shown to be able to track time-varying characteristics of dynamic cerebral autoregulation. In this work, it is first shown that by having P_{ETCO_2} as the secondary input, the $NMSE$ is improved compared to univariate models (as mathematically necessary). However in this work only training data could be used and no validation dataset was available.

Previous finding of other authors [91, 138] showed a low coherence value at low frequencies which suggested that univariate models cannot explain the variability of $CBFV$ at these low frequencies. It was also shown that the phase lead between ABP and $CBFV$ can be used in the univariate time-varying RLS method as an assessment of autoregulation. The results now show that multivariate time-varying model ($MI - RLS$) with ABP and P_{ETCO_2} can overcome the overshoot at the beginning of the transient in the set of data from normo- to hypercapnia.

In this chapter it is also shown that the effect of P_{ETCO_2} on the variation of $CBFV$ is more significant when the subject is in hypercapnia. The result also indicated that the multivariate time-varying model can improve our coherence value at low frequency range and also at the transient between normocapnia and hypercapnia and vice versa.

Chapter 6 : Analysis of new protocol of data collection using pseudorandom step-wise changes in pressure using $\boldsymbol{LBNP}$

6.1 Introduction

In the previous chapters data from spontaneous variations in $CBFV$ and ABP were analyzed during NC and HC. For the measurement of dynamic cerebral autoregulation many different experimental and signal analysis methods have been proposed, without a "gold-standard" having emerged [139]. The exploitation of spontaneous variations in arterial blood pressure (ABP) and cerebral blood flow velocity ($CBFV$) is now perhaps most common, as it requires minimal interference with the patients. However, low variability in arterial blood pressure has been associated with limited performance [139]. Different techniques have been employed to oscillate arterial blood pressure but measurement reproducibility has been poor. Some of these approaches to create blood pressure stimuli which have been widely used are: complex changes from natural spontaneous variation [2, 32, 75, 85], periodic variation induced by rhythmic postural changes or slow breathing [65] , step changes induced by the use of thigh cuffs or carotid artery compression [5, 63]. All these techniques generate a time series with blood pressure as the input and blood flow velocity as the output.

At Southampton General Hospital a new hardware and software system was developed, for the measurement of blood flow control, which allowed the inducement of small random, step-wise changes in blood pressure and inspired carbon dioxide (CO_2) level that can be easily and safely repeated and may be applicable as a clinical tool. This new tool was used to collect a dataset from 31 healthy subjects in two separate sections. The current chapter presents initial results from that dataset.

This experiment benefited from the use of $LBNP$ (Lower-body-negative pressure) discussed in section 2.9.1 which generates a controllable pressure variation, around the lower limbs of a subject resulting in temporary lowering the blood pressure [64]. The experiment also used a valve system to control the flow of inspired air/CO_2 mixture.

The main aim of this newly proposed experimental paradigm is to increase the variability in the changes in blood pressure in order to obtain more robust assessment of cerebral autoregulation, given that it has already been established that increasing ABP variability can improve estimates of cerebral autoregulation [74, 97]. The protocol of pseudorandom step-wise changes in pressure is well tolerated by the volunteers. It appears promising for the study of cerebral autoregulation, as a means of inducing small, well controlled transient increases in blood flow and pressure and is, somewhat surprisingly, associated with increased performance of autoregulation.

A new GUI (Graphical User Interface) is also built in order to review and edit the collected data and save it in different formats for further use (Appendix IV).

The first section introduces the experiment and data collection procedure. In the following sections, data collection procedure and results from the analysis of cerebral autoregulation during different experimental phases are presented and discussed.

6.2 Methods

6.2.1 Data Collection

All the measurements were performed on 31 healthy adult volunteers between the age of 18 and 50 with no history of cardiovascular disease or other serious medical conditions, under no medication, not pregnant and with waist measurements below 40 inches.

Each data from each subject were collected in two separate seasons. One subject did not come back for the second recording (61 recordings all together).

The measurement of blood pressure was carried out using Finapres (section 2.8.2) (Ohmeda Finapres 2300). The finger which was used for the measurement of blood pressure was rested at approximately the level of the heart. The blood flow velocity was monitored with a $2\ MHz$ pulsed transcranial Doppler ultrasound (ulti-Dop T, manufactured by DWL Elektronische Systeme GmbH, Sipplingen, Germany) from both middle cerebral arteries. The probes were held in position by an elastic head strap. For the measurement of end tidal carbon dioxide, a computer controlled valve switched inspired air to $5\%\ CO_2$ in air mixture (fed from a $200\ litre$ Douglas bag). The experiment consisted of 6 procedures carried out in random order (apart from baseline which was always collected at the beginning of the experiment).

1. Baseline (NC); the volunteer at rest
2. Hypercapnia (HCO_2); $5\%\ CO_2$/air

3. Random lower body negative pressure ($LBNP$)
4. Hypercapnia+lower body negative pressure ($HCO_2 - LBNP$)
5. Random 5% CO_2 ($RHCO_2$)
6. Random 5% CO_2 +lower body negative pressure ($RHCO_2 - LBNP$)

6.2.2 Data pre-processing

A typical raw data from all the channels is shown in Figure 6-2. ABP, $CBFV$ and CO_2 were digitized at $250\ Hz$ whilst the original sampling frequency of ECG was $500\ Hz$ in order to be able to measure heart rate (HR) accurately.

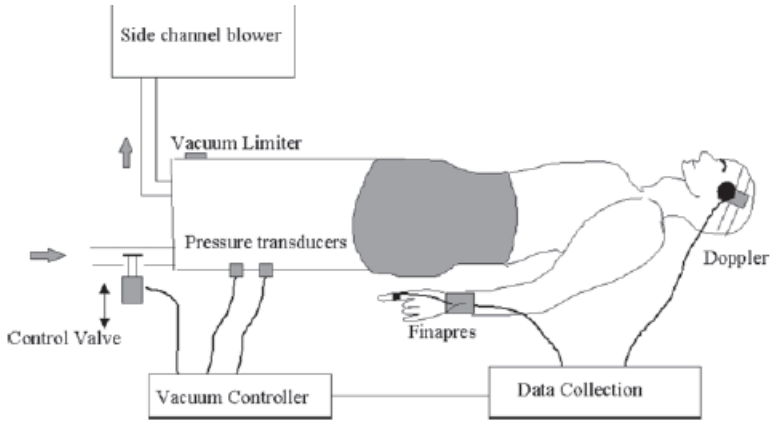

Figure 6-1 Schematic representation of the lower body negative pressure chamber. Taken from [139]

The signals are visually inspected, narrow spikes and artifacts were removed and the ABP signal calibrated at the beginning of each recording. The systolic and diastolic $CBFV$ and ABP were calculated automatically by identifying the maximum and minimum values in each heart-beat. Mean ABP ($MABP$) and $CBFV$ ($MCBFV$) were calculated with a 3^{rd} order Butterworth filter (applied in the forward and reverse direction to give zero phase shift) with a cut-off frequency of $0.5\ Hz$. The start of each heart cycle was automatically identified from both left and right ABP and ECG and HR is calculated from these signals. HR was calculated from all these three different signals (left ABP, right ABP and ECG).

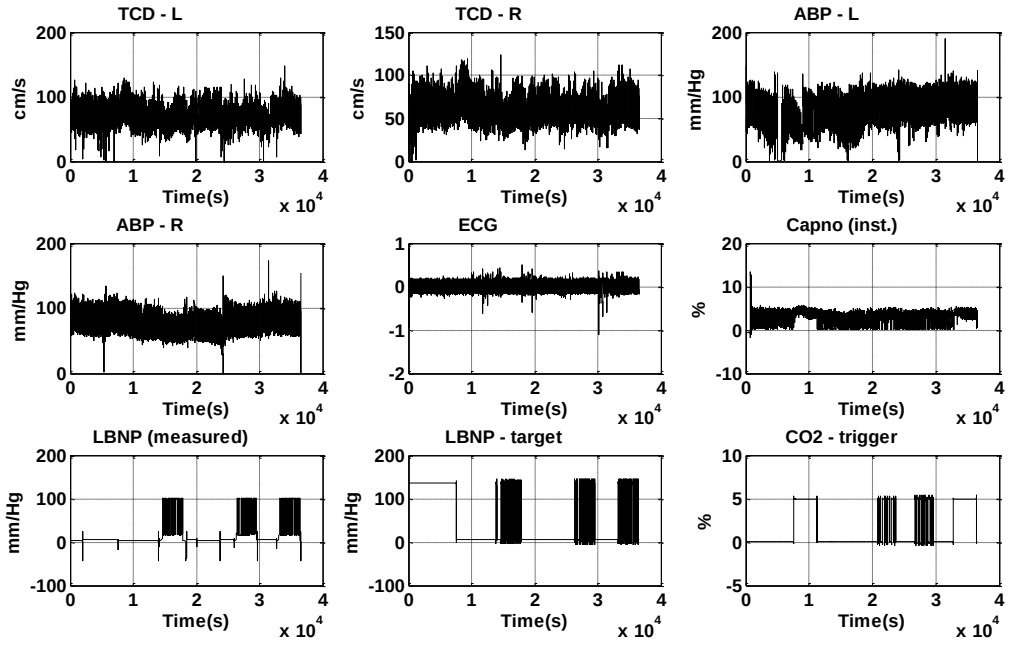

Figure 6-2 typical recorded signals

The signals are then down-sampled to $1\,Hz$ to increase numerical robustness in parameter estimation. The resampled data are then band-pass filtered using a 3^{rd} order Butterworth filter with a cuff-off frequency of $0.03\,Hz$ and $0.4\,Hz$ to remove very slow variation and baseline shift and high frequency components. The removed sections in the data are marked as $NaNs$ (Not-A-Number) in the calculations. Data are then normalized by their mean value using the following equation to give the relative changes in the signals

$$\Delta X = \frac{X - X_{mean}}{X_{mean}} \qquad 6.1$$

Where X in above equation refers to both ABP and $CBFV$ and ΔX is the normalized variation of the data.

The start and end of different procedures are automatically selected from the trigger signals of $LBNP$ and CO_2 switch valve (Appendix IV).

In this work, following visual inspection, $MABP$ and $CBFV$ signals from either the left or right side from Finapres or MCA respectively are chosen for further analysis. Other signals extracted from the measurements are available for future analysis.

6.3 Analysis of autoregulation

The phase at $0.1\ Hz$ ($P1$) [52, 73, 116] and second coefficient of an FIR filter with 2 lags ($H1$) [74] are used (section 3.4.2) as parameters for the assessment of cerebral autoregulation. $P1$ has been extensively used in the literature and shown to be a powerful and easy parameter to extract from recorded data [52, 73, 116]. In Chapter 3 it was shown that $H1$, despite its simplicity can provide robust assessment of autoregulation. In this work, these two autoregulatory parameters for this preliminary analysis of the novel protocol for data collection are studied. Mont-Carlo simulation is also used to measure the variability of these autoregulatory parameters as discussed in Chapter 3.

6.3.1 Statistical analysis

The Wilcoxon signed-rank is adopted as a non-parametric statistical hypothesis test to compare the effect of selected parameters on the classification of autoregulatory responses. It is also used to test the mean values of ABP and $CBFV$ and their variations during different protocols. The variation of different autoregulatory parameters ($P1, H1$) calculated from Monte-Carlo simulation is also tested. A significance level of 5% is used.

6.3.1.1 Intraclass correlation (ICC)

Intraclass correlation (ICC) is a measure of the reliability of measurements. It is a general measurement of agreement, where the measurements used are assumed to be continuous and have a normal distribution. It is widely used when agreement between two or more evaluation methods on the same set of subjects is assessed. It can be used to assess the agreement between repeated measurements [147].

The key difference between ICC and Pearson correlation coefficient is that in ICC the data are centered and scaled using a pooled mean and standard deviation (STD), whilst in the Pearson correlation, each individual variable is centered and scaled by its own mean and STD therefore Pearson's correlation quantifies how close two measurements are to a best-fit straight lit but not how the values agree [147].

Intraclass correlation (r) for two groups consisting of N paired data points ($x_{n,1}, x_{n,2}$) is introduced as [147]

$$\bar{x} = \frac{1}{2N}\sum_{n=1}^{N}(x_{n,1} + x_{n,2}) \tag{6.2}$$

$$s^2 = \frac{1}{2N-1}\left\{\sum_{n=1}^{N}(x_{n,1} - \bar{x})^2 + (x_{n,2} - \bar{x})^2\right\} \tag{6.3}$$

$$r = \frac{1}{(N-1)s^2}\sum_{n=1}^{N}(x_{n,1} - \bar{x})(x_{n,2} - \bar{x}) \tag{6.4}$$

where in above equation $2N - 1$ is the number of degree of freedom.

6.4 Results

As previously mentioned, a total of 31 subject of age 18 to 50 are studied on two separate days. All volunteers came back for the second measurement apart from one. Total number of 61 measurements were collected. All these measurements are of sufficient quality to be analyzed. After some initial adjustments to the protocol to increase comfort, the procedure was generally considered acceptable by the volunteers; the need for a face-mask to deliver and measure CO_2 levels, was deemed the least comfortable aspect. The average drop in blood pressure following each 'suction' is 7.5%, confirming that the gas mixture was inspired. This is calculated by synchronizing the falling edge and raising edge of $LBNP$ during each suction for each recording and calculating the mean drop in pressure for all measurements (Figure 6-3).

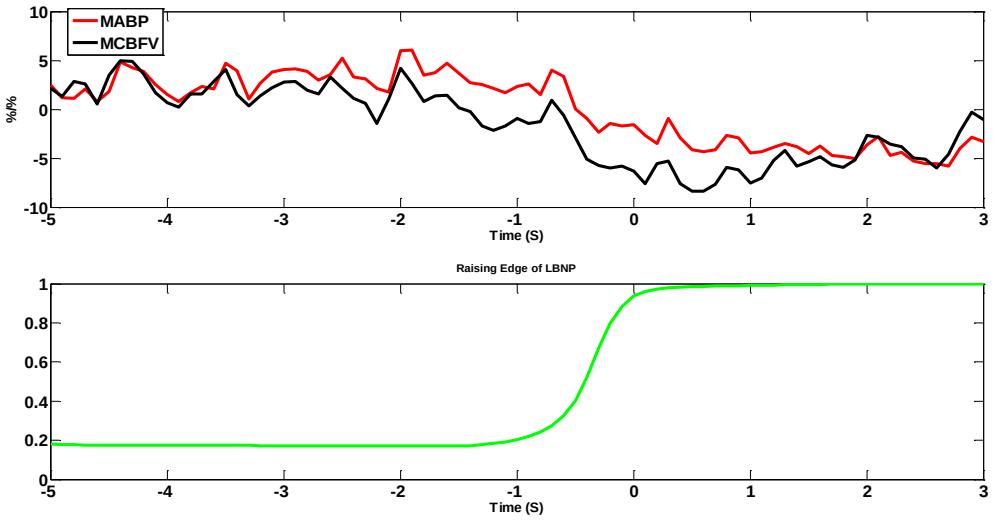

Figure 6-3 Normalized $MABP$ and $MCBFV$ during the raising edge of $LBNP$ averaged over all recordings

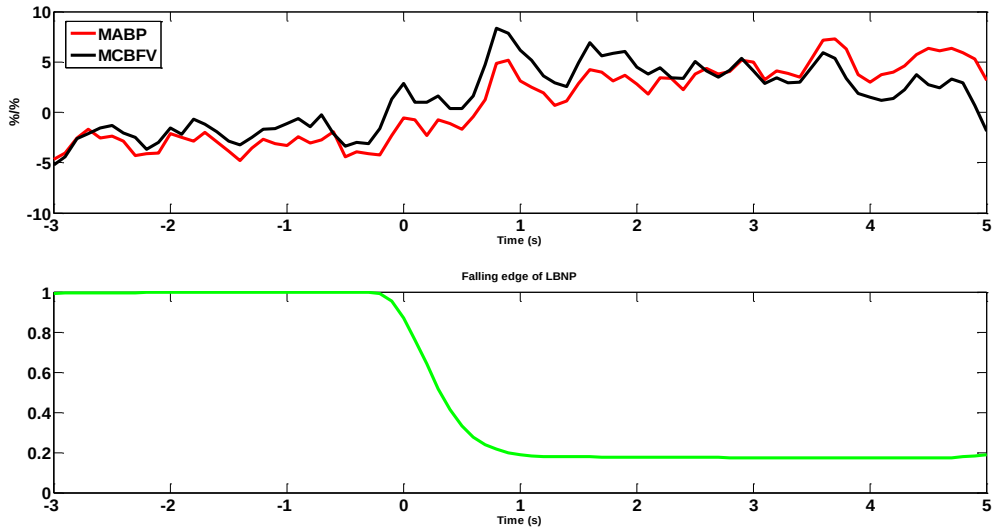

Figure 6-4 Normalized $MABP$ and $MCBFV$ during the falling edge of $LBNP$ averaged over all recordings

An overview of the mean$\pm STD$ of $ABP, CBFV$ and CO_2 for different protocols is presented in Table 6.1. The increase in mean $CBFV$ from baseline to HCO_2 by $7.66\ cm.s^{-1}$ shows the effect of high CO_2. The 5% increase in CO_2 from baseline to HCO_2 is also apparent from the result. The ABP during all procedures is in the range 80 to $90\ mmHg$.

Signals	NC	$LBNP$	HCO_2	$HCO_2 - LBNP$	$RHCO_2$	$RHCO_2 - LBNP$
	Mean$\pm STD$	Mean$\pm$ STD	Mean$\pm$ STD	Mean$\pm$ STD	Mean$\pm$ STD	Mean$\pm$ STD
$ABP\ (mmHg)$	86.45 ± 12.52	80.99 ± 12.53	89.39 ± 14.59	83.90 ± 13.35	84.90 ± 15.91	84.30 ± 12.10
$CBFV\ (cm/s)$	66.58 ± 12.15	62.92 ± 11.19	74.24 ± 14.07	70.89 ± 12.93	68.98 ± 11.83	65.21 ± 11.77
$ETCO_2(\%)$	4.72 ± 0.41	5.07 ± 0.33	5.44 ± 0.34	5.29 ± 0.39	5.01 ± 0.33	4.89 ± 0.35

Table 6.1 An overview of signals during different procedures averaged across 61 recordings

Table 6.2 depicts the result from p-values using Wilcoxon signed-rank pair-wise test on the mean values of ABP and $CBFV$ during different procedures. The results show that the mean $CBFV$ is significantly different between all measurements apart from between baseline and $LBNP$.

Procedures	$LBNP$		HCO_2		$HCO_2 - LBNP$		$RHCO_2$		$RHCO_2 - LBNP$	
	$CBFV$	ABP	$CBFV$	ABP	$CBFV$	ABP	$CBFV$	ABP	$CBFV$	ABP
NC	$\mathbf{2.7 \times 10^{-7}}$	$\mathbf{0.002}$	$\mathbf{2.3 \times 10^{-10}}$	$\mathbf{0.016}$	$\mathbf{3.5 \times 10^{-5}}$	0.194	$\mathbf{0.003}$	0.777	0.50	0.088
$LBNP$			$\mathbf{5.1 \times 10^{-10}}$	$\mathbf{3.3 \times 10^{-}}$	$\mathbf{1.8 \times 10^{-9}}$	0.22	$\mathbf{8.8 \times 10^{-9}}$	$\mathbf{0.002}$	$\mathbf{8.7 \times 10^{-6}}$	$\mathbf{0.04}$
HCO_2					$\mathbf{0.002}$	$\mathbf{0.008}$	$\mathbf{2.1 \times 10^{-7}}$	0.123	$\mathbf{2.6 \times 10^{-9}}$	$\mathbf{0.004}$
$HCO_2 - LBNP$							$\mathbf{0.005}$	0.297	$\mathbf{3.6 \times 10^{-6}}$	0.93
$RHCO_2$									$\mathbf{8.8 \times 10^{-4}}$	0.257

Table 6.2 p-values calculated using significance test (Wilcoxon) between the mean value of ABP and $CBFV$ during different procedures (Significant difference is indicated by bold numbers)

The main aim of this new protocol is to increase the variability in ABP and as a result of that, obtain better estimation of autoregulation. For this purpose, the effect of different procedures on the variability (STD) of both ABP and $CBFV$ is studied. The average of the variation of different procedures across all recordings through the period of the data collection is given in Table 6.3. It can be seen that the ABP has increased in procedures with $LBNP$ compared to the respective procedure without $LBNP$ ($NC \rightarrow LBNP, HCO_2 \rightarrow HCO_2 - LBNP$ and $RHCO_2 \rightarrow RHCO_2 - LBNP$).

Signals	NC	$LBNP$	HCO_2	$HCO_2 - LBNP$	$RHCO_2$	$RHCO_2 - LBNP$
	STD	STD	STD	STD	STD	STD
$ABP\ (mmHg)$	3.02	4.06	3.17	4.22	3.02	4.15
$CBFV\ (cm/s)$	3.10	4.02	3.18	4.08	3.17	4.44
$ETCO_2(\%)$	0.31	0.33	0.17	0.16	0.31	0.32

Table 6.3 STD of different procedures averaged across all recordings through the period of data collection

Table 6.4 shows the result of this significance test. The results show that STD of ABP and $CBFV$ during baseline are significantly different to corresponding ABP and $CBFV$ during $LBNP, HCO_2 - LBNP$ and $RHCO_2 - LBNP$ but not to others ($p < 10^{-8}$). On the other hand, the STD of ABP and $CBFV$ signals are not significantly different from the $LBNP$ to $HCO_2 - LBNP$ and $RCO_2 - LBNP$. No significant difference was also seen between HC and NC for either of the measured signals.

Procedures	$LBNP$		HCO_2		$HCO_2 - LBNP$		$RHCO_2$		$RHCO_2 - LBNP$	
	$CBFV$	ABP	$CBFV$	ABP	$CBFV$	ABP	$CBFV$	ABP	$CBFV$	ABP
NC	$\mathbf{1.1 \times 10^{-8}}$	$\mathbf{1.5 \times 10^{-7}}$	0.493	0.204	$\mathbf{1.8 \times 10^{-8}}$	$\mathbf{4.2 \times 10^{-9}}$	0.789	0.659	$\mathbf{4.9 \times 10^{-9}}$	$\mathbf{5.6 \times 10^{-8}}$
$LBNP$			$\mathbf{3.3 \times 10^{-6}}$	$\mathbf{7.1 \times 10^{-5}}$	0.34	0.16	$\mathbf{8.9 \times 10^{-9}}$	$\mathbf{7.6 \times 10^{-8}}$	0.088	0.964
HCO_2					$\mathbf{1.7 \times 10^{-7}}$	$\mathbf{4.4 \times 10^{-7}}$	0.547	0.183	$\mathbf{4.3 \times 10^{-8}}$	$\mathbf{8.1 \times 10^{-6}}$
$HCO_2 - LBNP$							$\mathbf{9.8 \times 10^{-9}}$	$\mathbf{8.6 \times 10^{-9}}$	0.122	0.383
$RHCO_2$									$\mathbf{3 \times 10^{-9}}$	$\mathbf{8.36 \times 10^{-8}}$

Table 6.4 p-values calculated using significance test between the STD of ABP and $CBFV$ during different procedures

The above table shows that by introducing $LBNP$, the variability in ABP has increased (from baseline $\rightarrow LBNP$,$HCO_2 \rightarrow HCO_2 - LBNP$ and $RHCO_2 \rightarrow RHCO_2 - LBNP$) which is in agreement with the expectation that $LBNP$ increases variability and suggests that the protocol is affecting ABP and $CBFV$ as expected. Next, different autoregulatory parameters are studied to test whether this increase in variability has led to better assessment of autoregulation.

Table 6.5 shows the mean$\pm STD$ of the chosen autoregulatory parameters ($P1$ and $H1$) for all available measurements during the different procedures carried out. Figure 6-5 shows the autoregulatory parameters extracted from each volunteer recording during different procedures plotted against each other. The $P1$ for all procedures is positive, and larger at baseline compared to HCO_2 which is in agreement with the finding of others [52, 65, 73, 116]. The reduction in $P1$ from $LBNP$ to $HCO_2 - LBNP$ can also be seen in Table 6.5, which is in agreement with the expectation in previous works [52, 73, 116].

The result of $H1$ also met our expectation [74] with larger mean absolute values (less negative) in hypercapnia compared to the relevant normocapnia stages. It can be seen that during normocapnia the majority of $P1$ are larger in NC than HCO_2 and thus lie below the line of identity. The result also shows that $P1$ during $LBNP$ is larger than during HC. The reason being that during $LBNP$ the subject is still in normocapnia and is expected to behave in that manner. The same structure of result is also delivered by $H1$ where, $H1$s are larger (less negative) in hypercapnia compared to both normocapnia and $LBNP$. However the comparison between HCO_2 and $HCO_2 - LBNP$ for both $P1$ and $H1$ suggests that the values not to be clearly different.

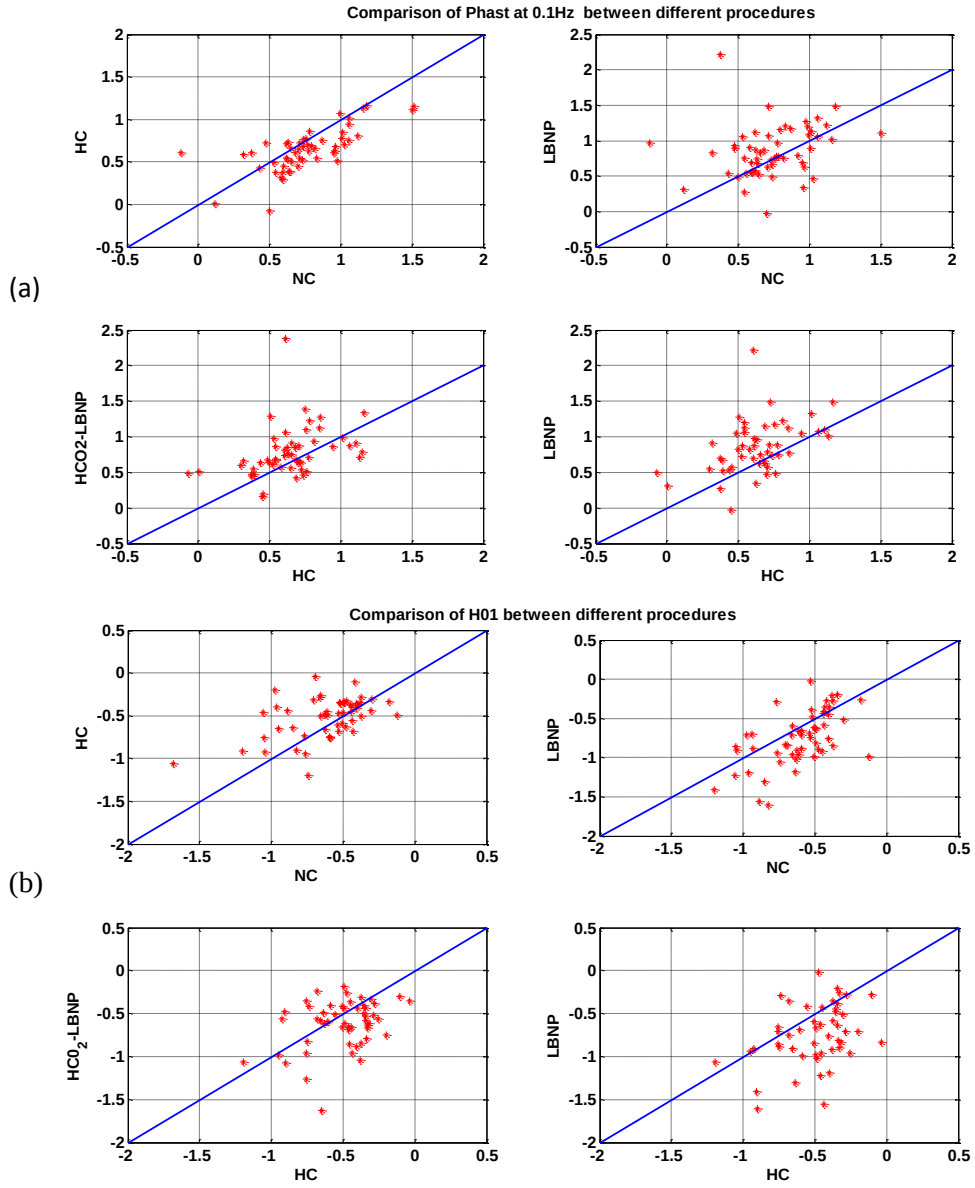

Figure 6-5 Comparison between different autoregulatory parameters for $P1$ (top two rows) and $H1$ (bottom two rows). In this plot each point represents one recording from one subject. The blue line is the separation line and is used for better visual observation

	Mean$\pm STD$ of $P1$	Mean$\pm STD$ of $H1$
NC	0.754 ± 0.286	-0.62 ± 0.27
$LBNP$	0.855 ± 0.361	-0.77 ± 0.40
HCO_2	0.643 ± 0.251	-0.52 ± 0.24
$HCO_2 - LBNP$	0.790 ± 0.343	-0.65 ± 0.34
$RHCO_2$	0.776 ± 0.283	-0.66 ± 0.36
NC	0.774 ± 0.280	-0.76 ± 0.43

Table 6.5 Mean$\pm STD$ of different autoregulatory parameters for different procedures

However in order to test whether these differences shown in Table 6.5 are significant, Wilcoxon signed-rank pair-wise tests for both $P1$ and $H1$ during these different procedures is used (Table 6.6). The results show that baseline $P1$ is significantly different to $P1$ for $LBNP$ and HCO_2, but not others. The result also shows that $P1$ for HCO_2 is significantly different to all other procedures.

Procedures	$LBNP$		HCO_2		$HCO_2 - LBNP$		$RHCO_2$		$RHCO_2 - LBNP$	
	$P1$	$H1$	$P1$	$H1$	$P1$	$H1$	$P1$	$H1$	$P1$	$H1$
NC	$\mathbf{0.034}$	$\mathbf{6.4 \times 10^{-4}}$	$\mathbf{3.1 \times 10^{-5}}$	$\mathbf{0.018}$	0.97	0.523	0.852	0.619	0.482	$\mathbf{0.004}$
$LBNP$			$\mathbf{2.1 \times 10^{-5}}$	$\mathbf{1.5 \times 10^{-5}}$	$\mathbf{0.016}$	$\mathbf{0.002}$	$\mathbf{0.006}$	$\mathbf{4.1 \times 10^{-4}}$	0.067	0.291
HCO_2					$\mathbf{0.004}$	$\mathbf{0.007}$	$\mathbf{0.005}$	$\mathbf{0.013}$	$\mathbf{8.6 \times 10^{-4}}$	$\mathbf{4.2 \times 10^{-5}}$
$HCO_2 - LBNP$							0.996	0.564	0.305	$\mathbf{0.049}$
$RHCO_2$									0.575	$\mathbf{0.034}$

Table 6.6 Wilcoxon signed-rank test for $P1$ and $H01$ during different procedures over all measurements

The results for $H1$ show that during baseline they are significantly different to HCO_2 and $LBNP$ and $RHCO_2 - LBNP$ but not the others. It can also be seen that $H1$ during $LBNP$ is significantly different to all other procedures but to $RHCO_2 - LBNP$. On the other hand the $H1$ autoregulatory parameter during HCO_2 is significantly different to all other procedures.

As mentioned before, the main aim of this new protocol is to obtain a more robust assessment of autoregulation. In order to study the robustness of this protocol, Monte-Carlo simulation introduced in section 3.4.2.3 is used to measure the variability of $P1$ and $H1$ during these different procedures and then Wilcoxon signed-rank pair-wise test is used to compare the variability between them.

	Mean$\pm STD$ of STD of $P1$	Mean$\pm STD$ of STD of H1
NC	0.133 ± 0.063	0.101 ± 0.048
$LBNP$	0.106 ± 0.065	0.095 ± 0.037
HCO_2	0.101 ± 0.053	0.071 ± 0.035
$HCO_2 - LBNP$	0.123 ± 0.196	0.084 ± 0.046
$RHCO_2$	0.135 ± 0.058	0.095 ± 0.041
$RHCO_2 - LBNP$	0.132 ± 0.125	0.110 ± 0.652

Table 6.7 Mean$\pm STD$ of the variation of the autoregulatory parameters ($P1, H1$) during different procedures over all recordings

Table 6.7 shows the overall Mean $\pm STD$ of variation of both $P1$ and $H1$ during all 6 procedures carried out and Table 6.8 the corresponding p-values computed from these parameters. The result shows reduction of the mean and the variation of both $P1$ and $H1$ from baseline to $LBNP$. The result of the mean variation of our autoregulatory parameters from HCO_2 to $HCO_2 - LBNP$ shows an increase in variability which is in contradiction our initial expectation that $LBNP$ will provide more robust assessment of autoregulation (reduction in variability in autoregulatory parameters).

Procedures	$LBNP$		HCO_2		$HCO_2 - LBNP$		$RHCO_2$		$RHCO_2 - LBNP$	
	$P1$	$H1$	$P1$	$H1$	$P1$	$H1$	$P1$	$H1$	$P1$	$H1$
NC	$\mathbf{0.03}$	0.94	$\mathbf{4.1 \times 10^{-4}}$	$\mathbf{4.7 \times 10^{-7}}$	$\mathbf{1.6 \times 10^{-16}}$	$\mathbf{0.005}$	0.548	0.108	0.132	0.323
$LBNP$			0.16	$\mathbf{3.5 \times 10^{-5}}$	$\mathbf{0.002}$	$\mathbf{6.49 \times 10^{-4}}$	$\mathbf{0.007}$	$\mathbf{0.005}$	0.258	0.391
HCO_2					$\mathbf{4.01 \times 10^{-18}}$	0.07	$\mathbf{2.5 \times 10^{-4}}$	$\mathbf{7.4 \times 10^{-4}}$	0.107	$\mathbf{3.5 \times 10^{-8}}$
$HCO_2 - LBNP$							$\mathbf{0.003}$	0.063	$\mathbf{0.008}$	$\mathbf{4.9 \times 10^{-5}}$
$RHCO_2$									0.197	$\mathbf{0.007}$

Table 6.8 Wilcoxon signed-rank test of the variation of autoregulatory parameters ($P1, H1$) during different procedures over all measurements

It can be seen in Table 6.8 that the variability of $P1$ and $H1$ during NC are only significantly different to, HCO_2 and $HCO_2 - LBNP$.

In order to test the agreement between repeated measurements on different days, intraclass correlation (ICC) introduced in section 6.3.1.1 between the autoregulatory parameters obtained on different days. The results are shown in Table 6.9. The results show that ICC for $P1$ has increased from $NC \rightarrow LBNP$ and $RHCO_2 \rightarrow RHCO_2 - LBNP$, which indicates better repeatability can be

achieved with $LBNP$. However the results from $H1$ is not in agreement with $P1$. On the other hand reasonably high value of ICC for $RHCO_2$ requires further analysis.

	ICC for $P1$	ICC for $H1$
NC	0.29	0.1843
$LBNP$	0.34	0.0474
HCO_2	0.57	0.1615
$HCO_2 - LBNP$	0.43	0.2405
$RHCO_2$	0.14	0.6924
$RHCO_2 - LBNP$	0.30	0.0024

Table 6.9 Intraclass correlation for the autoregulatory parameters ($P1$ and $H1$) on different days

6.5 Discussion

The results from the mean of our signals shown in Table 6.1 and Table 6.2 demonstrated a significant increase in $CBFV$ from baseline to HCO_2 and $HCO_2 - LBNP$ (10.21% and 6.08% respectively) which reflects the known cerebral vasodilation as the effect of increased arterial tension of CO_2 [5, 23, 141]. Significant reduction in both ABP and $CBFV$ from baseline to $LBNP$ is also observed which is in agreement of the finding of others [130, 148] and expected from pooling of blood in the legs. The point that has to be emphasized here is that the volunteers in $LBNP$ stage are still in normocapnia and are expected to behave in similar format to baseline with respect to hypercapnia. The results in Table 6.2, confirmed this, as a significant difference between HCO_2 and baseline for both ABP and $CBFV$ is also observed in $LBNP$. The results also showed significance different between $HCO_2 - LBNP$ with $LBNP$ and NC for $CBFV$ but not for APB ($p = 19\%$ and $p = 22\%$ respectively for ABP, Table 6.2). These results seem to confirm the observation of Balldin and Sun *et al.* [130, 148] that $CBFV$ reduces with $LBNP$.

As mentioned in the introduction, the main aim of this new study is to increase variability in ABP and $CBFV$ and hopefully as the result of that, obtain more robust assessment of autoregulation. In Table 6.4, it is observed that a significant differences in the variation of ABP and $CBFV$ as the result of $LBNP$. The results in Table 6.7 show that $P1$ during $LBNP$ provides the lowest within measurement variability compared to all other procedures apart from HCO_2. It is also shown by Birch *et al.* [139] that $LBNP$ increases variability in ABP. The result of significance test between procedures without $LBNP$ (baseline, HCO_2 and $RHCO_2$) and corresponding procedures with $LBNP$ ($LBNP$, $HCO_2 - LBNP$ and $RHCO_2 - LBNP$) agreed with the finding of Birch *et al.* [139] regarding

the increase in variability of ABP and $CBFV$. The result shows very clear effect of $LBNP$ on our volunteers.

Two independent autoregulatory parameters ($P1$; phase at $0.1\ Hz$ of the frequency response, $H1$; second coefficient of FIR filter with 2 lags) are measured and used for the assessment of autoregulation. Table 6.5 shows the calculated autoregulatory parameters from all our measurements. A significant increase of 14.72% and reduction 16.12% for $P1$ and $H1$ from baseline to HCO_2 is observed, which is in agreement of findings of others [52, 65, 73, 74, 116]. The same changes is also observed from $LBNP$ to $HCO_2 - LBNP$ for both $P1$ and $H1$ (7.6% and 15.58% respectively). No significant difference is observed for either $P1$ and $H1$ between baseline and $RHCO_2$ ($p = 85\%$ and $p = 62\%$). The results also show no significant difference for $P1$ between $RHCO_2$ and $RHCO_2 - LBNP$ ($p = 57\%$). This may be due to the fact that $RHCO_2$ does not impair autoregulation significantly and it takes some time for autoregulation to respond (see Chapter 5 and [86, 114]). On the other hand $LBNP$ enhances cerebral autoregulation and $RHCO_2$ reduces it, so they may have little overall effect.

In order to study the effect of $LBNP$ on more robust assessment of autoregulation, Table 6.7 shows the Mean$\pm STD$ of variation of our autoregulatory parameters. The results show smaller variations in autoregulatory parameters and as the result of that, better assessment of autoregulation was achieved from $NC \rightarrow LBNP$ and $RHCO_2 \rightarrow RHCO_2 - LBNP$. Table 6.7 shows significant reduction in variability for both $P1$ and $H1$ from baseline to $LBNP$ of (20.3% and 5.94% respectively), however the result of variation between HCO_2 and $HCO_2 - LBNP$ did not follow the reduction pattern expected, and an increase of 15.47% and 17.88% for $P1$ and $H1$ respectively is observed. This might be due to individual movement of the head-mask and induce leakage in mask and as the result of this, $5\%\ CO_2$ is not achieved during the protocols as $LBNP$ pushes the volunteers into the chamber and introduces movement to the head-mask; however a more robust investigation is required.

The intra-subject analysis for two measurements is carried out on the same subject on two different days using intraclass correlation (ICC) (Table 6.9). The results show that by introducing $LBNP$ the ICC for $P1$ has increased and showed better agreement between the measurements on the same subject on two different days compared to NC. The same result is also observed from $RHCO_2 \rightarrow RHCO_2 - LBNP$, however $HCO_2 \rightarrow HCO_2 - LBNP$ did not show an expected increase in ICC which may again be due to a fault in the measurement or the head-mask during the protocols as discussed above. The small values of $ICCs$ also requires further analysis, and significance test between these values should be studied in more details.

Even though the current protocol is not appropriate for assessing dynamics of autoregulation due to it being quite uncomfortable and its distressing nature as the result of the force on the body induced by the vacuum. However it does have distinct advantages over previous methods. The autoregulatory parameters used in this chapter ($P1$ and $H1$) can be continuously calculated (it has to be noted these are not the only parameters that could be used) and the result of the measurement is a quantitative value on a continuous scale. This would allow us to study the changes and trends in a subject from one stage to another, which could be over a course of physiological events.

Some of the steps that can be taken in future are:

1. The number of recordings that were available in this protocol was limited. In order to limit the inter-subject variability and improve the robustness of the analysis, larger sample should be studied.
2. It can be argued that two measurements from the same subjects are not independent from each other and should not be studied as two independent measurements. This issue was tackled in Chapter 4 by removing the second recordings from the same subject. However deeper analysis should be carried out to study the repeatability within and between sessions.
3. In Figure 6-3 and Figure 6-4, the speed of changes in ABP and $CBFV$ to rising and falling edge of $LBNP$ was shown. However deeper analysis of the speed of response to $LBNP$ can be carried out. This can also be done on the falling and raising edge of CO_2 and the speed of response to the changes in CO_2 can be studied.
4. It was shown in Chapter 3 and many others [35, 46, 86, 92, 93, 135, 137] that cerebral autoregulation is a nonlinear system. Non-linear effects comparing the transients to increase and decrease in blood pressure induced by $LBNP$ can be carried out in future work to investigate whether nonlinearity is more evident with the larger transitions induced by $LBNP$.

6.6 Conclusion

In this chapter a new dataset collected from 31 healthy volunteers at Southampton General Hospital using a new hardware and software system for the measurement of blood flow control, which allowed the inducement of small random, step-wise changes in blood pressure and inspired carbon dioxide (CO_2) level was analysed. This new experiment used $LBNP$ to generate controllable pressure variation and also used a valve system to control the flow of inspired air/CO_2 mixture. The main aim of this work was to increase variability in ABP and $CBFV$ and to study the robustness of

assessment of autoregulation. The results showed that the autoregulatory parameters had significantly lower variability with $LBNP$ compared to the corresponding recording section without it. The results from intraclass correlation (ICC) on the same subject on two different increased for $P1$ when $LBNP$ was present apart from when HCO_2 was studied. It could be as the result of a fault in the measurement or the mask-head, however this requires further analysis.

The result from this new protocol generated a more robust estimate of cerebral autoregulation compared to those obtained with conventional methods, however the improvement that could be obtained while ensuring user comfort still does not allow impairment to be detected in every individual subject and further analysis and refinement is still required.

Chapter 7 : Conclusion and Future Work

7.1 Conclusion

The research presented in this thesis has used different mathematical, signal processing and measurement methodology methods to investigate the cerebral autoregulation process in different experiments that were designed to assess a subject's autoregulatory state. It has been shown that these new approaches have provided us with deeper insight into understanding of non-invasive assessment of cerebral autoregulation. The main conclusions are summarized for each of the main elements of the thesis.

7.2 Physiological parameters and measurement techniques

Cerebral autoregulation is an active physiological process by which cerebral blood flow is controlled at an approximately steady level despite changes in arterial blood pressure, providing other physiological conditions are maintained in a stable level. This physiological control system is highly complex and yet not fully understood. There are no 'gold standard' methods for assessing dynamic autoregulation, and clinical use is still very limited.

The advent of transcranial Doppler ultrasonography (TCD) for the measurement of cerebral blood flow velocity ($CBFV$) usually from the middle cerebral artery ($MCBFV$) and servo-controlled finger photoplethysmography (Finapres) for continuous measurement of arterial blood pressure (ABP), have enabled the investigation of the dynamical relationship between ABP and $MCBFV$ of the cerebral circulation. It is also known that cerebral autoregulation is very sensitive to CO_2 [23, 53, 89, 91, 98, 138], and end-tidal pCO_2 is a good indicator of cerebral autoregulation for healthy individual subjects under a range of experimental conditions.

Simultaneous measurement of ABP, $CBFV$ and end-tidal CO_2 (P_{ETCO_2}), under normocapnia and hypercapnia condition were carried out in this research. This procedure enables the relationship between different inputs (ABP and P_{ETCO_2}) and $CBFV$ as output to be modeled and finally the state of cerebral autoregulation to be assessed.

7.3 Autoregulation models and parameters

In this thesis, different methods for assessment of autoregulation were studied. Most of the concentration of work in this field has been on the relationship between spontaneous fluctuations of

ABP and $CBFV$ [3, 39, 47, 52, 53, 65, 69, 73, 84, 112, 133, 134, 149, 150]. Cerebral blood flow is also affected by other physiological signals such as CO_2 [23, 53, 89, 91, 98, 138]. A linear relationship between ABP and $CBFV$ is assumed by many authors (section 2.12). The effect of CO_2 and metabolic activity on flow is another assumption that is usually made when linear relationship between ABP and $CBFV$ is studied.

In Chapter 3, the combination of Laguerre expansion with feedforward artificial neural networks in the form of a Laguerre-Volterra network, which has been shown to provide a good estimate of nonlinear systems with short input-output records [151], was used to model the cerebral autoregulation system. It was found that by having two-input nonlinear (second-order) models the performance of the model based on the $NMSE$ improved by 10% in validation data. This result provided further indication for the existence of nonlinearity in the autoregulatory system as found by other authors [23, 35, 46, 92, 93, 137].

Neural networks were previously used by Mitsis *et al.* [35, 137]. However in his work, the characteristic of the system was fixed for all recordings as mentioned before it is known that there is no 'gold standard', and cerebral autoregulation varies from one individual to another. Another limitation of the work by Mitsis *et al.* [35, 137], was that only the existence of nonlinearity and the impulse response of the system were studied, no assessment of autoregulation was reported from that model. In Chapter 3, in order to study the effect of nonlinearity in individuals, the characteristics of Laguerre-Volterra network was optimized. The results showed that the effect of CO_2 (its contribution toward $CBFV$) and the cross-kernel (the effect of nonlinear interaction between ABP and CO_2 toward changes in $CBFV$) vary between subjects and even within subjects. In that chapter, different indices for the assessment of dynamic cerebral autoregulation, based on the changes provoked by altering P_{ETCO_2} levels, which leads to temporary impairment of autoregulation in order to assess autoregulation, were studied. The Pressure pulse response (PPR) was used (section 3.3.2) as an autoregulatory parameter as it is more physiologically realistic compared to step or impulse inputs usually (section 3.3.2). The amplitude of the response at 1.5 seconds ($A1.5$) and 8 seconds ($A8$) were selected as autoregulatory parameters from this novel input. It was found that $A8$, when extracted from two-input nonlinear models, especially when the cross-kernel terms were included, provided the lowest variability (inter- and intra-subject) and the best separation between P_{ETCO_2} levels and thus autoregulation. However a very simple parameter ($H1$; second coefficient of an FIR filter with 2 lags proposed by Simpson *et al.* [74]) provided good performance in terms of variability with the added advantage of suitability for use in a very short dataset in comparison to nonlinear

multivariate models where in order to train the system, large data samples are required. With $H1$ as the result of the small number of free parameters this is not the case.

A major challenge of the methods used for the assessment of autoregulation is the issue of choosing an autoregulatory parameter that could work on different datasets collected from different patients under different physiological conditions. Furthermore the lack of a "gold standard" for assessment of dynamic cerebral autoregulation does not allow a robust reference, to which alternative methods could be compared. Autoregulatory parameters are sensitive to many physiological variables that can influence CBF ($P_{ETCO_2,}$brain activity, O_2 content, haemotacrit, temperature) as has already been observed by other authors [52, 90, 92]. Furthermore, there is a dearth of studies using multiple methods or performing inter-method comparisons [32]. Dynamic cerebral autoregulation can also vary from one patient to another and over time [115]. In Chapter 4, a new data-driven method for assessing autoregulation using subspace distance (SSD) between two autoregressive moving average ($ARMA$) models was proposed and tested, without studying primarily the performance of the models in term of data fit or choosing an arbitrarily autoregulatory parameter by visual inspection, as used in section 3.3.2 Martin *et al.* [119] showed that by treating an $ARMA$ model as a complex rational function, one can define a metric on the set of complex rational functions, and measure the distance between two $ARMA$ models. In that chapter it was first shown that the Tiecks model corresponding to a 2^{nd} order $ARMA$ model can be used to measure the $CBFV$ responses. Building on this, the distance between two $ARMA$ models was measured. This could also be extended to higher orders. The results from this work showed that subspace distance can provide a basis for assessing autoregulation, and the results using cross-validation suggest better performance than more conventional alternatives (Chapter 4). The main advantage of this method is that it does not require picking parameters to assess autoregulation, and it is driven by the data (and the model) itself.

In Chapter 5, we tackle time-varying characteristic of cerebral autoregulation as another issue in the assessment of autoregulation (section 2.12) using both univariate and multivariate models and both RLS and moving window approaches. These methods were applied during step-wise changes in CO_2 levels. $ABP - CBFV$ and $ABP, PETCO_2 - CBFV$ during step-wise changes in $PETCO_2$ respectively were studied. The results showed that by including $PETCO_2$ in a univariate model ($ABP - CBFV$) in addition to the improvement to the model fit, we can also get better assessment of autoregulation using different autoregulatory parameters (phase lead; $P1$, and amplitude using pressure pulse input (PPR); $A8$). The results also showed that the contribution of $PETCO_2$ towards the spontaneous changes in $CBFV$ is significantly higher in hypercapnia compared to normocapnia. It was also shown

that the multivariate coherence provided higher values at the transient between hypercapnia to normocapnia and vice versa and we also showed that it is significantly different to univariate models during these transients and at low frequencies ($f < 0.1\ Hz$) (Figure 5-6). This was concluded that the effect of $PETCO_2$ on the variation of $CBFV$ is more significant when the subject is in hypercapnia. The result also indicated that the multivariate time-varying model can improve our coherence value at low frequency range and also at the transient between normocapnia and hypercapnia and vice versa.

In Chapter 6, a new experimental approach for generating small random step-wise changes in blood pressure and inspired carbon dioxide (CO_2) level was studied. The aim was to test a protocol that can be easily and safely repeated and may be applicable as a clinical tool. In this approach pseudorandom lower-body negative pressure ($LBNP$) variations were applied as a means to provoke a small increase in blood pressure variability. This study consisted of 31 subjects, with two sessions for each subject. A total number of 61 recordings were available for this study. The increase in mean $CBFV$ from baseline to HCO_2 by $7.66\ cm.s^{-1}$ shows the effect of high CO_2 on cerebral vasodilation. The ABP during all procedures was in the range of 80 to $90\ mmHg$ (see Table 6.1). Significant difference in the variation of ABP and $CBFV$ as the result of $LBNP$ was also observed .The average drop across all recording in blood pressure following each 'suction' was 7.5%. This was calculated by synchronizing the falling edge and raising edge of $LBNP$ during each suction for each recording and calculating the mean drop in pressure for all measurements (Figure 6-3 and Figure 6-4). It was also shown that by introducing $LBNP$, the variability in ABP has increased (from baseline $\rightarrow LBNP$, $HCO_2 \rightarrow HCO_2 - LBNP$ and $RHCO_2 \rightarrow RHCO_2 - LBNP$) which is in agreement with the expectation that $LBNP$ increases variability and suggests that the protocol is affecting ABP and $CBFV$, as expected.

Significant change in autoregulatory parameters ($P1$ and $H1$) from baseline to HCO_2 and $LBNP$ to $HCO_2 - LBNP$ was observed. However no significant different between $RHCO_2$ and $RHCO_2 - LBNP$ was reported. This could be as the result of $RHCO_2$ does not impair autoregulation significantly. However a leakage in the face-mask was discovered, and as the result of that, $5\%\ CO_2$ was not fully achieved, and hypercapnia does not reduce autoregulation as strongly as expected, but this requires further analysis.

The results also showed significant reduction in the variability of autoregulatory parameters ($P1$ and $H1$) from baseline to $LBNP$. However the variation of the autoregulatory parameters from HCO_2 to $HCO_2 - LBNP$ did not follow this reduction, which could be as the result of individual movement of the head-mask during the protocols due to the heavy suction of the chamber. The results of

intraclass correlation for autoregulatory parameters from the same subject on different days showed better agreement between measurements during $LBNP$ compared to baseline and $RHCO_2$ to $RHCO_2 - LBNP$, but not from HCO_2 to $HCO_2 - LBNP$. However low values of ICC and their significance different should be studied in more depth. It was shown in this chapter that this new protocol can provide more robust estimates of cerebral autoregulation. However the improvement that could be obtained while ensuring user comfort still does not allow impairment to be detected in every individual subject and further analysis and refinement is required.

7.4 Future work

The cerebral haemodynamic system is known to be nonlinear and non-stationary [46, 87, 92, 135, 138, 146]. In this work, the nonlinear characteristics of this system were considered with Wiener-Laguerre models, but more sophisticated 'black-box' that could simultaneously address the non-stationary characteristics of cerebral autoregulation could be applied to this study in the future.

In chapter 5, a rather time-consuming approach to identifying the optimum system characteristics (Laguerre-Volterra Network model orders) for different models for each recording was studied. Even though this method resulted in better assessment of autoregulation, due to its computational cost this approach would not be feasible for clinical applications. Further investigation of the optimal choices for the nonlinear approach for the assessment of cerebral autoregulation would be beneficial.

The research in this thesis has focused on the assessment of autoregulation in healthy volunteers, and hypercapnia as the result of inhaling high CO_2 was assumed to behave in a similar way to that observed in different autoregulation impairments in clinical conditions. This assumption, made repeatedly in the field, should be tested on data from patients.

The intracranial pressure (ICP) has been assumed to be constant throughout this work. This assumption has led to another assumption that cerebral perfusion pressure (CPP) changes is proportional to ABP. However in patients with severe head injury or pathological conditions this may not necessary be the case, and more sophisticated model of the relationship between ABP,ICP and CPP may be needed.

Another assumption that was made in Chapter 6 was that the two measurements from the same subjects are independent; however measurements from the same subjects are not independent

from each other and should not be studied as two independent measurements. The same approach has been used in some earlier work [47, 50]. This issue was tackled in Chapter 4 by removing the second recordings from the same subject. However deeper analysis should be carried out to study the repeatability within and between sessions.

It was shown in Chapter 3 and many others [35, 46, 86, 92, 93, 135, 137] that cerebral autoregulation is a nonlinear system. Non-linear effects comparing the transients of increasing and decreasing in blood pressure induced by $LBNP$ on data collected in Chapter 6 can be carried out in future work to investigate whether nonlinearity is more evident with the larger transitions induced by $LBNP$.

A comparison between repeatability of different protocols (data collection from Leicester and Southampton) and ability to distinguish between normocapnia and hypercapnia using different methods for assessment of autoregulation studied throughout in this thesis should also be studied.

Appendix

Appendix I. Volterra Models

The development of Volterra series relies on mathematical notion of the Volterra series (power series expansion), introduced by the Italian mathematician Vito Volterra in 1930. The Volterra series can be viewed as a generalization of the Taylor multivariate series expansion of an analytic function, f, of m variables as $m \to \infty$. The multivariate Taylor series expansion of an analytic function $f(x_1, \dots, x_m)$ about a reference point $(x_1^*, \dots, x_m^*)$ in the m-dimensional vector space is defined by these m variables as:

$$f(x_1, \dots, x_m) = f(x_1^*, \dots, x_m^*) + \sum_{i=1}^{m} a_i(x_i - x_i^*) + \sum_{i_1=1}^{m}\sum_{i_2=1}^{m} a_{i_1,i_2}\left(x_{i_1} - x_{i_1}^*\right)\left(x_{i_2} - x_{i_2}^*\right) + \cdots$$

And if $m \to \infty$, it will evolves into the Volterra function power series, where the origin of the real axis is used as the reference point. Then the vector $[x_1, \dots, x_m]$ turns into a continuous function $x(\lambda)$ for λ in the interval $[a, b]$. The Volterra series expansion can be expressed as:

$$F[\,x(\lambda)] = k_0 + \int_a^b k_1(\lambda)x(\lambda)d\,\lambda + \int_a^b \int k_2(\lambda_1, \lambda_2)x(\lambda_1)\,x(\lambda_2)d\,\lambda_1 d\lambda_2 + \cdots$$
$$+ \int_a^b \dots \int k_r(\lambda_1, \dots, \lambda_r)x(\lambda_1) \dots x(\lambda_r)d\,\lambda_1 \dots d\lambda_r + \cdots$$

In the above equation k_r represents the limit of the multivariate Taylor expansion coefficients $a_{i_1,\dots,i_r}$and is called the "Volterra kernel" of r^{th} order. The multiple integrals are called "Volterra functional".

Another form of the Volterra series that is more commonly used is in the form that can relate to the output of a time invariant stable causal system in terms of its input signal using the equation below:

$$y(t) = k_0 + \int_0^\infty k_1(\tau)x(t-\tau)d\tau$$
$$+ \int\int_0^\infty k_2(\tau_1, \tau_2)x(t-\tau_1)x(t-\tau_2)d\tau_1 d\tau_2 + \cdots$$
$$+ \int_0^\infty \dots \int k_r(\tau_1, \dots, \tau_r)x(t-\tau_1) \dots x(t-\tau_r)d\tau_1 \dots d\tau_r + \cdots$$

The first-order Volterra kernel, $k_1(\tau)$, is the same as the impulse response function of linear system and can be viewed as the linear component of the nonlinear system. The second-order kernel $k_2(\tau_1, \tau_2)$ represents the lowest order nonlinear interactions in the Volterra framework, and can be viewed as the two-dimensional pattern by which the system weighs all possible pair-wise product combinations of input in order to generate the second-order component of the system output. Higher-order kernels represent the patterns of nonlinear interactions among a number of input epoch values equal to the order of the kernel.

Appendix II: Wiener-Laguerre

To date, the best method (in terms of the number of Kernels required) for estimating the kernel expansion is the use of discrete Laguerre functions [151]. Laguerre is based on Wiener's original suggestion or expansion of the Wiener kernels, because Laguerre functions are orthonormal over the domain from zero to infinity and have a built-in exponential.

A set of real function $w_m(t)$ is said to be orthonormal over the interval (a, b) if

$$\int_a^b w_m(t)w_n(t)dt = \delta_{mn} = \begin{cases} 0 & for\ m \neq n \\ 1 & for\ m = n \end{cases}$$

It is shown [35] that function $f(t)$ for which $\int_a^b f^2(t)dt < \infty$ can be approximated by N members of an orthonormal set with minimum integral-square error over the interval (a, b) as

$$f(t) \approx \sum_{n=1}^{N} c_n w_n(t)$$

In which the coefficients $c_n$have the value

$$c_n = \int_a^b f(t)w_n(t)dt$$

The value of the resulting integral-square error is

$$E_N = \int_a^b [f(t) - \sum_{n=1}^{N} c_n w_n(t)]^2\, dt = \int_a^b f^2(t)dt - \sum_{n=1}^{N} c_n^2$$

Also, if the set $\{w_n(t)\}$ is complete, $E_N \to 0\ as\ N \to \infty$.

An important complete set of orthonormal functions is the set of Laguerre functions, which can be obtained by forming an orthonormal set from the linearly independent set of functions:

$$v_m(t) = \begin{cases} 0 & for\ t < 0 \\ (pt)^m e^{-pt} & for\ t \geq 0\ \ m = 0,1,2 \ldots \end{cases}$$

The positive real constant p is a scale factor by which the functions $v_n(t)$ can be stretched out or compressed on the time scale. The Laguerre functions $I_m(t)$ are defined in terms of the set $v_m(t)$ as:

$$I_n(t) = \sum_{m=0}^{n} c_{mn} v_m(t)$$

With the orthonormal property

$$\int_0^\infty I_m(t)I_n(t)dt = \delta_{mn}$$

So the nth-Laguerre function is a linear combination of the first n members of the set $\{v_n(t)\}$.

APPENDIX III: $ARMA$ model of Tiecks model

Tiecks *et al.* [5] proposed a second-order differential equation to predict the changes in cerebral blood flow velocity ($CBFV(t)$) to changes in arterial blood pressure ($ABP(t)$), where:

$$dP(t) = \frac{P(t)}{1 - CrCP}$$

where in the above equation $dP(t)$ is the normalized pressure change and $CrCP$ is a fraction of the baseline pressure ($CrCP = 0$ was used in Chapter 4). The relative velocity $\widehat{CBFV}(t)$ can be calculated using:

$$\widehat{CBFV}(t) = 1 + dP(t) - K \times x_2(t)$$

where K in above equation is a gain parameter, and different values of gain selected by Tiecks *et al.* [5] is shown in Table 2.1.

The estate variable equations can be expressed based on below second-order linear differential equations:

$$x_1(t) = x_1(t-1) + \frac{dP(t-1) - x_2(t-1)}{f \times T}$$

$$x_2(t) = x_2(t-1) + \frac{x_1(t-1) - 2 \times D \times x_2(t-1)}{f \times T}$$

Where in the above equations f is the sampling frequency, T is the time-interval and D is the damping factor. K, T and D are also pre-defined values and only 10 combinations of these parameters are reported by Tiecks *et al.* [5] (shown in Chapter 4) and each combination represents one value for ARI.

By taking a $z-$transforms of above the equations, the transfer function between $ABP(t)$ and $CBFV(t)$ can be obtained

$$CBFV(z) = ABP(z) - KX_2(z)$$

$$X_1(z) = z^{-1}X_1(z) + \frac{P(z) - z^{-1}X_2(z)}{T'}$$

$$X_2(z) = z^{-1}X_2(z) + \frac{X_1(z) - 2Dz^{-1}X_2(z)}{T'}$$

where in the above equation $T' = f \times T$. Solving above equations leads to the transfer function between $CBFV$ and ABP

$$\frac{CBFV(z)}{ABP(z)} = \frac{\left(1 - \frac{K}{T'}\right)^2 + z^{-1}\left(\frac{1}{T'^2} + \frac{2D}{T'} - 2\right) + z^{-2}(1 - \frac{2D}{T'})}{1 + z^{-1}\left(\frac{1}{T'^2} + \frac{2D}{T'} - 2\right) + z^{-2}(1 - \frac{2D}{T'})}$$

The above equation can be re-written as:

$$\frac{CBFV(z)}{ABP(z)} = \frac{a + bz^{-1} + cz^{-2}}{1 + bz^{-1} + cz^{-2}}$$

Where $a = \left(1 - \frac{K}{T'}\right)^2$, $b = \left(\frac{1}{T'^2} + \frac{2D}{T'} - 2\right)$ and $c = (1 - \frac{2D}{T'})$

By applying the inverse z −transform to above equation, we get:

$$CBFV(n) = aABP(n) + b[ABP(n-1) - CBFV(n-1)] + c[ABP(n-2) - CBFV(n-2)]$$

As it can be seen from above equation, it is indeed has a format of an $ARMA$ model, where the past samples of both $CBFV$ and ABP are weighted by the same coefficients.

Appendix IV: Manual for "Graphical User Interface (GUI)" for Data Analysis

A GUI interface was created to ease the process of data analysis and visualization. In this program four different channels can be observed at the same time with two channels being plotted on top of each other to ease comparison. It also gives the option to the user to zoom into the channels and look at the signals in more details. The data can be saved as .mat files.

Some snapshots of the GUI for different signals for an arbitrary recording are shown below.

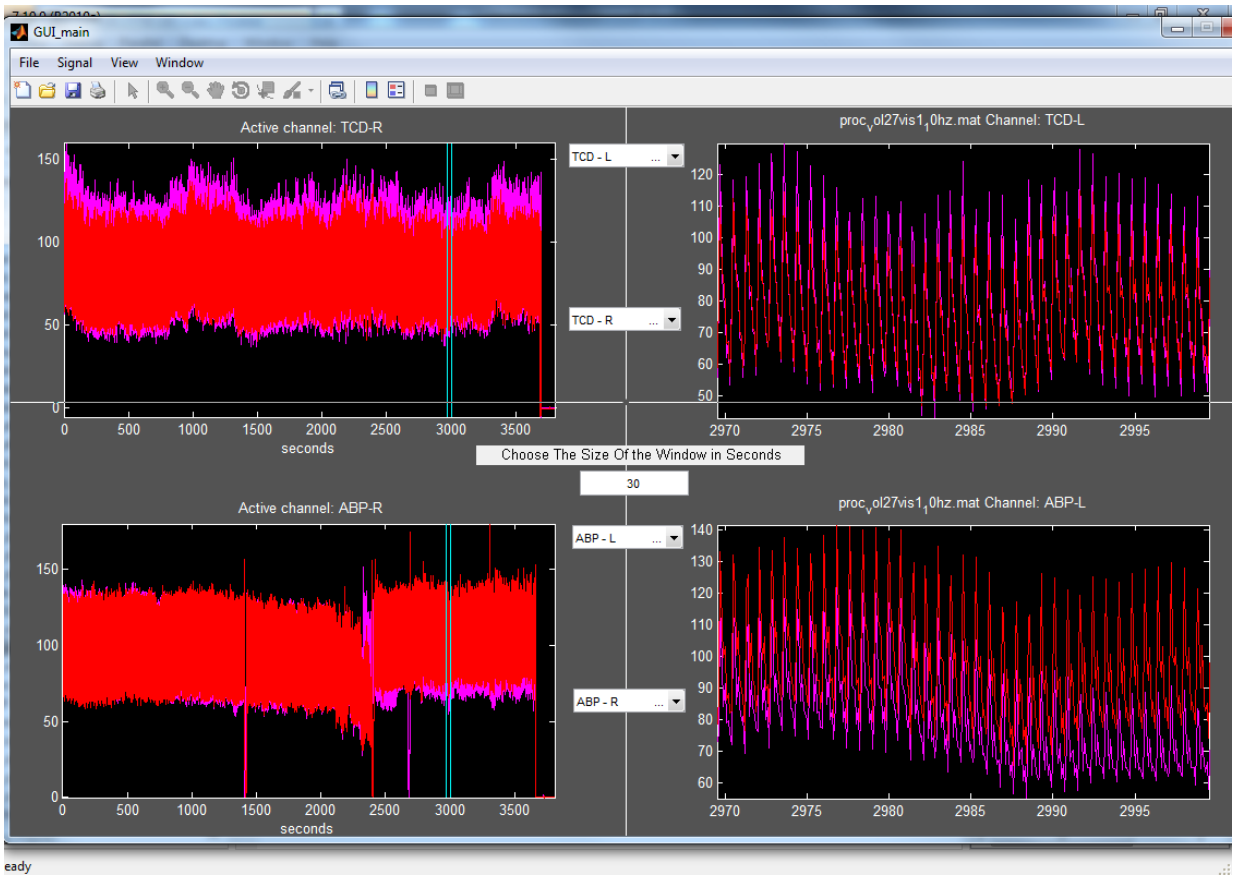

Measured $CBFV$ from left and right TCD are shown in the top frames and ABP measured from left and right hands are plotted in the bottom frames for an arbitrary recordings

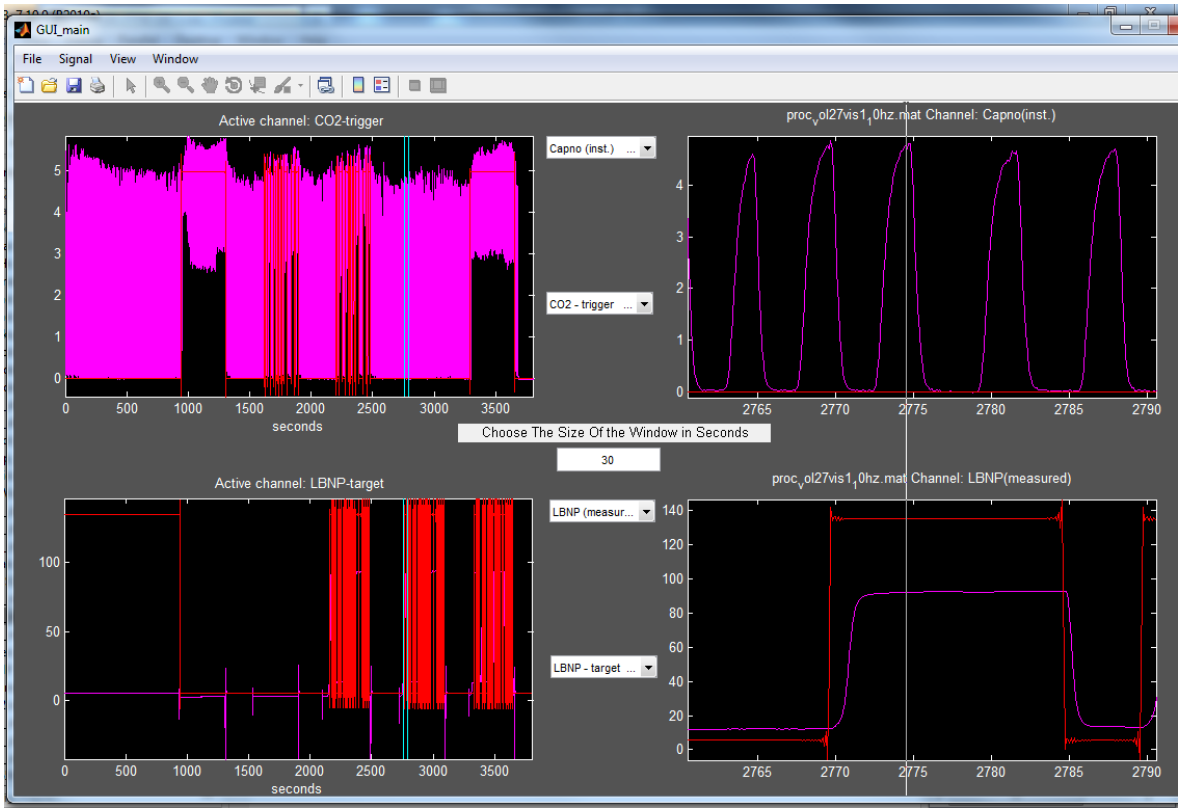

Measured CO_2 level and the trigger CO_2 are shown in top frames. And below frames shows the measured and target lower body negative pressure ($LBNP$) for an arbitrary recordings

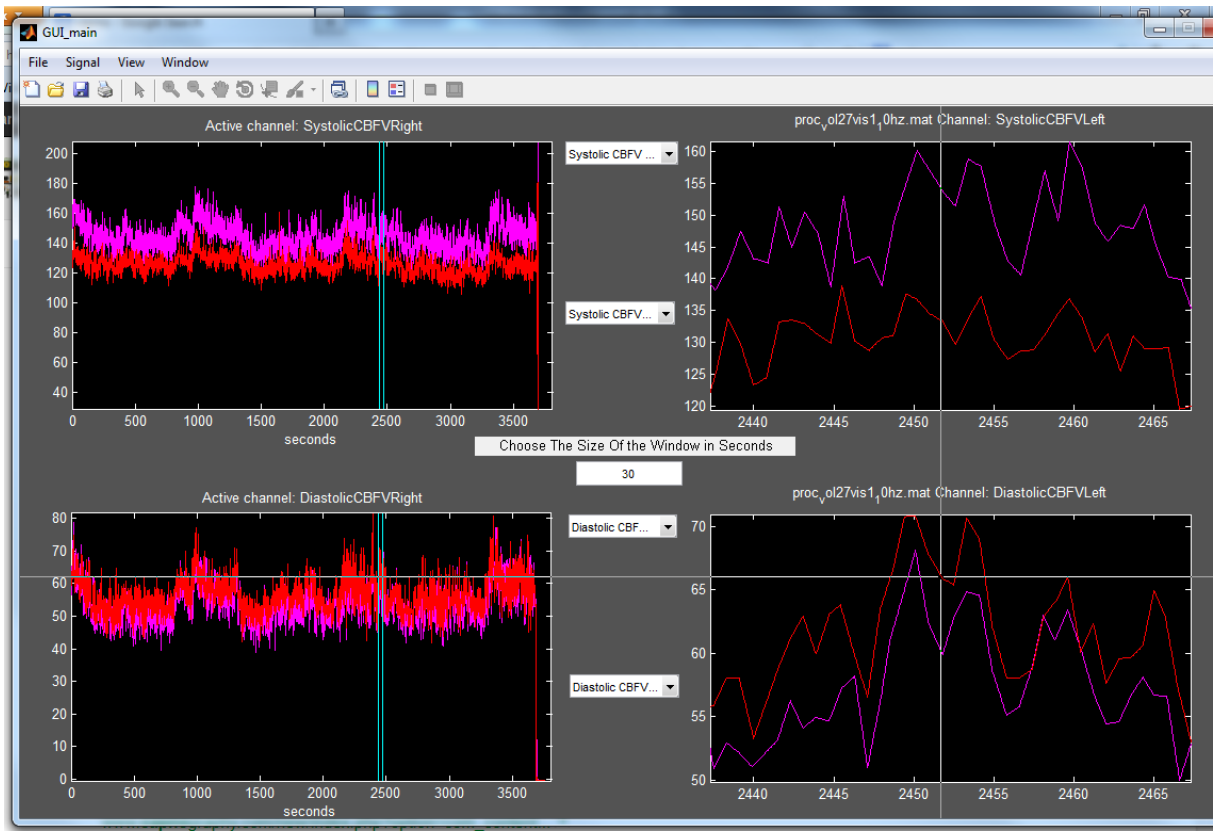

Systolic $CBFV$ from left and right TCD are shown in above frames (cyan and red respectively). Diastolic $CBFV$ from left and right TCD are shown in bottom frames (cyan and red respectively)

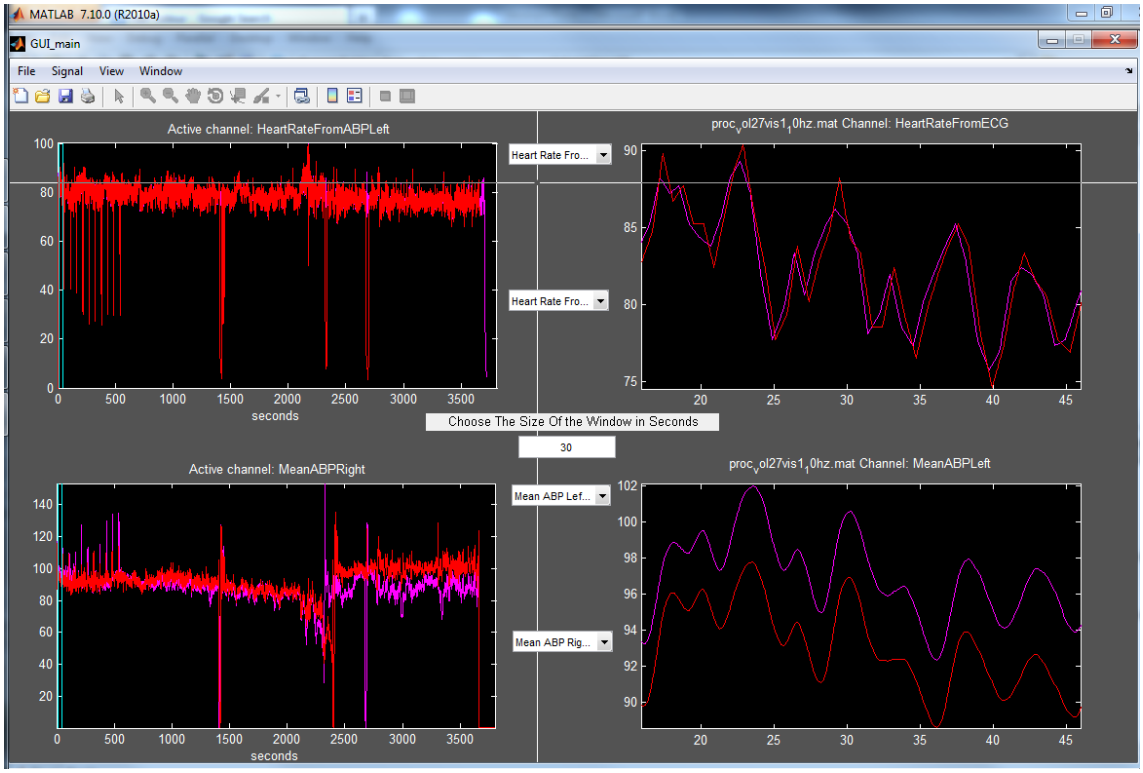

Heart rate calculated from ECG and ABP are shown in above frames (cyan and red respectively). Mean ABP calculated from left and right hands are shown in bottom frames (cyan and red respectively).

Command lists

1. The user can press “cnt+o” or choose from the top bar to open a new file. The program can read matlab files (.m) or .par files which was the original format for the collected data from our collaborator in Leicester
2. The program saves the modified data as matlab files (.m).
3. Pressing “cnt+s” or choosing from the top bar allows the user to save the data.
4. To remove a section: Press “a” at the beginning and “b” at the end of the end of the desired section to be removed. If the section that is required to be removed is at the end of a signal, just press “a” at the beginning and the end would automatically be the end of the signal. If the section that is required to be removed is at the beginning of the signal, just press “b” at the end of the section that is required to be removed. The removed section will be shown in “blue”. The start and the end of the removed section are shown with red and green vertical lines (below figure).

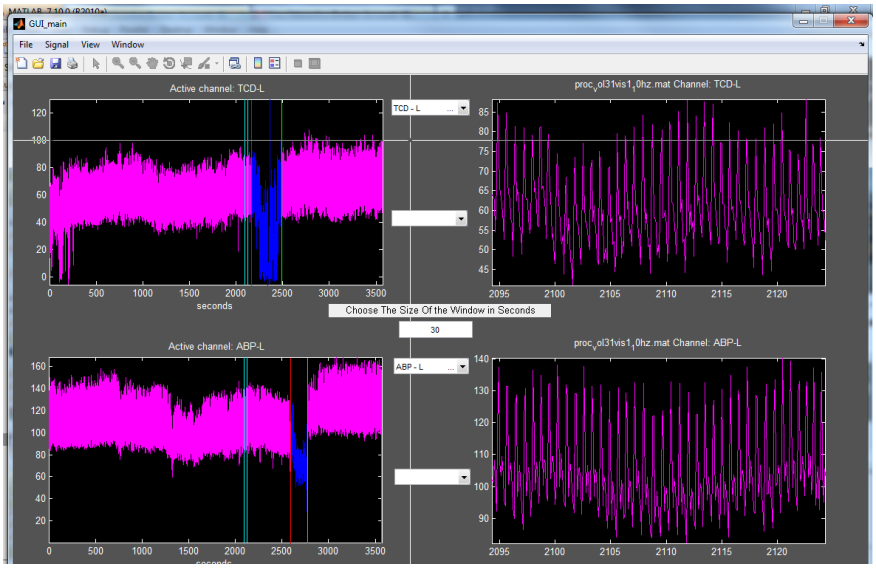

Start and end of a section to be removed are shown with red and green vertical lines using “a” and “b” commands

5. To delete a mark (such as ‘a’ or ‘b’) that was previously applied, press “d” near where it was applied.
6. Pressing “q”, “h”, “j” and “k” puts a marker on the signal with different colours (To mark start or end of experimental protocol).
7. Pressing “s” would switch between the top and bottom plots. This can also be done by just clicking on the desired plot.
8. Pressing “E” would automatically select different protocols from the data, this protocols are: high CO_2 (HCO_2), low CO_2 (LCO_2),Random high CO_2($RHCO_2$), $LBNP$, high CO_2 with $LBNP$ ($HCO_2 - LBNP$)and $LBNP$ with random high CO_2($RHCO_2 - LBNP$) . It also saves these sections in different folders. If the program does not manage to find any of these protocols, it only saves the one that it finds. If the program finds two or more section with the same property of a protocol (HCO_2 for example), it chooses the longer section. The program also removes the first 5 sec from each section. If the user has already applied markers in the original recordings, the markers and those changes will be automatically applied and saved in each section.
9. By pressing “w” once the program puts a green vertical line on that signal with circles on the ends, if “w” is pressed again somewhere else on that signal another green vertical line is plotted. Now by pressing the “c” command the program cuts that specific section and allows the user to save that section under a different name in a folder. This can be used to manually select different sections in different protocols.

10. To manually modify a signal (if there is glitch or artefact in signal), the user can press “i” on a signal and the program replace the nearest point of that signal to the curser with the value of the curser on the plot, however the usage of this property is very time-consuming.
11. To recalculate all the parameters from the recorded signals (systolic, diastolic and mean, left and right $CBFV$ and ABP, heart rate from ECG and ABP left and right, $ETCO_2$, $R-R$ intervals, respiratory from CO_2, $CrCP$ and RAP), press “m” command. This would enable the user the recalculate these parameters if any change or modification was done on any recorded signal.

The main GUI function is called *GUI_main.m* (*GUI_main.fig* for the interface) and the functions it required are listed below:

1. Aread.m
2. chop_spa.m
3. edit_data.m
4. find_etco2.m
5. nan_interp.m
6. nan_sig.m
7. peakfinder.m
8. plottting_data.m
9. Save_Box.m
10. save_hco2_lco2.m
11. save_LBNP.m
12. save_txt.m
13. sig_calc.m
14. sig_calc_2.m

References

1. Evans, D.H., W.N. Mcdicken, R. Skidmore, and J.P. Woodcock, *Doppler ultrasound: Physics, Instumentation and clinical applications.* John Wiley and Sons, 1989.
2. Blaber, A.P., R.L. Bondar, F. Stein, P.T. Dunphy, P. Moradshahi, M.S. Kassam, and R. Freeman, *Transfer function analysis of cerebral autoregulation dynamics in autonomic failure patients.* Stroke, 1997. **28**: p. 1686-1692.
3. Aaslid, R. and A.O. Brubakk, *Accuracy of an ultrasound doppler servo method for non-invasive determination of instantaneous and mean arterial blood pressure.* Circulation, 1981. **64**: p. 753-759.
4. Maneen, M.J., R. Hannah, L. Vitullo, N. DeLance, and M.J. Cipolla, *Peroxynitrite diminishes myogenic activity and is associated with decreased vascular smooth muscle F-actin in rat posterior cerebral arteries.* Stroke, 2006. **37**(3): p. 894-899.
5. Tiecks, F.P., A.M. Lam, R. Aaslid, and D.W. Newell, *Comparison of static and dynamic cerebral autoregulation measurements.* Stroke, 1995. **26(6)**: p. 1014-1019.
6. Siegel, G.J., B.W. Agranoff, R.W. Albers, S.K. Fisher, and M.D. Uhler, *Basic Neurochemistry: Molecular, Cellular and Medical Aspects.* 1999, Philadelphia: Lippincott.
7. Lennox, W.G., F. A. Gibbs, and E. L. Gibbs, *Relationship of unconsciousness to cerebral blood flow and to anoxemia.* Arch. Neurol. Psychiatry, 1935: p. 34: 1001-1013.
8. Ganong., W.F., *Review of medical physiology.* Vol. 23. 2005, Appleton and Lange: McGraw-Hill Professional.
9. Gray, H. and P.L. Williams, *Gray's Anatomy*. 1989, Edinbrugh: Churchill Livingstone.
10. Marieb, E.N. and K. Hoehn, *Human Anatomy and Physiology*. Vol. Seven. 1991: Benjamin/Cummings Pub Co.
11. Czosnyka, M., P. Smielewski, S. Piechnik, L.A. Steiner, and J.D. Pickard, *Cerebral autoregulation following head injury.* Journal of Neurosurgery, 2001. **95**(5): p. 756-763.
12. Blomquist, A.J., R.M. Benjamin, and R. Emmers, *Thalamic localization of afferents from the tongue in squirrel monkey (Saimiri sciureus).* Jour Comp Neurol, 1962. **118**((1)): p. 77-87.
13. Lundberg.N, *The saga of the Montro-Kellie doctrine*. 1983, Berlin-Heidelberg: Springer-Verlag.
14. Marmarou, A., K. Shulman, and R.M. Rosende, *Non-linear analysis of cerebrospinal- fluid system and intracianial-pressure dynamics.* Journal of Neurosurgery, 1978. **48**(3): p. 332-344.
15. Ursino, M. and P. Digiammarco, *A mathematical model of the relationship between cerebral blood volume and intracranial pressure changes- The generation of plateau waves.* Annals of Biomedical Engineering, 1991. **19**(1): p. 15-42.
16. Aaslid, R., T.M. Markwalder, and H. Nornes, *Noninvasive transcranial doppler ultrasound recording of flow velocity in basal cerebral arteries.* J Neurosurg, 1982: p. 57:769-774.
17. Lang, E.W., J. Lagopoulos, J. Griffith, K. Yip, Y. Mudaliar, H.M. Mehdorn, and N.W.C. Dorsch, *Noninvasive cerebrovascular autoregulation assessment in traumatic brain injury: Validation and utility.* Journal of Neurotrauma, 2003. **20**(1): p. 69-75.
18. Steinmeier, R., C. Bauhuf, U. Hubner, R.D. Bauer, R. Fahlbusch, R. Laumer, and I. Bondar, *Slow rhythmic oscillations of blood pressure, intracranial pressure, microcirculation, and cerebral oxygenation - Dynamic interrelation and time course in humans.* Stroke, 1996. **27**(12): p. 2236-2243.
19. Allen, R., *Time-Series methods in the monitoring of intracranila-pressure.2. comparative study and initial assessment.* Journal of Biomedical Engineering, 1983. **5**(2): p. 103-109.
20. Schmidt, B., J.J. Schwarze, M. Czosnyka, D. Sander, I. Wittich, and J. Klingelhofer, *A method for a simulation of continuous intracranial pressure curves.* Computers and Biomedical Research, 1998. **31**(4): p. 231-243.

21. Swiercz, M., Z. Mariak, J. Krejza, J. Lewko, and P. Szydlik, *Intracranial pressure processing with artificial neural networks: Prediction of ICP trends.* Acta Neurochirurgica, 2000. **142**(4): p. 401-406.
22. Czosnyka, M., D. Radolovich, M. Balestreri, A. Lavinio, P. Hutchinson, I. Timofeev, P. Smielewski, and J.D. Pickard. *Gender-related differences in intracranial hypertension and outcome after traumatic brain injury*. in *13th International Symposium on Intracranial Pressure and Brain Monitoring*. 2007. San Francisco, CA: Springer-Verlag Wien.
23. Ursino, M. and C.A. Lodi, *Interaction among autoregulation, CO2 reactivity, and intracranial pressure: a mathematical model.* American Journal of Physiology-Heart and Circulatory Physiology, 1998. **274**(5): p. H1715-H1728.
24. Hagstadius, S. and J. Risberg, *Regional cerebral blood-flow characteristics and variations with age in resting normal subjecs.* Brain and Cognition, 1989. **10**(1): p. 28-43.
25. Lassen, N.A., *Cerebral blood flow and oxygen consumption in man.* Physiol Rev, 1959. **39**(2): p. 183-238.
26. Aaslid, R., K.F. Lindegaard, W. Sorteberg, and H. Nornes, *Cerebral auto-regulation dynamics in humans.* Stroke, 1989. **20**(1): p. 45-52.
27. Jensen, E.C., L. Bennet, S.J. Guild, L.C. Booth, J. Stewart, and A.J. Gunn, *The role of the neural sympathetic and parasympathetic systems in diurnal and sleep state-related cardiovascular rhythms in the late-gestation ovine fetus.* American Journal of Physiology-Regulatory Integrative and Comparative Physiology, 2009. **297**(4): p. R998-R1008.
28. Czosnyka, M., P. Smielewski, P. Kirkpatrick, D.K. Menon, and J.D. Pickard, *Monitoring of cerebral autoregulation in head-injured patients.* Stroke, 1996. **27**(10): p. 1829-1834.
29. Paulson, O.B., S. Strandgaard, and L. Edvinsson, *Cerebral autoregulation.* Cerebrovasc Brain Metab Rev, 1990. **2**: p. 161-192.
30. Nelson, R.J., M. Czosnyka, J.D. Pickard, W. Maksymowicz, S. Perry, J.L. Martin, A.H.J. Lovick, L.F. Marshall, and H.D. Portnoy, *Experimental aspects of cerebrospinal hemodynamics- The relationship between blood-flow velocity waveform and cerebral autoregulation.* Neurosurgery, 1992. **31**(4): p. 705-710.
31. Folkow, B., *Description of the myogenic hypothesis.* Circulation Research, 1964. **15**: p. SUPPL:279-87.
32. Panerai, R.B., *Assesssment of cerebral pressure autoregulation in humans: a review of measurement methods.* Physiological measurement, 1998. **19**: p. 305-338.
33. Busija, D.W. and D.D. Heistad, *Effects of indomethacin on cerebral blood flow during hypercapnia in cats.* American Journal of Physiology, 1983. **244**(4): p. H519-H524.
34. Schmidt, J.F., G. Waldemar, S. Vorstrup, A.R. Andersen, F. Gjerris, and O.B. Paulson, *Computerized analysis of cerebral blood flow autoregulation in humans: validation of a method for pharmacologic studies.* J Cardiovasc pharmacol, 1990. **15**: p. 983-988.
35. Mitsis, G.D., R. Zhang, B.D. Levine, and V.Z. Marmarelis, *Modeling of nonlinear physiological systems with fast and slow dynamics. II. Application to cerebral autoregulation.* Annual Biomedical Engineering, 2002. **30**: p. 555-565.
36. Morita, Y., J.E. Hardebo, and E. Bouskela, *Influence of cerebrovascular sympathetic, parasympathetic and sensory nerves on autoregulation and sppontaneous vasomotion.* Acta Physiologica Scandinavica, 1995. **154**(2): p. 121-130.
37. Tennant, R., M.A. Mohammed, J.J. Coleman, and U. Martin, *Monitoring patients using control charts: a systematic review.* International Journal for Quality in Health Care, 2007. **19**(4): p. 187-194.
38. Strandgaard, S. and O.B. Paulson, *Cerebral Autoregulation.* Stroke, 1984. **15**: p. 413-416.
39. Carey, B.J., P.J. Eames, M.J. Blake, R.B. Panerai, and J.F. Potter, *Dynamic cerebral autoregulation is unaffected by aging.* Stroke, 2000. **31**: p. 2895-900.
40. Obrist, W.D., H.K. Thompson, H.S. Wang, and W.E. Wilkinson, *Regional cerebral blood flow estimated by Xenon inhalation.* Stroke, 1975. **6**: p. 245-256.

41. Hagstadius, S. and J. Risberg, *Regional cerebral blood flowcharacteristics and variations with age in resting normal subjects.* Brain & Cognition, 1989. **10**.
42. Obrist WD, T.H., Wang HS, Wilkinson WE, *Regional cerebral blood flow estimated by Xenon inhalation.* Stroke, 1975. **6**: p. 245-256.
43. Berg, R.M.G., G.I. Strauss, F. Tofteng, T. Qvist, L. Edvinsson, J. Fahrenkrug, J. Qvist, L. Fonsmark, P. Skinhoj, and K. Moller, *Circulating levels of vasoactive peptides in patients with acute bacterial meningitis.* Intensive Care Medicine, 2009. **35**(9): p. 1604-1608.
44. Bouma, G.J. and J.P. Muizelaar, *Relationship between cardiac output and cerebral blood flow in patients with intact and with impaired autoregulation.* Journal of Neurosurgery, 1990. **73**(3): p. 368-374.
45. Victor, S., R.E. Appleton, M. Beirne, A.G. Marson, and A.M. Weindling, *The relationship between cardiac output, cerebral electrical activity, cerebral fractional oxygen extraction and peripheral blood flow in premature newborn infants.* Pediatric Research, 2006. **60**(4): p. 456-460.
46. Panerai, R.B., S.L. Dawson, and J.F. Potter, *Linear and Nonlinear analysis of human dynamic cerebral autoregulation.* Americal Journal of physiology, 1999. **277**: p. H1089-H1099.
47. Panerai, R.B., B.J. Carey, and J.F. Potter, *Short-term variability of cerebral blood flow velocity responses to arterial blood pressure transients.* Ultrasound in Medicine & Biology, 2003. **29(1)**.
48. S. Satomura, Z.K., *Ultrasonic blood rheogprah*. 1960: Proceeding of the 3rd International Conference on Medical Electronics. p. 254-258.
49. Kinefuchi, Y., H. Fukuyama, T. Suzuki, M. Kanazawa, and M. Takiguchi, *Development of a new catheter-tip pressure transducer.* Tokai Journal of Experimental and Clinical Medicine, 1999. **24**(3): p. 85-92.
50. Pinna, G.D., R. Maestriy, and A. Mortaraz, *Estimation of arterial blood pressure variability by spectral analysis: comparison between Finapres and invasive measurements.* Physiol meas, 1996. **17**: p. 147–169.
51. Imholz, B.P., W. Wieling, G.A. Van Montfrans, and K.H. Wesseling, *Fifteen years experience with finger arterial pressure monitoring: assessment of the technology.* Cardiovascular Research, 1998. **38**: p. 605-16.
52. Panerai, R.B., J.M. Rennie, A.W.R. Kelsall, and D.H. Evans, *Frequency-domain analysis of cerebral autoregulation from spontaneous fluctuations in arterial blood pressure.* Medical and Biological Engineering and Computing, 1998. **36**.
53. Dineen, N.E., F.G. Brodie, T.G. Robinson, and R.B. Panerai, *Continuous estimates of dynamic cerebral autoregulation during transient hypocapnia and hypercapnia.* Journal of Applied Physiology, 2010. **108**(3): p. 604-613.
54. Raamat, R., K. Jagomagi, J. Talts, K. Toska, and L. Walloe, *Recording of short-term finger blood pressure changes induced by an arterial occlusive thigh cuff: comparison between the modified oscillometric and Finapres techniques.* Physiol meas, 2001. **22**: p. N13-N20.
55. Penaz, J., A. Voigt, and W. Teichmann, *[Contribution to the continuous indirect blood pressure measurement].* Z Gesamte Inn Med, 1976. **31**(24): p. 1030-3.
56. Ristuccia, H.L., P. Grossman, L.L. Watkins, and B. Lown, *Incremental bias in finapres estimation of baseline blood pressure levels over time.* Hypertension, 1997. **29**: p. 1039-43.
57. Birch, A.A. and S.L. Morris, *Do the FinapresTM and ColinR radial artery tonometer measure the same blood pressure changes following deflation of thigh cuffs?* Physiol meas, 2003. **24**: p. 653-660.
58. Sato, T., M. Nishinaga, A. Kawamoto, T. Ozawa, and H. Takatsuji, *ccuracy of a continuous blood pressure monitor based on arterial tonometry.* Hypertension, 1993. **21**(6): p. 866-874.
59. Nelesen, R.A. and J.E. Dimsdale, *Use of radial arterial tonometric continuous blood pressure measurement in cardiovascular reactivity studies.* Blood pressure monitoring, 2002. **7**(5): p. 259-263.

60. Birch, A.A., *Sympathetic peripheral vasoconstriction may be measured using an artifact of the Finapres volume clamp technique.* Blood pressure monitoring, 2007. **12**(5): p. 315-319.
61. Rapela, C.E. and H.D. Green, *Autoregulation of canine cerebral blood flow.* Circ Res, 1964. **15**: p. SUPPL:205-12.
62. Greenfield, J.C., J.C. Rembert, and G.T. Tindall, *Transient changes in cerebral vascular resistance during the Valsalva maneuver in man.* Stroke, 1984. **15**(1): p. 76-79.
63. Aaslid, R., K.F. Lindegaard, S. W., and N. H., *cerebral autoregulation dynamics in humans.* stroke, 1989. **20**: p. 45-52.
64. Stevens, P.M. and L.E. Lamb, *Effects of lower body negative pressure on the cardiovascular system.* The American journal of cardiology, 1965. **16**(4): p. 506-15.
65. Birch, A.A., M.J. Dirnhuber, R. Hartley-Davies, F. Iannotti, and G. Neil-Dwyer, *Assessment of autoregulation by means of periodic changes in blood pressure.* Stroke, 1995. **26**: p. 834-7.
66. Carey, B.J., R.B. Panerai, and J.F. Potter, *Effect of aging on dynamic cerebral autoregulation during head-up tilt.* Stroke, 2003. **34**(8): p. 1871-1875.
67. Giller, C.A., A.M. Giller, C.R. Cooper, and M.R. Hatab, *Evaluation of the cerebral hemodynamic response to rhythmic handgrip.* Journal of Applied Physiology, 2000. **88**(6): p. 2205-2213.
68. Sprangers, R.L.H., K.H. Wesseling, A.L.T. Imholz, B.P.M. Imholz, and W. Wieling, *Initial blood pressure fall on stand up and exercise explained by changes in total peripheral resistance.* Journal of Applied Physiology, 1991. **70**(2): p. 523-530.
69. Diehl, R.R., D. Linden, D. Lucke, and P. Berlit, *Phase relationship between cerebral blood flow velocity and blood pressure. A clinical test of autoregulation.* stroke, 1995. **26**: p. 1801-1804.
70. Aaslid, R., M. Blaha, G. Sviri, C.M. Douville, and D.W. Newell, *Asymmetric dynamic cerebral autoregulatory response to cyclic stimuli.* Stroke, 2007. **38**(5): p. 1465-1469.
71. Gigli, G., G. Reggiardo, M. Casu, M. Perocchio, M. Iannetti, and S. Parodi, *Multiple sequential spectral analysis (MSSA): A new approach to R-R variability spectral analysis.* Journal of the Autonomic Nervous System, 1993. **43**(SUPPL.): p. 79-80.
72. van Beek, A., J. Claassen, M. Rikkert, and R. Jansen, *Cerebral autoregulation: an overview of current concepts and methodology with special focus on the elderly.* Journal of cerebral blood flow and metabolism, 2008. **28**(6): p. 1071-1085.
73. Giller, C.A., *The frequency-dependent behavior of cerebral autoregulation.* Neurosurgery, 1990. **27**: p. 362-8.
74. Simpson, D.M., R.B. Panerai, and D.H. Evans, *A parametric approach to measuring cerebral blood flow autoregulation from spontaneous variations in blood pressure.* Annals of Biomedical Engineering, 2001. **29**: p. 18-25.
75. Zhang, R., J.H. Zuckerman, C.A. Giller, and B.D. Levine, *Transfer function analysis of dynamic cerebral autoregulation in humans* American Journal of Physiology-Heart and Circulatory Physiology, 1998. **11**: p. 2567-2577.
76. Christ, M., F. Noack, T. Schroeder, A. Hagmueller, R. Koch, S.A. May, U. Morgenstern, M. Ragaller, and R. Steinmeier, *Continuous cerebral autoregulation monitoring by improved cross-correlation analysis: comparison with the cuff deflation test.* Intensive Care Medicine, 2007. **33**(2): p. 246-254.
77. Kuo, T.B.J., C.M. Chern, W.Y. Sheng, W.J. Wong, and H.H. Hu, *Frequency domain analysis of cerebral blood flow velocity and its correlation with arterial blood pressure.* Journal of cerebral blood flow and metabolism, 1998. **18**(3): p. 311-318.
78. Diehl, R.R., D. Linden, D. Lucke, and P. Berlit, *Spontaneous blood pressure oscillations and cerebral autoregulation.* Clinical Autonomic Research, 1998. **8**(1): p. 7-12.
79. Ogawa, Y., K. Iwasaki, S. Shibata, J. Kato, S. Ogawa, and Y. Oi, *The effect of sevoflurane on dynamic cerebral blood flow autoregulation assessed by spectral and transfer function analysis.* Anesthesia and analgesia, 2006. **102**(2): p. 552-559.

80. Parati, G., P. Castiglioni, S. Omboni, A. Pedotti, and G. Mancia, *Sequential spectral analysis of 24-h blood pressure and pulse interval in humans.* Hypertension, 1990. **16**: p. 414-421.
81. Sahuquillo, J., S. Amoros, A. Santos, M.A. Poca, H. Valenzuela, M. Baguena, and A. Garnacho. *False autoregulation (pseudoautoregulation) in patients with severe head injury. Its importance in CPP management*. in *11th International Brain Oedema Symposium*. 1999. Newcastle Tyne, England: Springer-Verlag Wien.
82. Panerai, R.B., M. Chacon, R. Pereira, and D.H. Evans, *Neural network modelling of dynamic cerebral autoregulation: assessment and comparison with established methods.* Medical Engineering & Physics, 2004. **26**(1): p. 43-52.
83. Mitsis, G.D., R. Zhang, B.D. Levine, and V.Z. Marmarelis, *Modeling of nonlinear physiological systems with fast and slow dynamics. II. Application to cerebral autoregulation.* Annals of Biomedical Engineering, 2002. **30**(4): p. 555-565.
84. Giller, C.A. and M. Mueller, *Linearity and non-linearity in cerebral hemodynamics.* Medical Engineering & Physiscs, 2003. **25**: p. 633-646.
85. Zernikow, B., E. Michel, G. Kohlmann, J. Steck, R.M. Schmitt, and G. Jorch, *Cerebral autoregulation of preterm neonates- a nonlinear control-system.* Archives of disease in childhood, 1994. **70(3)**: p. F166-F173.
86. Liu, J., D.M. Simpson, and R. Allen, *Tracking the Dynamics of the Cerebral Autoregulation Response to Sudden Changes of PaCO2*, in *World Congress on Medical Physics and Biomedical Engineering, Vol 25, Pt 4: Image Processing, Biosignal Processing, Modelling and Simulation, Biomechanics*, O. Dossel and W.C. Schlegel, Editors. 2010, Springer: New York. p. 1-4.
87. Chon, K.H., Y. Zhong, L.C. Moore, N.H. Holstein-Rathlou, and W.A. Cupples, *Analysis of nonstationarity in renal autoregulation mechanisms using time-varying transfer and coherence functions.* American Journal of Physiology-Regulatory Integrative and Comparative Physiology, 2008. **295**(3): p. R821-R828.
88. Poulin, M.J., P.J. Liang, and P.A. Robbins, *Dynamics of the cerebral blood flow response to step changes in end-tidal P-CO2 and P-O2 in humans.* Journal of Applied Physiology, 1996. **81**(3): p. 1084-1095.
89. Poulin, M.J., P.J. Liang, and P.A. Robbins, *Fast and slow components of cerebral blood flow response to step decreases in end-tidal PCO2 in humans.* Journal of Applied Physiology, 1998. **85**(2): p. 388-397.
90. Panerai, R.B., D.M. Simpson, S.T. Deverson, P. Mahony, P. Hayes, and D.H. Evans, *Multivariate dynamic analysis of cerebral blood flow regulation in humans.* Ieee Transactions on Biomedical Engineering, 2000. **47**(3): p. 419-423.
91. Peng, T.Y., A.B. Rowley, P.N. Ainslie, M.J. Poulin, and S.J. Payne, *Multivariate system identification for cerebral autoregulation.* Annals of Biomedical Engineering, 2008. **36**(2): p. 308-320.
92. Mitsis, G.D., M.J. Poulin, P.A. Robbins, and V.Z. Marmarelis, *Nonlinear modeling of the dynamic effects of arterial pressure and CO2 variations on cerebral blood flow in healthy humans.* Ieee Transactions on Biomedical Engineering, 2004. **51**(11): p. 1932-1943.
93. Kouchakpour, H., R. Allen, and D.M. Simpson, *Nonlinear, multiple-input modeling of cerebral autoregulation using Volterra Kernel estimation.* Conference proceedings : ... Annual International Conference of the IEEE Engineering in Medicine and Biology Society. IEEE Engineering in Medicine and Biology Society. Conference, 2010. **2010**: p. 2375-8.
94. Carey, B.J., P.J. Eames, M.J. Blake, R.B. Panerai, and J.F. Potter, *Dynamic cerebral autoregulation is unaffected by aging.* Stroke, 2000. **31**(12): p. 2895-2900.
95. Lipsitz, L.A., M. Gagnon, M. Vyas, I. Iloputaife, D.K. Kiely, F. Sorond, J. Serrador, D.M. Cheng, V. Babikian, and L.A. Cupples, *Antihypertensive therapy increases cerebral blood flow and carotid distensibility in hypertensive elderly subjects.* Hypertension, 2005. **45**(2): p. 216-221.

96. Narayanan, K., J.J. Collins, J. Hamner, S. Mukai, and L.A. Lipsitz, *Predicting cerebral blood flow response to orthostatic stress from resting dynamics: effects of healthy aging.* American Journal of Physiology-Regulatory Integrative and Comparative Physiology, 2001. **281**(3): p. R716-R722.
97. Panerai, R.B., P.J. Eames, and J.F. Potter, *Variability of time-domain indices of dynamic cerebral autoregulation.* Physiological measurement, 2003. **24**: p. 367-381.
98. Liu, J., D.M. Simpson, and R. Allen, *High spontaneous fluctuation in arterial blood pressure improves the assessment of cerebral autoregulation.* Physiological measurement, 2005. **26**(5): p. 725-741.
99. Manly, B.F.J., *Randomization, bootstrap and Monte Carlo methods in biology*. 1997: Chapman & Hall.
100. Marmarelis, V.Z., *Nonlinear dynamic modeling of physiological systems*. 2004, IEEE press series in biomedical engineering: EMB.
101. Westwick, D.T. and R.E. Kearney, *Identification of nonlinear physiological systems*. 2003: IEEE press/Wiley, Piscataway, NJ.
102. Simpson, D.M. and A.A. Birch, *Optimizing the assessment of autoregulation from black-box models.* 4th IET International Conference on Advances in Medical, Signal and Information Processing, MEDSIP 2008, 2008: p. P17 (4 pp.)-P17 (4 pp.)P17 (4 pp.).
103. Zhang, R., J.H. Zuckerman, and B.D. Levine, *Deterioration of cerebral autoregulation during orthostatic stress: insights from the frequency domain.* Journal of Applied Physiology, 1998. **85**(3): p. 1113-1122.
104. Angarita-Jaimes, N., H. Kouchakpour, J. Liu, R.B. Panerai, and D.M. Simpson, *Optimizing the assessment of cerebral autoregulation from black box models.* Medical Engineering and Physics, 2013.
105. Panerai, R.B., J.M. Rennie, A.W.R. Kelsall, and D.H. Evans, *Frequency-domain analysis of cerebral autoregulation from spontaneous fluctuations in arterial blood pressure.* Medical & Biological Engineering & Computing, 1998. **36**(3): p. 315-322.
106. Piechnik, S.K., X. Yang, M. Czosnyka, P. Smielewski, S.H. Fletcher, A.L. Jones, and J.D. Pickard, *The continuous assessment of cerebrovascular reactivity: a validation of the method in healthy volunteers.* Anesthesia and analgesia, 1999. **89(4)**: p. 944-949.
107. Marple S.L, *Digital spectral analysis : with applications*, ed. P.-H.s.p. series. 1987: Englewood Cliffs, N.J.: Prentice-Hall.
108. Soderstorm, T. and P. Stoica, *System Identification*. 1988: Prentice Hall international series in systems and control engineering.
109. Fraser, C.D., K.M. Brady, C.J. Rhee, R.B. Easley, K. Kibler, P. Smielewski, M. Czosnyka, D.W. Kaczka, D.B. Andropoulos, and C. Rusin, *The frequency response of cerebral autoregulation.* Journal of applied physiology (Bethesda, Md. : 1985), 2013. **115**(1): p. 52-6.
110. Panerai, R.B., M. Moody, P.J. Eames, and J.F. Potter, *Dynamic cerebral autoregulation during brain activation paradigms.* American Journal of Physiology-Heart and Circulatory Physiology, 2005. **289**(3): p. H1202-H1208.
111. Panerai, R.B., V. Hudson, L. Fan, P. Mahony, P.M. Yeoman, T. Hope, and D.H. Evans, *Assessment of dynamic cerebral autoregulation based on spontaneous fluctuations in arterial blood pressure and intracranial pressure.* Physiological measurement, 2002. **23**(1): p. 59-72.
112. Newell, D.W., R. Aaslid, R. Stooss, and H.J. Reulen, *The relationship of blood flow velocity fluctuations to intracranial pressure B waves.* Neurosurgery, 1992. **76**: p. 415-421.
113. Steinmeier, R., C. Bauhuf, U. Hubner, R.D. Bauer, R. Fahlbusch, R. Laumer, and I. Bondar, *Slow rhythmic oscillations of blood pressure, intracranial pressure, microcirculation, and cerebral oxygenation.* Stroke, 1996. **27**: p. 2236-2243.

114. Liu, J., M.D. Simpson, J.Y. Yan, and R. Allen, *Tracking time-varying cerebral autoregulation in response to changes in respiratory PaCO(2).* Physiological measurement, 2010. **31**(10): p. 1291-1307.
115. RangeL-Castilla, L., J. Gasco, H.J.W. Nauta, D.O. Okonkwo, and C.S. Robertson, *Cerebral pressure autoregulation in traumatic brain injury.* Neurosurgical Focus, 2008. **25**(4).
116. Kuo T.B.J, C.M.C., W.Y. Sheng, W.J. Wong, H.H. Hu,, *Frequency domain analysis of cerebral blood flow velocity and its correlation with arterial blood pressure.* Journal of cerebral blood flow and metabolism, 1998. **18**: p. 311-318.
117. Percival, D.B. and A.T. Walden, *Spectral Analysis for Physical Applications.* Cambridge University Press, 1993.
118. Budohoski, K.P., M. Czosnyka, N. de Riva, P. Smielewski, J.D. Pickard, D.K. Menon, P.J. Kirkpatrick, and A. Lavinio, *The Relationship Between Cerebral Blood Flow Autoregulation and Cerebrovascular Pressure Reactivity After Traumatic Brain Injury.* Neurosurgery, 2012. **71**(3): p. 652-660.
119. Martin, R.J., *A metric for ARMA processes.* Ieee Transactions on Signal Processing, 2000. **48**(4): p. 1164-1170.
120. Bissacco, A. and S. Soatto, *Hybrid Dynamical Models of Human Motion for the Recognition of Human Gaits.* International Journal of Computer Vision, 2009. **85**(1): p. 101-114.
121. Vidal, R., A. Chiuso, S. Soatto, and S. Sastry, *Observability of linear hybrid systems*, in *Hybrid Systems: Computation and Control, Proceedings*, O. Maler and A. Pnueli, Editors. 2003, Springer-Verlag Berlin: Berlin. p. 526-539.
122. Cuntoor, N.P. and R. Chellappa, *Epitomic representation of human activities.* CVPR '07. IEEE Conference on Computer Vision and Pattern Recognition, 2007: p. 1336-13431343.
123. Bissacco, A., A. Chiuso, M. Yi, and S. Soatto, *Recognition of human gaits.* Proceedings of the 2001 IEEE Computer Society Conference on Computer Vision and Pattern Recognition. CVPR 2001, 2001: p. II-52-II-II-7 vol.2II-II-7 vol.2.
124. Soderstrom, T. and P. Stoica, *System Identifiation*. 1989: Prentice Hall International Series In Systems And Control Engineering
125. Bogert. B.P, Healy. M.J.R, and T. J.W, *The Quefrency Alanysis of Time Series for Echoes: Cepstrum, Pseudo Autocovariance, Cross-Cepstrum and Saphe Cracking*. Proceedings of the Symposium on Time Series Analysis (M. Rosenblatt, Ed) 1963, New York: Wiley.
126. Nikias, C.L., *HIGHER-ORDER SPECTRA IN SIGNAL-PROCESSING*. Signal Processing V : Theories and Applications, Vols 1-3, ed. L. Torres, E. Masgrau, and M.A. Lagunas. 1990, Amsterdam: Elsevier Science Publ B V. 35-41.
127. Martin, R.J., *Autoregression and cepstrum-domain filtering.* Signal Processing, 1999. **76**(1): p. 93-97.
128. Kohavi, R., *A study of cross-validation and bootstrap for accuracy estimation and model selection.* IJCAI-95. Proceedings of the Fourteenth International Joint Conference on Artificial Intelligence, 1995: p. 1137-43 vol.243 vol.2.
129. Aaslid, R., M. Blaha, G. Sviri, C.M. Douville, and D.W. Newell, *Asymmetric dynamic cerebral autoregulatory response to cyclic stimuli.* Stroke, 2007. **38**: p. 1465-1469.
130. Sun, X.Q., Y.J. Yao, C.B. Yang, S.Z. Jiang, C.L. Jiang, and W.B. Liang, *Effect of lower-body negative pressure on cerebral blood flow velocity during 21 days head-down tilt bed rest.* Medical Science Monitor, 2005. **11**(1): p. CR1-CR5.
131. De Cock, K. and B. De Moor, *Subspace angles between ARMA models.* Systems & Control Letters, 2002. **46**(4): p. 265-270.
132. Childers, D.G., D.P. Skinner, and R.C. Kemerait, *CEPSTRUM - GUIDE TO PROCESSING.* Proceedings of the Ieee, 1977. **65**(10): p. 1428-1443.
133. Panerai, R.B., E.L. Sammons, M. Smith, W.E. Rathbone, S. Bentley, P.J. F., and N.J. Samani, *Continuous estimates of dynamic cerebral autoregulation: influence of non-invasive arterial blood pressure measurements.* Physiol meas, 2008. **29**: p. 497-513.

134. Panerai, R.B., *Cerebral autoregulation: From models to clinical applications.* Cardiovascular Engineering, 2008. **8**(1): p. 42-59.
135. Rowley, A.B., S.J. Payne, I. Tachtsidis, M.J. Ebden, J.P. Whiteley, D.J. Gavaghan, L. Tarassenko, M. Smith, C.E. Elwell, and D.T. Delpy, *Synchronization between arterial blood pressure and cerebral oxyhaemoglobin concentration investigated by wavelet cross-correlation.* Physiological measurement, 2007. **28**(2): p. 161-173.
136. Latka, M., M. Turalska, M. Glaubic-Latka, W. Kolodziej, D. Latka, and B.J. West, *Phase dynamics in cerebral autoregulation.* American Journal of Physiology-Heart and Circulatory Physiology, 2005. **289**(5): p. H2272-H2279.
137. Mitsis, G.D., R. Zhang, B.D. Levine, and V.Z. Marmarelis, *Cerebral hemodynamics during orthostatic stress assessed by nonlinear modeling.* Journal of Applied Physiology, 2006. **101**(1): p. 354-366.
138. Panerai, R.B., P.J. Eames, and J.F. Potter, *Multiple coherence of cerebral blood flow velocity in humans.* American Journal of Physiology-Heart and Circulatory Physiology, 2006. **291**(1): p. H251-H259.
139. Birch, A.A., G. Neil-Dwyer, and A.J. Murrills, *The repeatability of cerebral autoregulation assessment using sinusoidal lower body negative pressure.* Physiol meas, 2002. **23**: p. 73-83.
140. Panerai, R.B., *Transcranial Doppler for evaluation of cerebral autoregulation.* Clinical Autonomic Research, 2009. **19**(4): p. 197-211.
141. Giller, C.A., G. Bowman, H. Dyer, L. Mootz, W. Krippner, C.M. Loftus, and J.P. Muizelaar, *Cerebral arterial diameters during changes in blood pressure and cerbon dioxide durig craniotomy.* Neurosurgery, 1993. **32**(5): p. 737-742.
142. Strebel, S., A.M. Lam, B. Matta, T.S. Mayberg, R. Aaslid, and D.W. Newell, *Dynamic and static cerebral autoregulation during Isoflurane, Desflurane, and propofol Anesthesia.* Anesthesiology, 1995. **83**(1): p. 66-76.
143. Edwards, M.R., D.L. Devitt, and R.L. Hughson, *Two-breath CO2 test detects altered dynamic cerebrovascular autoregulation and CO2 responsiveness with changes in arterial PCO2.* American Journal of Physiology-Regulatory Integrative and Comparative Physiology, 2004. **287**(3): p. R627-R632.
144. Haykin. S, *Adaptive Filter Theory*. Vol. Fourth 1996: Englewood Cliffs, NJ:Prentice-Hall.
145. Liu, Y. and R. Allen, *Analysis of dynamic cerebral autoregulation using an ARX model based on arterial blood pressure and middle cerebral artery velocity simulation.* Medical & Biological Engineering & Computing, 2002. **40**(5): p. 600-605.
146. Peng, T.Y., A.B. Rowley, P.N. Ainslie, M.J. Poulin, and S.J. Payne, *Wavelet Phase Synchronization Analysis of Cerebral Blood Flow Autoregulation.* Ieee Transactions on Biomedical Engineering, 2010. **57**(4): p. 960-968.
147. Koch, G.G., *Intraclass correlation coefficient*. 1982, New York: John Wileyt & Sons.
148. Balldin, U.I., L.P. Krock, N.L. Hopper, and W.G. Squires, *Cerebral artery blood flow velocity changes following rapid release of lower body negative pressure.* Aviation Space and Environmental Medicine, 1996. **67**(1): p. 19-22.
149. Hu, H.-H., T. Kuo B-J., W.-J. Wong, Y.-O. Luk, C.-M.Chern, L.-C. Hsu, and W.-Y. Sheng, *Transfer function analysis of cerebral hemodynamics in patients with carotid stenosis.* Cerebral Blood Flow Metabolism, 1999. **19**: p. 460-465.
150. Chuang-Chien Chiua, S.-J.Y., *Assessment of cerebral autoregulation using time-domain cross-correlation analysis.* computers in biology and medicine, 2001. **31**: p. 471-480.
151. Kearney, R. and D. Westwick, *Nonlinear identification methods for modeling biomedical systems*. Proceedings of the 1998 2nd International Conference Biomedical Engineering Days. 1998, New York: Ieee. 1-10.